THE UNIVERSITY OF MICHIGAN

INDUSTRY PROGRAM OF THE COLLEGE OF ENGINEERING

REDUNDANCY IN COHERENT IMAGING SYSTEMS

by
Robert Warren Lewis

A dissertation submitted in partial fulfillment
of the requirements for the degree of
Doctor of Philosophy in the
University of Michigan
Department of Electrical Engineering

January, 1973

IP-850

Doctoral Committee:

Professor Emmett N. Leith, Chairman
Professor Frederick J. Beutler
Associate Professor William B. Ribbens
Professor Thomas B. A. Senior
Doctor Carl C. Aleksoff
Lecturer Juris Upatnieks

ABSTRACT

REDUNDANCY IN COHERENT IMAGING SYSTEMS

by
Robert Warren Lewis

Chairman: Emmett N. Leith

Diffuse coherent illumination has a wide spatial bandwidth with no dominant frequency components. This type of illumination makes a holographic recording redundant since any small part of the hologram can reconstruct the entire object field. Because of this redundancy property, a diffuse holographic recording is rather insensitive to scratches and other system artifacts. Unfortunately, diffuse coherent illumination results in a multiplicative noise granularity called laser speckle. The spectral density of laser speckle has a significant low frequency contribution which limits both image quality and resolution. Mixed-integration processing can utilize excess system bandwidth to suppress speckle. The statistical speckle fluctuation is reduced by adding uncorrelated samples noncoherently. This paper establishes an equivalence between noncoherent techniques which continuously sample a signal's spectrum and a simple irradiance filter.

Most optical noise suppression techniques for coherent spatial filtering systems involve transverse displacement of the optical signal relative to the optical axis together with noncoherent addition. An effective moving grating method is presented for introducing redundancy into coherent spatial filtering systems.

For holographic systems, special redundancy modulation is needed to obtain a high quality image of a continuous-tone transparency. Redundancy modulation must satisfy two constraints. First, the modulation must be free of low frequency speckle. Second, the spectral density of the modulation must be bandlimited and must satisfy certain uniformity conditions. Numerical results obtained compare the characteristics of several functions which appear to satisfy these constraints.

Periodic functions are the most promising class of redundancy modulation for the high density storage of continuous-tone transparencies. The class of speckle-free periodic modulation proposed by Gabor has been studied and new solutions with uniform spectral characteristics have been determined using numerical methods. Several methods exist for synthesizing this speckle-free modulation. Two indirect synthesis methods are presented which require a spatial filtering operation. The noise suppression performance of periodic functions has been analyzed in terms of a family of redundancy parameters. Redundancy modulation with good diffraction efficiency characteristics can be obtained by using a coarse lens array in tandem with a periodic grating solution. Experimental results demonstrate that the addition of a lens array can improve the noise suppression characteristics of this class of functions.

ACKNOWLEDGMENTS

I wish to thank the members of my dissertation committee for their service. A special note of thanks is given to Professor Leith for his interest and helpful discussions while serving as Chairman. Professor Senior provided important advice during the early stages of my dissertation work. Juris Upatnieks, Dr. Aleksoff and several other members of the Radar and Optics Laboratory provided helpful comments during the course of my research.

Special appreciation is expressed to my wife Jill for her encouragement, and for editing the manuscript.

Thanks are due to Carole Newton for typing the dissertation.

A major portion of this dissertation work was supported by NSF Grant GK-31474. A portion of the work was supported by the Air Force Avionics Laboratory, Air Force Systems Command, Wright-Patterson Air Force Base, under Contract No. F33615-70-C-1433.

TABLE OF CONTENTS

Page

LIST OF FIGURES

LIST OF TABLES

LIST OF SYMBOLS

a_n	n-th complex Fourier series coefficient
$\arg\{\bullet\}$	denotes the argument of a complex number
b_R	free real parameter represented as BR in computer subroutines
BR	subroutine variable equal to b_R
BW	bandwidth
circ(r)	defined on page 17
d(x)	dust diffraction pattern
E_s	the percent of the light energy within the system bandpass
$E\{\bullet\}$	expected value operator
Eq. (N, k)	k-th equation of Eqs. (6) on page 84
F	F-number of lens
f	focal length of lens
f_o	reciprocal of the period of a grating
$FT\{\bullet\}$	Fourier transform operator
G_α	general redundancy parameter (see Condition B, page 41)
g(x)	final average image irradiance
$g_I(x)$	impulse response of low-pass irradiance filter
H	frequency transfer function
h(x)	impulse response
$h_I(x)$	impulse response of irradiance filter
$h_\nu(t)$	impulse response for slit at position ν
$\hat{h}(f_x)$	Fourier transform of h(x)
I_k	modulus of the k-th Fourier series coefficient of periodic $\lvert q(x) \rvert^2$

I_M	output irradiance of mixed integrator
$I(x)$	output irradiance of imaging system
J_1	first order Bessel function
$J(x)$	output of low-pass irradiance filter (see Condition A, page 39)
k	equal to $(2\pi)/\lambda$
L	constant often used as upper bound for V (page 41)
M	irradiance modulation (see page 49)
m	mean value
$\hat{m}(\nu)$	weighting function dependent on scanning position
m^2/σ^2	defined for Condition (A) on page 39
N	positive integer
$\hat{n}(f_x)$	Fourier transform of n(x)
$P(x)$	phase of q(x)
$p(x, z)$	impulse response for free space propagation (see page 71)
p_{coh}	PDF for coherent image irradiance
p_{MI}	PDF for image irradiance after mixed integration
PDF	probability density function
Q	constant usually representing the space bandwidth parameter of a quadratic phase signal (see page 42)
q_A	periodic quadratic phase modulation (page 42)
q_B	periodic quadratic phase modulation with continuous dP(x)/dx (page 43)
q_o	periodic q(x) after one order a_{n_o} is attenuated
$q(x)$	complex amplitude transmittance representing redundancy modulation
$\hat{q}(n/X)$	n-th complex Fourier series coefficient of periodic q(x)
R_M	redundancy parameter for periodic redundancy modulation (page 46)
rect(x)	defined on page 31
RDC	1/(duty cycle)

S	power spectrum
s_o	DC term of $s(x)$
$s(x)$	input signal amplitude
$\text{sinc}(x)$	$\sin(\pi x)/(\pi x)$
S/N	signal-to-noise ratio
u	diameter of a dust particle
V	width of an elementary element of $q(x)$ (page 40)
$\text{Var}\{\bullet\}$	variance operator
W	constant often used for bandwidth
w_o	equals $2\pi f_o$
$w(x)$	impulse response of coherent processor
X	period of grating
Z	output amplitude for white complex Gaussian input
$\Gamma(N)$	gamma function
$\delta(x)$	Dirac delta function
ϵ	small positive constant
λ	light wavelength
σ	standard deviation

1
PARTIALLY COHERENT PROCESSING TECHNIQUES TO REDUCE LASER SPECKLE

1.1. INTRODUCTION

Coherent imaging differs from noncoherent imaging systems in several important respects. A coherent system is linear in complex amplitude, while a noncoherent system can be described as a linear mapping of intensity or irradiance. The lensless recording of the complex amplitude of light afforded by holography can be exploited for signal processing, data storage, and many other applications. Unfortunately coherent imaging has certain characteristics which limit its utility in many applications. For example, if non-diffuse objects such as transparencies are imaged with a uniform beam of coherent light, system artifacts such as a small scratch, bubble, or dust particle introduce dark diffraction patterns at the image plane. For diffuse objects with many random scatterers in a resolution cell or when imaging transparencies backlighted with diffuse illumination from fine ground glass, small system artifacts no longer limit image quality. However, now superimposed on the average reflectivity of the object is a multiplicative "noise" granularity referred to in the literature as laser speckle [1]. It will be seen that laser speckle limits both image quality and system resolution. It will be demonstrated that excess system bandwidth together with a controlled reduction in coherence can suppress optical noise and decrease speckle modulation.

1.2. CHARACTERISTICS OF LASER SPECKLE

For diffuse objects imaged with spatial bandlimited coherent optical systems, a multiplicative "noise" granularity is superimposed on the average reflectivity or transmittance density of the image. This granularity, known as laser speckle, limits the resolution and image fidelity of such systems. Speckle can be modeled as white, complex Gaussian clutter with a zero mean [2]. Such a model is a good approximation if large numbers of scattering centers exist in a resolution cell, in which case linear filtering (such as low-pass filtering) results in a zero-mean, stationary, complex Gaussian process. The spatial power spectrum of the image amplitude is usually bandlimited and uniform. The fineness of the image speckle is determined by its autocorrelation width, which is approximately equal to the reciprocal of the bandwidth of the image signal amplitude. The $(\text{modulus})^2$ of the image amplitude has an exponential probability density function (PDF), $(1/\sigma)\exp(-u/\sigma)$, with domain $0 \le u < \infty$. This PDF has a variance σ^2 and a mean $m = \sigma$ and thus a $(\text{mean})^2/\text{variance}$ of unity. The ratio m^2/σ^2 can be considered a signal-to-noise ratio which measures image fidelity. It will be seen in the next section that mixed integration can be used to increase m^2/σ^2 by decreasing the achievable system resolution. The image irradiance at the output of a mixed integrator is the sum of N identically distributed, uncorrelated random variables, each with an exponential distribution. For this sum $m^2/\sigma^2 = N$, and the PDF is the gamma distribution

$$\frac{1}{(\sigma/N)\,\Gamma(N)}\left(\frac{u}{\sigma/N}\right)^{N-1} e^{-u/(\sigma/N)}$$

with domain $0 \le u < \infty$.

1.3. MIXED-INTEGRATION PROCESSING

1.3.1. INTRODUCTION

Mixed integration is a method of processing a coherent image which reduces speckle granularity but also decreases the achievable resolution [2, 3]. This processing method is equivalent to introducing a system diversity parameter. The method usually involves processing portions of the signal spectrum separately and then noncoherently summing the energy densities of a family of images. The noncoherent summation reduces the statistical fluctuation of the speckle. An equivalence will be established between sampling portions of the signal's spatial spectrum and sampling the coherently processed image to accomplish the noncoherent addition.

1.3.2. DESCRIPTION OF MIXED-INTEGRATION PROCESSING

There exist several discrete and continuous types of mixed integration. Three types will now be considered.

Case A: Discrete Sampling in the Frequency Plane

Mixed integration can be introduced into an optical processor by processing N equal nonoverlapping portions of a signal's spectrum separately and then by summing N output image irradiances noncoherently. Let $s(x)$ be the input signal and represent bandlimited white complex Gaussian speckle. Since the N sections of the spectrum do not overlap, mixed-integration processing performed in this way results in the noncoherent addition of N independent samples. The output resolution-cell width is N times the width that would be obtained with coherent processing.

Case B: Discrete Sampling at the Image Plane

Instead of sampling the signal's spectrum to achieve N independent additions, a mixed-integration operation can be introduced as shown in Fig. 1-1. The signal s(x) is first coherently processed by means of a filter with impulse response w(x) and is then square-law envelope detected to yield an output irradiance $|f(x)|^2$. The output irradiance $|f(x)|^2$ is filtered with a linear filter with an impulse $h_I(x)$ to yield a final image irradiance g(x). Let $w(x) = \frac{(\sin \pi x)}{\pi x}$ be the impulse response of a coherent processor. Then if

$$h_I(x) = \sum_{n=0}^{N-1} \delta(x - n)$$

the resolution-cell width will increase by a factor N. Since the autocorrelation function for the speckle is $\frac{\sin(\pi x)}{\pi x}$ and the speckle has Gaussian statistics, the output irradiance for each point x_o of g(x) is the sum of the irradiances of N independent coherent image points.

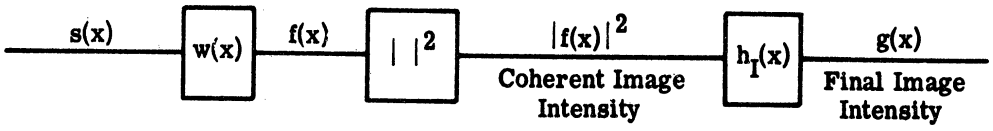

Figure 1-1. Block Diagram for a Processor with Type B or C Mixed Integration

Case C: Continuous Sampling of the Signal Spectrum with a Scanning Slit

Case C, which utilizes continuous sampling of the signal spectrum, can be represented by the same block diagram as that shown in Fig. 1-1. This type of mixed integration is implemented by scanning the signal spectrum with a slit, while integrating the output irradiance over one scan time. One scan time is the time it takes for the slit to pass completely across the spectral window. To simplify the derivation of the mixed-integration transfer function, let $f(x) = s(x) * w(x)$ represent the coherently processed signal amplitude used as the input to a mixed integrator, where the symbol * denotes the convolution operator. Let $h(x)$ be proportional to the Fourier transform of the scanning slit, and let $\hat{m}(\nu)$ be a weighting function dependent on the scanning position ν. Then the mixed integrator has the following form: $f(x)$ is the input signal, and $g(x)$ is the average output irradiance averaged over one scan time of the scanning aperture. Thus

$$g(x) = \frac{1}{2\pi} \int_{-\infty}^{\infty} \left| a(x;\ \nu) \right|^2 \hat{m}(\nu)\, d\nu$$

where

$$a(x;\ \nu) = \int_{-\infty}^{\infty} f(x - t) h_{\nu}(t)\, dt$$

and where $h_{\nu}(t)$ = the impulse response for the system when the scanning slit is centered at position ν in the frequency plane. Hence, $g(x)$ can be written as

$$g(x) = \iint_{-\infty}^{\infty} f(x - t)f(x - \tau)^* \left[\frac{1}{2\pi} \int_{-\infty}^{\infty} h_\nu(t)h_\nu^*(\tau)\hat{m}(\nu)\, d\nu \right] dt\, d\tau$$

Let

$$Q(t, \tau) = \frac{1}{2\pi} \int_{-\infty}^{\infty} h_\nu(t)h_\nu^*(\tau)\hat{m}(\nu)\, d\nu$$

For the mixed integrator being discussed,

$$h_\nu(t) = h(t)e^{-i\nu t}$$

and

$$\hat{m}(\nu) = \text{constant}$$

Then, to within a constant of proportionality

$$Q(t, \tau) = h(t)h(\tau)^* \delta(\tau - t)$$

and

$$g(x) = \int_{-\infty}^{\infty} \left| f(x - t) \right|^2 \left| h(t) \right|^2 dt$$

Thus, the output of a processor using Type C mixed integration is

$$g(x) = \left| s(x) * w(x) \right|^2 * \left| h(x) \right|^2$$

where s(x) is the amplitude of the input signal to the processor. For the discrete sampling method discussed in Case A, $\hat{m}(\nu)$ takes the form

$$\sum_{n=-\infty}^{\infty} \delta(\nu - nD)$$

where D represents the width of the scanning slit. In summary, $f(x) = s(x) * w(x)$ is the processor's output amplitude that has been coherently processed over the full input signal bandwidth. The mixed integrator that continuously samples the Fourier transform of the signal performs a simple low-pass video filtering operation on the output signal intensity of the form

$$g(x) = |f(x)|^2 * h_I(x)$$

where

$$h_I(x) = |h(x)|^2$$

and h(x) is simply the Fourier transform of the scanning aperture, if the usual scale factors introduced by lenses are set equal to unity.

1.3.3. EFFECT OF MIXED INTEGRATION ON THE VARIANCE/(MEAN)^2 OF LASER SPECKLE

Mixed integration compresses the dynamic range of laser speckle. For complex Gaussian speckle, mixed integrators A and B reduce the variance/(mean)^2 of the processed image irradiance from 1 to 1/N, if N independent samples are noncoherently added. Calculations in this section will show how mixed integrator C affects the variance/(mean)^2 characteristics of complex Gaussian speckle.

Before determining the effect of mixed integrator C on the variance/(mean)^2 of speckle, the power spectrum of complex Gaussian speckle must be determined. Let Z(x, y) be the output amplitude of an imaging system with a linear transfer function $H(f_x, f_y)$ and an input which is a stationary white complex Gaussian random process with zero mean. Since the statistics of Z are also Gaussian, the following theorem [4] will be used to calculate the correlation function for $|Z|^2$.

If Z_1, Z_2, Z_3, and Z_4 are complex jointly Gaussian random variables with zero means, then

$$E(Z_1Z_2Z_3Z_4) = E(Z_1Z_2)E(Z_3Z_4) + E(Z_1Z_3)E(Z_2Z_4)$$

$$+ E(Z_1Z_4)E(Z_2Z_3)$$

where E is the expected value operator. Let the irradiance of the imaging system be

$$I(x, y) = |Z_1(x, y)|^2$$

when this theorem is used

$$E[I(x, y)I(x + t_1, y + t_2)] = \{E[I(x, y)]\}^2$$

$$+ E[Z_1^*(x + t_1, y + t_2)Z_1(x, y)]E[Z_1^*(x, y)Z_1(x + t_1, y + t_2)]$$

where t is a constant. Let the power spectrum of Z(x, y) be $S_Z(f_x, f_y)$. Then the power spectrum S, for I(x, y) is

$$S_I(f_x, f_y) = \{E[I(x, y)]\}^2\delta(f_x, f_y) + S_Z(f_x, f_y) * S_Z^*(-f_x, -f_y)$$

where δ is the Dirac δ function. Assume

$$S_Z(f_x, f_y) = S_Z^*(-f_x, -f_y) = \sqrt{C}\left|H(f_x, f_y)\right|^2$$

Then

$$S_I(f_x, f_y) = E^2(I)\delta(f_x, f_y) + C(|H|^2 * |H|^2)$$

Let σ_I^2 = variance of I, and $\mu_I = E(I)$ = mean of I. Then

$$\sigma_I^2 = \int_{-\infty}^{\infty} C\left[\left|H(f_x, f_y)\right|^2 * \left|H(f_x, f_y)\right|^2\right] df_x\, df_y$$

$$= C\left[FT^{-1}(|H|^2)\right]^2 \text{ at } x = y = 0$$

$$= C\left[\iint_{-\infty}^{\infty} \left|H(f_x, f_y)\right|^2 df_x\, df_y\right]^2$$

Since $\mu_I^2 = \sigma_I^2$ from Section 1.2

$$C = \frac{\mu_I^2}{\left[\iint_{-\infty}^{\infty} |H|^2\, df_x\, df_y\right]^2}$$

$$S_I = \mu_I^2\left[\delta(f_x, f_y) + \frac{|H|^2 * |H|^2}{\left(\iint_{-\infty}^{\infty} |H|^2\, df_x\, df_y\right)^2}\right]$$

Let the output intensity I_M result from a mixed-integration operation with impulse response $h_I(x, y)$.

$$I_M = I(x, y) * h_I(x, y)$$

The power spectrum for I_M is

$$S_{I_M}(f_x, f_y) = |H_I|^2 S_I \quad \text{where } H_I = FT(h_I)$$

Thus, the (mean)^2/variance ratio for I_M is

$$\left(\frac{\mu^2}{\sigma^2}\right) = \frac{|H_I(0, 0)|^2 \left[\int_{-\infty}^{\infty}\int |H(f_x, f_y)|^2 df_x df_y\right]^2}{\int_{-\infty}^{\infty}\int |H_I(f_x, f_y)|^2 \left[|H(f_x, f_y)|^2 * |H(f_x, f_y)|^2\right] df_x df_y} \quad (1)$$

A sample calculation for a Gaussian aperture derived from Eq. (1) is as follows:

$$H(f_1, f_2) = \prod_{i=1}^{2} e^{-\pi f_i^2}$$

then

$$|H|^2 * |H|^2 = \prod_{i=1}^{2} \frac{1}{2} e^{-\pi f_i^2}$$

$$h = FT^{-1}(H)$$

$$h(x_1, x_2) = \prod_{i=1}^{2} e^{-\pi x_i^2}$$

$$|h|^2 = \prod_{i=1}^{2} e^{-\pi(\sqrt{2}x_i)^2}$$

Let

$$h_I(x_1, x_2) = \prod_{i=1}^{2} e^{-\pi[(\sqrt{2}x_i)/(N_i)]^2}$$

Note that h_I is scaled N_i wider than $|h|^2$ along the x_i coordinate.

$$|H_I|^2 \propto \prod_{i=1}^{2} e^{-\pi(N_i f_i)^2}$$

when these expressions are substituted in Eq. (1)

$$\left(\frac{\mu^2}{\sigma^2}\right) = \frac{\left(\prod_{i=1}^{2} \int_{-\infty}^{\infty} e^{-2\pi f_i^2} \, df_i\right)^2}{\prod_{i=1}^{2} \left(\int_{-\infty}^{\infty} e^{-\pi(N_i f_i)^2} (1/2) e^{-\pi f_i^2} \, df_i\right)}$$

Using the fact that

$$\int_{-\infty}^{\infty} e^{-1/2(X/C)^2}\, dx = C\sqrt{2\pi}$$

Then

$$\left(\frac{\mu^2}{\sigma^2}\right) = \sqrt{N_1^2 + 1}\,\sqrt{N_2^2 + 1}$$

as $N_1,\ N_2 \to \infty,\ N_1 N_2(\sigma^2/\mu^2) \to 1.$

1.3.4. IMAGE CONTRAST

The nonlinearity introduced by recording film or by a human observer affects the final image contrast, when an estimate of the average image irradiance is sought for a small image patch containing many resolution cells. Consider an image patch which has an average irradiance σ. If there are many scatterers in a resolution cell, the PDF for the irradiance, w, at a single image point is

$$p_{coh}(w) = \frac{1}{\sigma} e^{-w/\sigma}$$

for a coherent image, and

$$p_{MI}(w) = \frac{1}{(\sigma/N)\Gamma(N)} \left(\frac{w}{\sigma/N}\right)^{N-1} e^{[-w/(\sigma/N)]}$$

for an image processed by mixed integration, which noncoherently adds N independent samples. $p_{coh}(w)$ and $p_{MI}(w)$

are both zero for $w < 0$, and the mean of each distribution is σ. The variance-to-(mean)^2 ratio is 1 for p_{coh} and $1/N$ for p_{MI}. These probability density functions can be found in Ref. [5].

Let $n_T(w)$, shown in Fig. 1-2, represent the transfer function relating w to the intensity transmittance of a positive transparency used to record a processed image. Let C be a positive constant. Then the space-averaged irradiance W of the light transmitted by the image transparency is

$$W_{coh} = C \int_0^\infty p_{coh}(w) n_T(w)\, dw$$

for the coherent image, and

$$W_{MI} = C \int_0^\infty p_{MI}(w) n_T(w)\, dw$$

for the image processed by means of mixed integration.

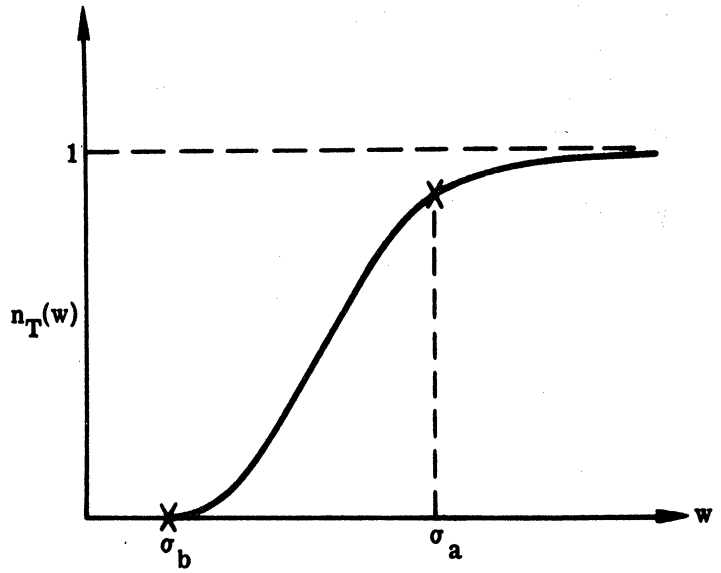

Figure 1-2. Intensity Transmittance of a Positive Transparency as a Function of the Image Irradiance

Consider points $w = \sigma_a$ and $w = \sigma_b$ in Fig. 1-2. If the average irradiance of the patch is σ_a, the mean σ for PDF's p_{coh} and p_{MI} is set equal to σ_a, and it is found that $W_{MI} > W_{coh}$. If σ_b is the average irradiance, $W_{MI} < W_{coh}$. An example of this characteristic is shown in Fig. 1-3, in which a resolution chart was coherently imaged with and without mixed-integration processing. Complex Gaussian speckle was introduced by placing a ground glass plate against the resolution chart. The pictures show that mixed-integration processing can improve contrast.

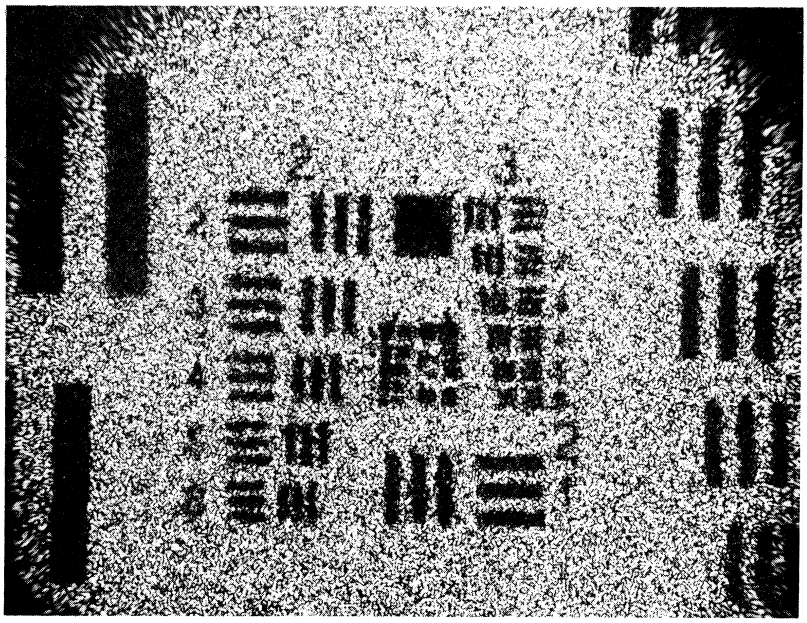

(a) Coherent Image Without Mixed Integration

Figure 1-3. Image Showing Laser Speckle With and Without Mixed Integration

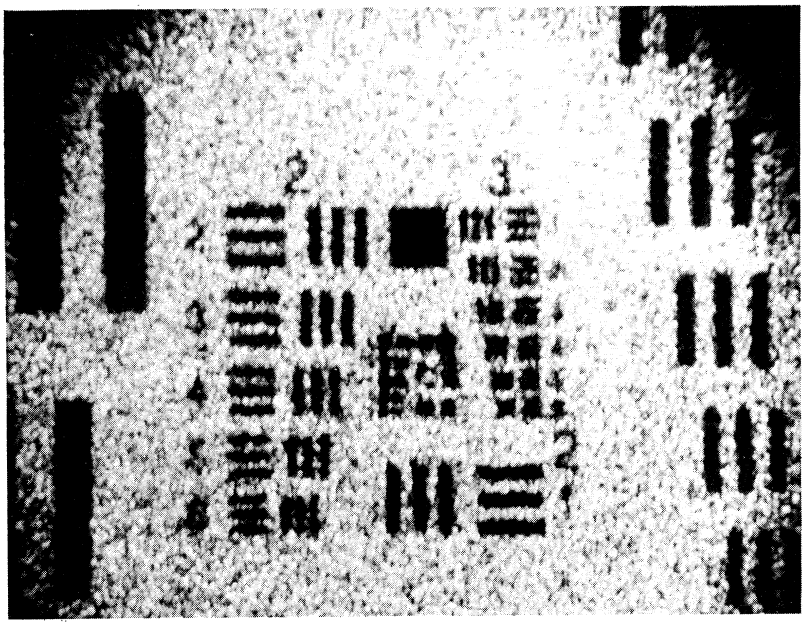

(b) Image With Mixed Integration

Figure 1-3. Image Showing Laser Speckle With and Without Mixed Integration (continued)

1.3.5. MIXED INTEGRATION USING A MOVING DIFFUSER

It was seen in Section 1.3.2 that mixed integration is equivalent to a noncoherent spatial filtering operation. A spatially noncoherent source can introduce this operation in holographic image reconstruction since a lateral shift in the reference beam source point causes a corresponding shift in the position of the image [2]. It will be seen in Section 1.4.2 that reducing the source coherence helps suppress artifact noise. An efficient means of achieving a spatially noncoherent source using laser light will now be given.

Consider the light distribution shown at Plane B of Fig. 1.4.

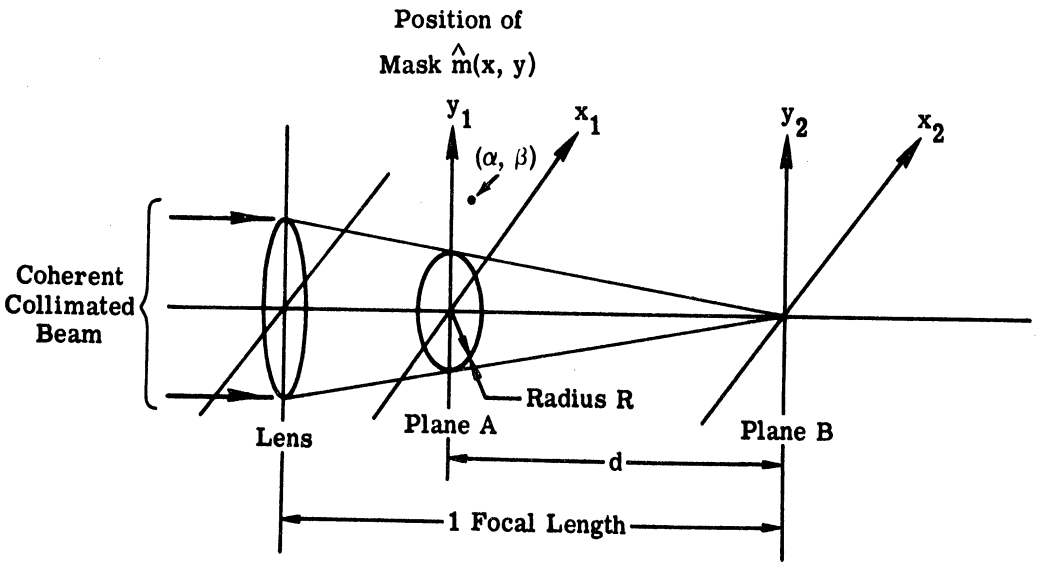

re 1-4. Construction of a Light Source for Mixed-Integration Processing

Let us examine the cross correlation of the light amplitude at two points in Plane B if the mask is moving. Let the coordinates of Plane A be the Cartesian coordinates x and y. If a mask, $\hat{m}(x, y)$, is centered at point (α, β) of Plane A, then the light distribution at Plane B is

$$u(f_x, f_y) = Ce^{-i\omega t} \int_{-\infty}^{\infty}\int \operatorname{circ}\left(\frac{r}{R}\right) \hat{m}(x - \alpha, y - \beta) e^{-i2\pi(f_x x + f_y y)} dx\, dy$$

where

$$f_x = \frac{x_2}{\lambda d}$$

$$f_y = \frac{y_2}{\lambda d}$$

$$r = \sqrt{x^2 + y^2}$$

$$FT[\hat{m}(x)] = m(f_x)$$

$$\operatorname{circ} r = \begin{cases} 1, & r \le 1 \\ 0, & \text{otherwise} \end{cases}$$

Then

$$u(f_x, f_y) = CR^2 e^{-i\omega t} \left\{ \left[\frac{J_1\left(2\pi R\sqrt{f_x^2 + f_y^2}\right)}{R\sqrt{f_x^2 + f_y^2}} \right] * \left[m(f_x, f_y) e^{-i2\pi(\alpha f_x + \beta f_y)} \right] \right\}$$

Defining

$$\hat{C}(f_x, f_y) \equiv CR^2 \frac{J_1\left(2\pi R\sqrt{f_x^2 + f_y^2}\right)}{R\sqrt{f_x^2 + f_y^2}}$$

Let

$$w(f_x, f_y, \alpha, \beta) = e^{-i\omega t}\left[\hat{C}(f_x, f_y) * m(f_x, f_y)e^{-i2\pi(\alpha f_x + \beta f_y)}\right]$$

When the mask $\hat{m}$ is moved to various positions during reconstruction or optical processing with the source formed at Plane B, it is necessary to determine the cross correlation

$$R(f_{x1}, f_{y1}; f_{x2}, f_{y2}) = \iint_{(\alpha,\beta)\in A\times B} w(f_{x1}, f_{y1}, \alpha, \beta)$$

$$w^*(f_{x2}, f_{y2}, \alpha, \beta)\, d\alpha\, d\beta$$

where the integration is over the Cartesian product $A \times B$, and $A = B = (-\infty, \infty)$. Or

A = N (spatial mask period along x coordinate)

B = N (spatial mask period along y coordinate)

if the mask is periodic in each coordinate, and N is a positive integer or $N >> 1$.

It is necessary to determine how far apart source points must be for the cross correlation to be zero. By interchanging integrals and integrating first over $A \times B$ it is found that

$$R(f_{x1}, f_{y1}; f_{x2}, f_{y2}) = \int_{-\infty}^{\infty}\int \hat{C}(\tau_{x1}, \tau_{y1})$$

$$\hat{C}\left[\tau_{x1} + (f_{x2} - f_{x1}), \tau_{y1} + (f_{y2} - f_{y1})\right]$$

$$\left| m(f_{x1} - \tau_{x1}, f_{y1} - \tau_{y1})\right|^2 d\tau_{x1}\, d\tau_{y1}$$

Since, $\hat{C}(\tau_{x1}, \tau_{y1}) \approx 0$ for $\sqrt{\tau_{x1}^2 + \tau_{y1}^2} > 1/R$, and the correlation coefficient

$$\rho = \frac{R(f_{x1}, f_{y1}; f_{x2}, f_{y2})}{\sqrt{R(f_{x1}, f_{y1}; f_{x1}, f_{y1})R(f_{x2}, f_{y2}; f_{x2}, f_{y2})}}$$

is approximately zero if

$$\sqrt{(f_{x2} - f_{x1})^2 + (f_{y2} - f_{y1})^2} > \frac{2}{R}$$

This result shows that the intensities of the images produced by source points spaced more than $2\lambda d/R$ apart on Plane B of Fig. 1.4 add together noncoherently to form the total output image irradiance. To achieve this noncoherent addition, the image irradiance must be time averaged over some time interval of length T. T is dependent on the time required for the integration over A × B. In practice a spinning lens array is a suitable choice for $\hat{m}$, since lens arrays with rather narrow circ function spectral densities exist, and good light efficiency can be achieved with such a diffuser. Amplitude weighting at

Plane B can help control the source shape. Section 1.4.2 will show the optical noise suppression characteristics of this type of spatially noncoherent source.

1.4. OPTICAL NOISE SUPPRESSION IN OPTICAL FILTERING

1.4.1. INTRODUCTION

Unless special techniques are employed, optical noise limits the performance of coherent optical spatial filtering systems. Because the output of a spatial filtering system is usually square-law envelope detected, this type of system is amenable to noncoherent noise suppression techniques.

Various methods have been used to reduce optical noise. One method which has proved effective in processing synthetic aperture radar data is to move the input and output films in synchronism [6]. Optical elements with rotational symmetry can be rotated during processing to reduce optical noise effects. In one technique the spatial carrier frequency of a filtering system is time varying and a spatial filter must track the transform plane motion [7]. If the spatial source coherence is reduced, it will be seen that optical noise can be dispersed and noncoherently added at the output plane. Unfortunately, decreasing the spatial coherence causes a loss of resolution at the Fourier transform plane of a filtering system. In Section 1.4.3 a moving grating technique for suppressing optical noise is presented. This technique does not reduce the resolution at either the image or the transform plane, and in general is one of the simplest and least expensive techniques to implement. This latter technique gives insight into the noise suppression techniques required for fully coherent systems which are considered in Chapter 2.

1.4.2. REDUCTION OF THE SPATIAL SOURCE COHERENCE

An experiment was conducted which illustrates the fact that reducing the spatial coherence of a source helps suppress optical noise in spatial filtering systems. Figure 1-5 shows a

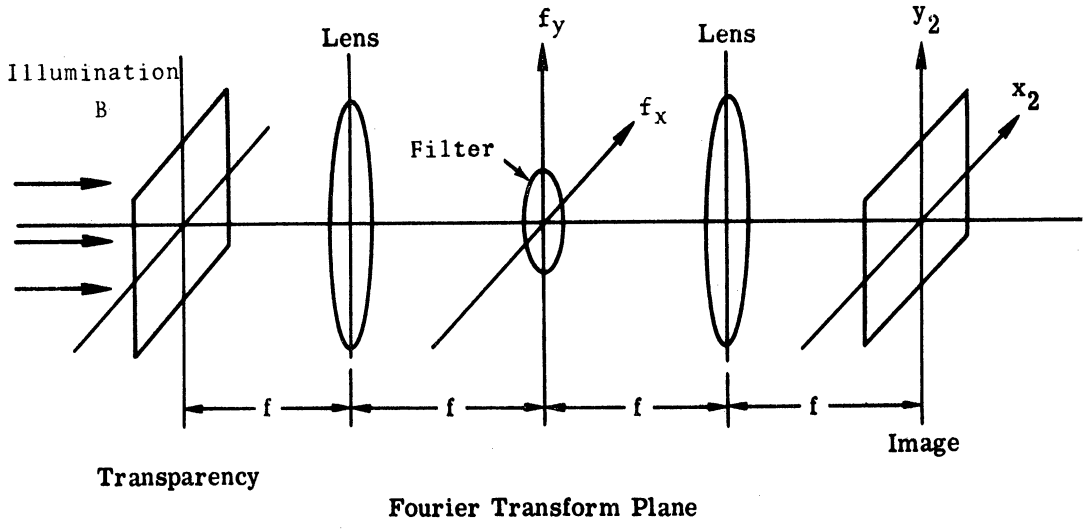

Figure 1-5. Coherent Spatial Filtering System

typical coherent spatial filtering system. In this example, a high-pass filter was created by placing a DC stop at the Fourier transform plane. The input transparency to be filtered in this example is shown in Fig. 1-6. Figure 1-7(a) shows the filtered output image when illumination B is a coherent collimated beam. It is seen that optical noise limits the output image quality. Instead of using a collimated coherent beam, consider illumination B shown in Fig. 1-8. Here a crossed 16 cycle per mm sinusoidal phase grating g_1 was used to generate 9 equal carriers. A spatially noncoherent source was created at Plane B using the technique described in Section 1.3.5. Since the DC

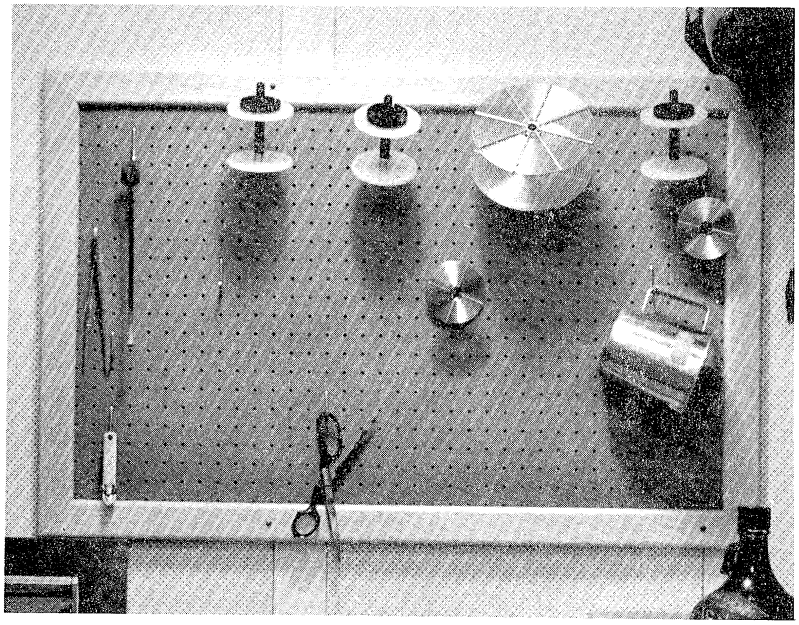

Figure 1-6. Original Transparency

component of the transparency now forms illumination

$$\sum_{n=-1}^{1} \sum_{m=-1}^{1} \operatorname{circ}\left[\frac{\sqrt{(f_x - n\Delta)^2 + (f_y - m\Delta)^2}}{R}\right]$$

consisting of an array of circular dots each with diameter 1 mm at the Fourier transform plane, an array of DC stops is now required in order to high-pass filter the input transparency. The filtered output using this illumination is shown in Fig. 1-7(b), and clearly illustrates the fact that the system with reduced spatial coherence gives superior performance.

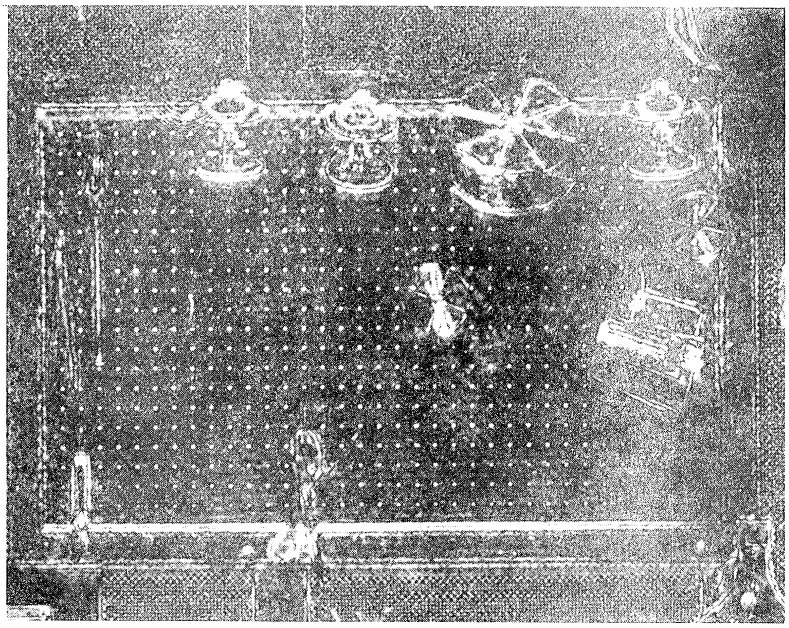

(a) Single Coherent Collimated Beam

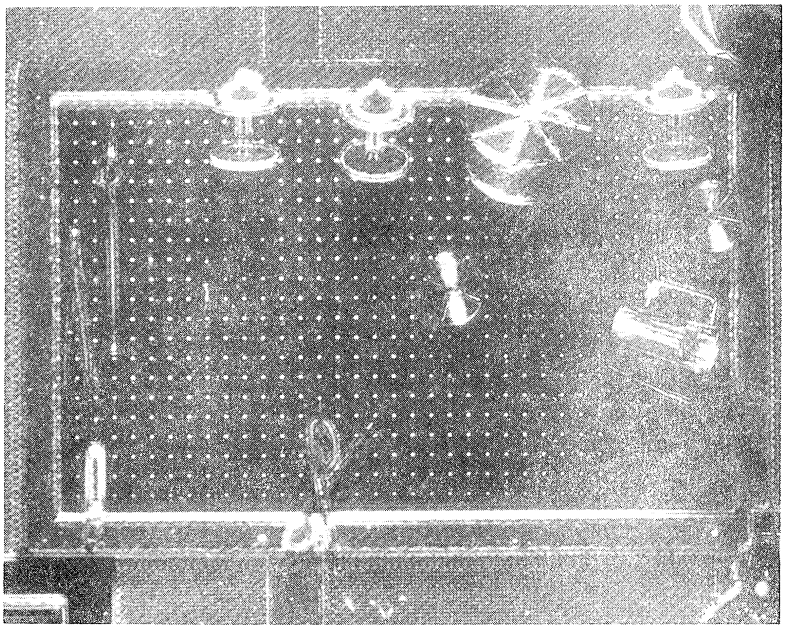

(b) An Array of Spatially Noncoherent Sources

Figure 1-7. Filtered Image

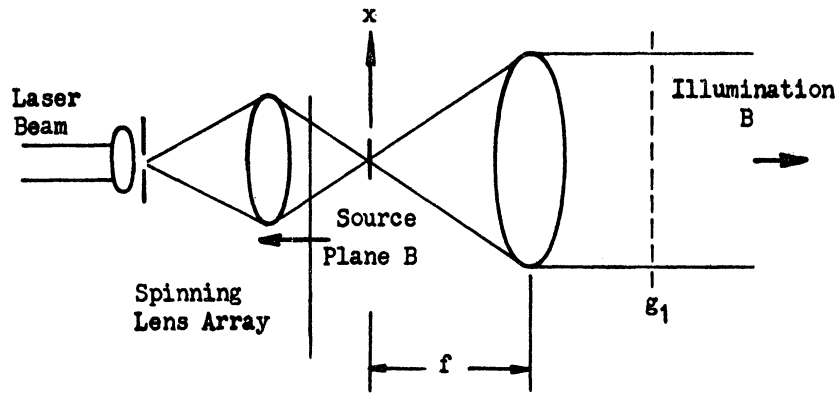

Figure 1-8. Construction of an Array of Spatially Noncoherent Sources

1.4.3. NOISE SUPPRESSION USING MOVING GRATINGS

A moving grating technique for suppressing optical noise will now be presented. This method does not reduce the resolution at the frequency plane of a spatial filtering system.

Consider Fig. 1-9 where a linear grating

$$g_1(x) = \sum_{n=-\infty}^{\infty} a_n e^{in2\pi f_o x}$$

is illuminated with a collimated beam of coherent light and is set in motion with constant velocity v in the x coordinate direction. If the temporal frequency of the beam is f_t, the n-th order plane wave generated by the grating has temporal frequency $f_t + nvf_o$. Redundancy can be introduced in an optical system such as Fig. 1-5 by using the above property to generate multiple carrier illumination B. Multicarrier illumination requires that an

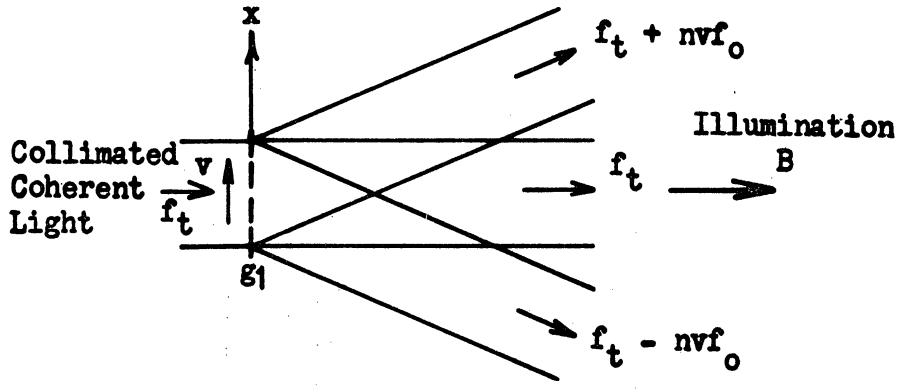

Figure 1-9. Generation of Multicarrier Illumination

array of spatial filters be placed at the Fourier transform plane of Fig. 1-5. Each carrier generated by the moving grating has a distinct temporal frequency. With the proper choice of recording parameters, it is possible to noncoherently add the output signal energies from each spatial carrier. Consider the temporal frequency difference vf_o for adjacent orders and let T equal the observation or exposure time. Then if $Tvf_o >> 1$ or Tvf_o is an integer, the output irradiance variation due to the presence of the grating is negligible since Tvf_o equals the number of cycles of translation of the grating. If more than one grating is used in tandem, care must be used to assure that each carrier has a distinct temporal frequency. A cross grating should be translated in a direction that is not parallel to the lines of the grating; a direction forming a 30 degree angle with a grating line would suffice.

Experimental results using moving grating illumination are given in Fig. 1-10. Here the filtering experiment of Section 1.4.2

was repeated using the moving grating technique. In this experiment, the spatially noncoherent source at source Plane B of Fig. 1-8 was replaced with a point source. Figure 1-10(a) shows the output of the system with a crossed phase grating stationary in the system. Figure 1-10(b) shows the same output when the gratings were translated during the exposure time. It is seen that translating the gratings removes the fringes shown in Fig. 1-10(a). By comparing Figs. 1-7(a) and 1-10(b), it is seen that although only nine carriers were employed, the moving grating method was quite effective in suppressing optical noise.

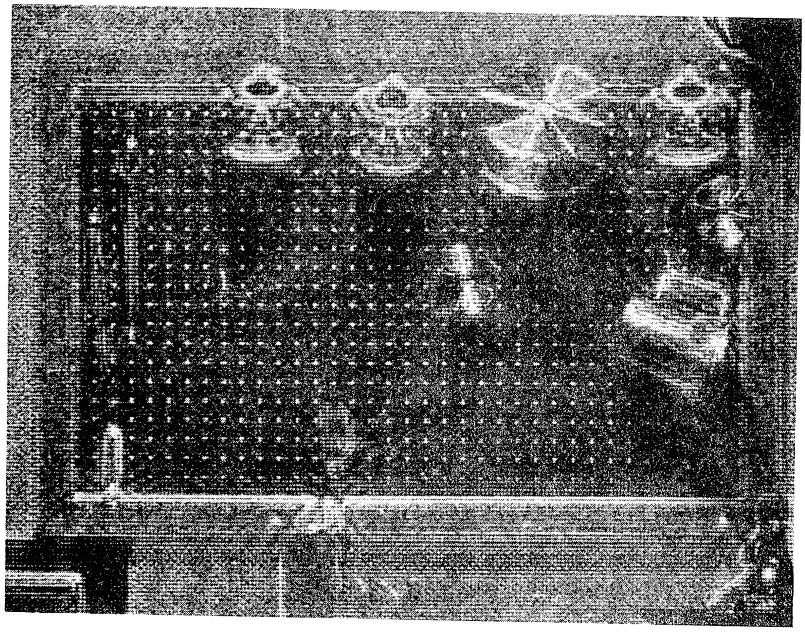

(a) Grating Stationary

Figure 1-10. Filtered Image
Using the Illumination of Fig. 1-9

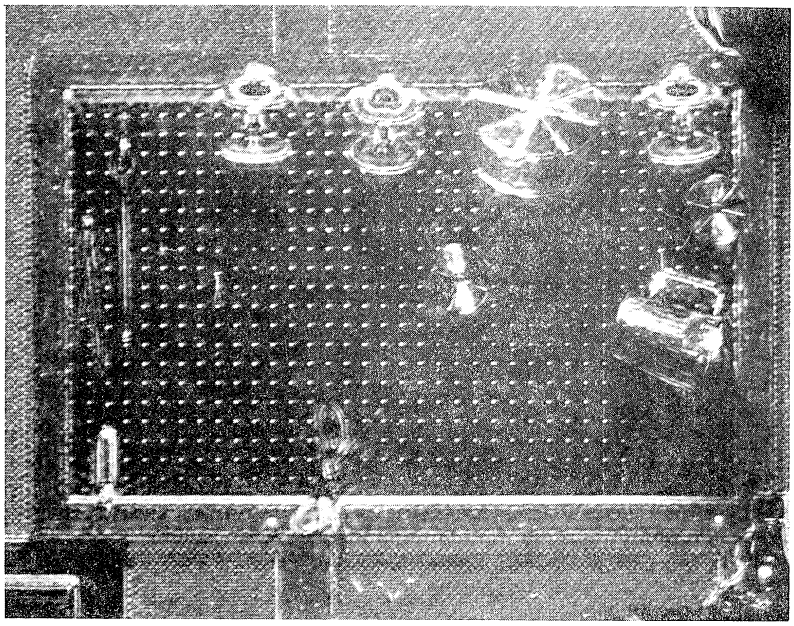

(b) Moving Grating

Figure 1-10. Filtered Image
Using the Illumination of Fig. 1-9 (continued)

Although it is permissible to use real amplitude gratings, phase gratings are more desirable to efficiently utilize the available light. The modulation provided by the moving grating technique can also be achieved by the generation of sound waves in a fluid gate to produce traveling waves which propagate across the optical channel. The moving grating technique is a simple practical means of achieving optical noise suppression. Since the gratings are translated during processing, the gratings' design requirements are reduced and the need for precise positioning of the gratings along the optical axis is usually eliminated.

The moving grating method was presented at the 1972 Fall OSA meeting [8]. Closely related work by Brandt was also presented at that meeting [9, 10].

1.5. SUMMARY

Diffuse coherent illumination has a wide spatial bandwidth with no dominant frequency components. This type of illumination makes a holographic recording redundant since any small part of the hologram can reconstruct the entire object field. This redundancy property makes a diffuse holographic recording rather insensitive to scratches and other system artifacts. Unfortunately, diffuse coherent illumination results in a multiplicative noise granularity called laser speckle. The spectral density of laser speckle has a significant low frequency contribution which limits both image quality and resolution. Mixed-integration processing can utilize excess system bandwidth to suppress speckle. The statistical speckle fluctuation is reduced by adding uncorrelated samples noncoherently. Synthetic aperture radars can use both angle and temporal diversity to obtain independent samples [3]. Temporal diversity can also be employed at optical wavelengths [11].

Optical artifact noise can be suppressed in coherent optical filtering systems by reducing the source coherence. It is thus advantageous that the source coherence not exceed the system requirements. Noncoherent techniques are permissible in coherent optical filtering systems since the output is usually square-law envelope detected. Most noise suppression techniques for such systems involve transverse displacement of the propagating signal relative to the noise scatterers together with noncoherent addition. Many of these techniques are costly and difficult to implement. Others place limits on processing speed and frequency plane resolution. A moving grating technique was presented which does not have the above limitations. This method can achieve noncoherent addition by translating a grating one grating period.

Most noncoherent noise suppression techniques are not useful for diffraction-limited holographic storage systems. The remaining chapters consider redundancy modulation for holographic systems. Mixed integration can be used to remove high frequency residual fringes which are introduced by periodic redundancy modulation. This is accomplished by using a spatially noncoherent source for image reconstruction.

2
REDUNDANCY MODULATION FOR COHERENT IMAGING SYSTEMS

2.1. INTRODUCTION

For the coherent optical processing systems considered in Chapter 1, transverse displacement of the propagating signal relative to the processing optics together with noncoherent addition was effective in suppressing optical noise. For fully coherent systems where noncoherent addition is not permitted, optical noise reduction is more difficult and special types of speckle-free redundancy modulation must be considered. In this chapter, redundancy modulation for imaging continuous-tone transparency signals will be investigated. This class of signals is especially susceptible to optical noise because a continuous-tone signal has a dominant DC frequency component. Leith and Upatnieks showed that the self-imaging characteristics of phase gratings are useful for generating diffuse speckle-free illumination, and for coherently imaging a volume [12]. This characteristic is analyzed in the next section.

2.2. THE SELF-IMAGING CHARACTERISTIC OF GRATINGS

It is well known that gratings have a self-imaging characteristic. This property is sometimes referred to as the Talbot effect [13]. Self-imaging will now be analyzed for a one-dimensional grating.

Consider the periodic grating function

$$q(x) = \sum_{n=-N}^{N} a_n e^{\frac{i2\pi nx}{X}}$$

with complex Fourier series coefficients

$$a_n = \frac{1}{X} \int_{-X/2}^{X/2} q(x)\, e^{-\frac{i2\pi nx}{X}}\, dx$$

If coherent collimated light is incident normal to the grating surface, let q(x, z) be the complex light distribution a distance z from the grating. Since q(x) is

$$q(x, 0) = \int_{-\infty}^{\infty} \hat{q}(f_x) e^{i2\pi f_x x}\, df_x$$

where f_x denotes spatial frequency, the free space transfer function $H(f_x)$ relating q(x, z) to q(x, 0) is [14]

$$H(f_x) = \text{rect}\left(\frac{\lambda f_x}{2}\right) e^{\frac{i2\pi z}{\lambda}\sqrt{1-(\lambda f_x)^2}} \qquad (2)$$

where rect(x) $\equiv$ 1 if $x \leq 1/2$

$\equiv$ 0 otherwise.

Since

$$\sqrt{1 - (\lambda f_x)^2} = 1 - \frac{1}{2}(\lambda f_x)^2 - \frac{1}{8}(\lambda f_x)^4 - \ldots, \qquad (3)$$

$H(f_x)$ becomes

$$H(f_x) = e^{\frac{i2\pi z}{\lambda}} \; e^{i2\pi z\lambda f_x^2} \; \text{rect}\left(\frac{\lambda f_x}{2}\right) \tag{4}$$

if f_x is sufficiently small. Let $f_o = 1/X$ be the fundamental frequency of the function q(x) and let $2z\lambda f_o^2 = J$. Then

$$q\left(x, \frac{J}{2\lambda f_o^2}\right) = \sum_{n=-N}^{N} a_n \, e^{iJ\pi n^2} \, e^{i2\pi n f_o x}$$

where complex constants such as $e^{\frac{i2\pi z}{\lambda}}$ are ignored. If J = 1, q(x, z) becomes

$$q\left(x, \frac{1}{2\lambda f_o^2}\right) = \sum_{n=-N}^{N} a_n \, e^{i2\pi n f_o\left(x+\frac{1}{2f_o}\right)}$$

$$= q\left(x + \frac{X}{2}, 0\right)$$

Thus q(x, 0) has a self-imaging distance

$$L = \frac{1}{2\lambda f_o^2}$$

where the same diffraction pattern forms, but is shifted transversely a distance X/2 which is one-half the period of q. From Eq. (3) the self-imaging property requires that the approximate inequality

$$\frac{2\pi z}{\lambda}\left[\frac{\lambda(Nf_o)}{8}\right]^4 < \frac{\pi}{20}$$

or

$$z < \frac{1}{5\lambda^3(Nf_o)^4}$$

be satisfied. If the bandwidth BW equals $2Nf_o$, the above inequality becomes

$$z < \frac{16}{5\lambda^3 (BW)^4}$$

The approximate number of self-imaging planes is thus $0.4\left(\lambda^2 f_o^2 N^4\right)^{-1}$. For a grating with a 100 cycle per millimeter bandwidth and a 0.1 millimeter period, the number of self-imaging planes is approximately 16 if λ equals 0.6328 microns. In practice, the flatness and uniformity of a grating often limit the number of image planes. Equation (4) can be used to determine the approximate focus sensitivity of self-imaging planes. A self-imaging plane is in focus if

$$2\pi \left| \Delta z \right| \lambda \left(Nf_o \right)^2 < 0.05\ \pi$$

or

$$\left| \Delta z \right| < \frac{0.05}{N^2} L$$

where the self-imaging distance L equals $\left(2\lambda f_o^2\right)^{-1}$. In terms of the bandwidth

$$BW = 2Nf_o$$

this inequality becomes

$$\left| \Delta z \right| < \frac{1}{10\ \lambda (BW)^2}$$

This is comparable with the approximate focal tolerance,

$$\Delta z = \pm \frac{1}{2\lambda(BW)^2} \qquad \text{where } BW = \frac{1}{\lambda(\text{F-number})}$$

given for a point target in Ref. [15]. A computer program was written which uses Eq. (2) to calculate $\left|q(x, z)\right|^2$ given

$$q(x, 0) = \sum_{n=-N}^{N} a_n e^{i2\pi n f_o x}$$

and z. The program can be used to determine the characteristics of a particular function q without using the above approximations.

2.3. OPTICAL NOISE SUPPRESSION USING GRATINGS

Leith and Upatnieks considered the problem of coherently imaging a three-dimensional object s(x, y, z) such as a transparent volume with various scattering centers; where the goal was to image a desired plane of the object without incurring the noise due to the scattering points of other planes or system artifacts [12]. They formulated criteria for image improvement and demonstrated how the self-imaging characteristic of gratings can be used to suppress the effects of system noise occurring throughout the system.

Consider the optical system in Fig. 2-1. If redundancy modulation were introduced by placing a mask with complex amplitude transmittance q(x) against s(x) at Plane B, noise introduced by system artifacts between Planes B and C could be suppressed. However, this would have no effect on noise effects from artifacts to the left of Plane B. A periodic mask with some

desirable complex amplitude transmittance q(x) can be placed at Plane A, and Plane B can be a self-imaging plane of the grating. Now noise effects due to grating defects and system artifacts occurring both to the left and right of Plane B can be attenuated. Leith and Upatnieks demonstrated that quasidiffusers such as phase gratings offered an improvement over imagery formed when the illumination is produced by an ordinary diffuser such as ground glass [12, 16].

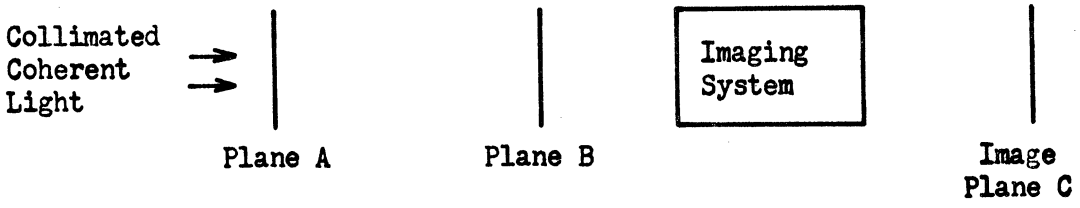

Figure 2-1. Coherent Imaging System

The results of an experiment which utilizes the self-imaging characteristics of phase gratings for optical noise suppression are now presented. The bandlimited coherent imaging system shown in Fig. 2-1 was used to image a continuous-tone transparency. Sinusoidal crossed phase gratings generated the redundancy modulation function

$$q(x, y) = \left(\sum_{n=-1}^{1} a_n e^{inw_o x} \right) \left(\sum_{n=-1}^{1} a_n e^{inw_o y} \right)$$

where $f_o = \frac{w_o}{2\pi}$ and $\{a_n\}_{n=-1}^{1} = \{i, 1, i\}$. The bandwidth of the system was $4f_o - \epsilon$ for each of the Cartesian coordinates x

y at the image Plane C. The positive constant ϵ was just large enough to block the second order terms of the phase grating. Figure 2-2 shows the image with no redundancy modulation present. Note the dark artifact diffraction pattern beneath the spool in the upper right hand corner. Figure 2-3 shows the speckle pattern introduced at the image plane if ground glass is placed at Plane A. Figure 2-4 shows that only high frequency speckle results if the crossed phase grating is placed at Plane A and signal Plane B is a self-imaging plane. The diffuser noise resulting from the redundancy modulation is seen to limit the image resolution. Figures 2-1, 2-2, and 2-3 show that by carefully choosing the redundancy modulation, optical noise can be suppressed without introducing low frequency laser speckle.

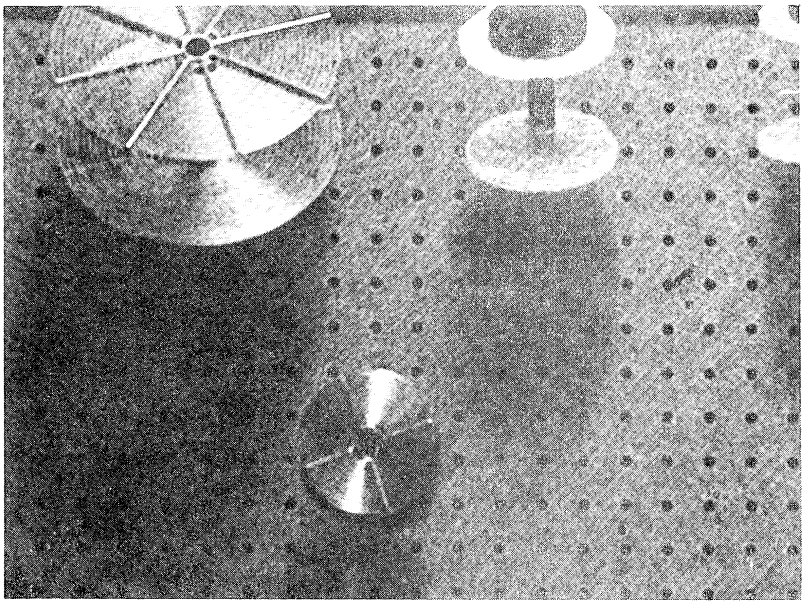

Figure 2-2. Image Plane C without Redundancy

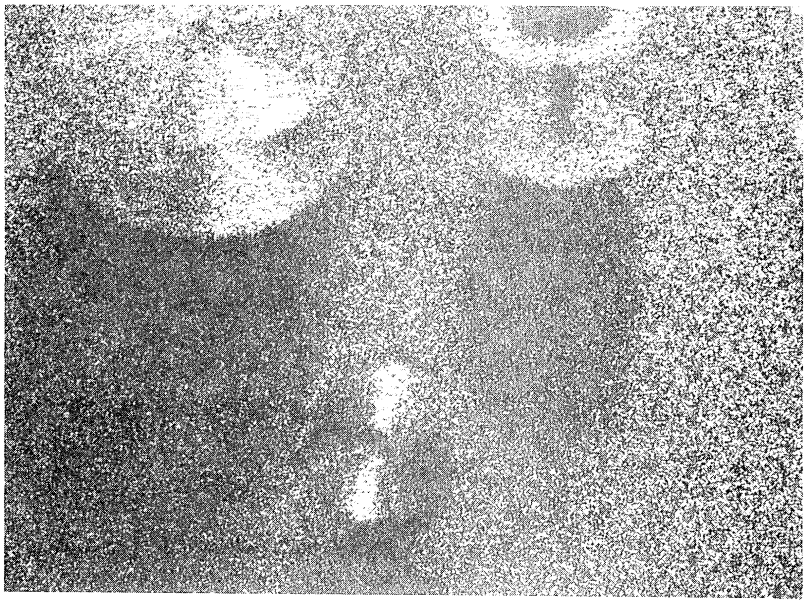

Figure 2-3. Image with Ground Glass Illumination

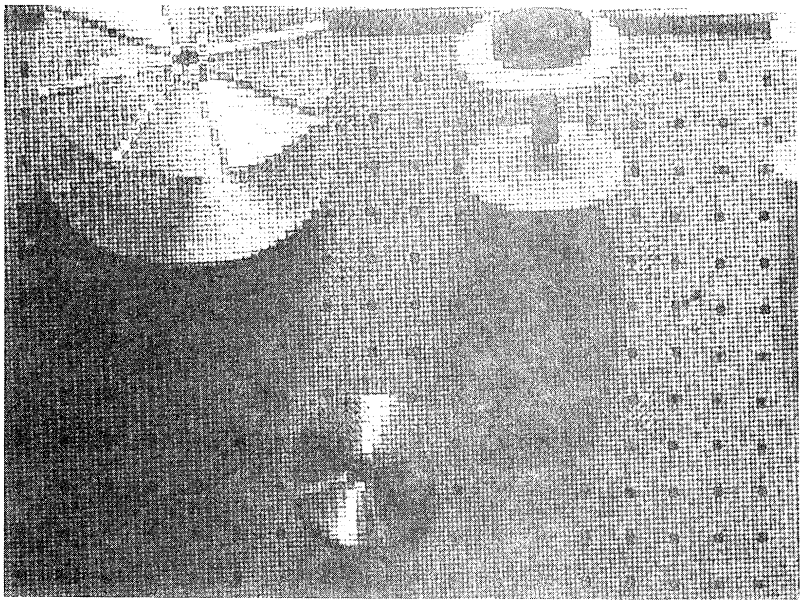

Figure 2-4. Image with Phase Grating q(x, y)

Although the self-imaging characteristic of gratings provides a convenient means of generating redundancy illumination, it is not absolutely required. If redundancy modulation with the proper characteristics is generated by a complex mask at the plane of the mask, the far field of a point source created with a lens pinhole assembly can provide a clean beam for illuminating the mask. In order to achieve a more compact system, a hologram of the above illumination can be made using a point source reference beam. If the hologram to mask distance is not too small, the quality of the illumination reconstructed by the hologram will not be sensitive to scratches and other artifacts on the hologram surface. Thus many holograms for generating redundancy modulation can be made from one high quality, extremely clean phase grating.

2.4. CONSTRAINTS FOR REDUNDANCY MODULATION

Constraints for redundancy modulation will now be specified and certain types of complex modulation will be considered which satisfy these constraints. Let $q(x)s(x)$ be the complex input signal amplitude for a bandlimited coherent imaging system where $s(x)$ is the amplitude transmittance of a continuous-tone transparency and $q(x)$ represents complex modulation used to increase the spatial bandwidth of the transparency. Suppose $h(x) = \text{sinc}(Wx)$ is the impulse response of the system, where $\text{sinc}(x)$ denotes $\frac{\sin(\pi x)}{\pi x}$. Then the frequency transfer function $\hat{h}(f_x) = FT\{h(x)\}$ of the system is rect (f_x/W), where $FT\{\cdot\}$ denotes the Fourier transform operation. In order to achieve high resolution and adequate image quality, it is necessary that the output image irradiance

$$\left| [q(x)s(x)] * h(x) \right|^2$$

be free of low frequency speckle. Since s(x) has a dominant DC frequency component, it is only necessary to place constraints on $\left| q(x) * h(x) \right|^2$ to satisfy this condition.

Suppose $g_I(x)$ is the impulse response of a low-pass irradiance filter and consider

$$J(x) = \left| q(x) * h(x) \right|^2 * g_I(x)$$

with mean m and variance σ^2. Then if the image is to be free of low frequency speckle, Condition (A) below must be satisfied.

$$\frac{m^2}{\sigma^2} \geq C_1 \qquad \text{(A)}$$

where C_1 represents some minimum signal-to-noise ratio. For best resolution, $g_I(x)$ must equal the Dirac delta function $\delta(x)$. When q(x) represents diffuse illumination from fine ground glass and $g_I(x)$ equals rect $\left[x/(Q/W)\right]$, $m^2/\sigma^2 \approx Q$ for $Q >> 1$ [2]. For a two-dimensional system, Condition (A) requires that the linear resolution be $\sqrt{\frac{C_1}{W}}$. Although plane wave illumination

$$q(x) = e^{iwx}$$

satisfies Condition (A), large dust diffraction patterns are superimposed on the reconstructed image when q(x)s(x) has a dominant frequency component. Therefore, a second condition must be established to assure that high redundancy and thus adequate noise suppression is obtained.

There are two mechanisms which improve image quality when optical noise occurs. The law of conservation of energy predicts

that dispersion of the noise diffraction patterns uniformly over the image space will improve the local signal to noise ratio S/N. Here, S/N is defined as the space average image irradiance to the change in the average signal irradiance for a local region of the image. A second mechanism is to demagnify or increase the spatial bandwidth of the noise diffraction pattern irradiance distribution. This decreases the area of the image affected by optical noise and helps preserve low frequency image detail. High frequency detail has appreciable bandwidth and is less susceptible to optical defects, but can be obscurred if the average irradiance in a local region is too low. It will become evident when quadratic phase modulation is considered that although dust diffraction patterns can be demagnified, their size cannot approach the optical system resolution. For this reason the principal mechanism for optical noise suppression is dispersion. In order for optical noise to be dispersed evenly over as large an image area as possible, it is necessary to establish certain uniformity conditions for the spectral density of q. Let

$$S(f_x, V, x_o) = \left| FT\left\{ \text{rect}\left(\frac{x - x_o}{V}\right) q(x - x_o) \right\} \right|^2$$

where V represents the width of an elementary element of q. Condition (B) requires that

$$\text{Envelope of } S(f_x, V, x_o) \approx \text{rect}\,(f_x/W) \qquad \text{(B)}$$

or that the parameter

$$G_\alpha = \frac{\int_{W/2}^{W/2} S(f_x, V, x_o)\, df_x}{\max_{\text{over } f_c} \int_{\frac{\alpha W}{2}}^{\frac{\alpha W}{2}} S(f_x - f_c, V, x_o)\, df_x}$$

be large for all x_o where $\alpha < 1$ and $V \leq L$. The constant WL is a system design parameter which is determined by certain system constraints. In general, L is dependent on the size and position of artifacts and the function q(x).

If q(x) is periodic with period X and L/X is greater than three or four, then Condition (B) is satisfied if

$$\text{Envelope of } \left| \text{FT} \{q(x)\} \right|^2 = \text{rect}\,(f_x/W)$$

If X exceeds a certain upper bound, optical noise will not be dispersed uniformly at the image plane. If q(x) is periodic and a system artifact is several times larger than the period X, the noise diffraction pattern will be multiply imaged with unity magnification at the image plane. If the main lobes of the multiple noise diffraction patterns do not overlap, dispersion and thus attenuation of the noise is assured. In Chapter 3 it will be shown that if a dust particle is in the far field relative to the image plane, overlap will not occur if X is smaller than the diameter of the dust particle. When many coherent overlapping patterns are formed, one cannot always be assured that even dispersion of the optical noise will occur. Careful examination of Fig. 2-4 shows that optical noise introduces fringes at the image plane with the same periodicity as q(x). This property also makes it desirable to limit the size of X.

2.5. QUADRATIC PHASE MODULATION

2.5.1. CHARACTERISTICS

A class of phase modulation will now be considered which under certain conditions has a rather uniform, bandlimited power spectrum, and thus appears to satisfy Conditions (A) and (B). A logical function q(x) to consider is a train of quadratic phase signals,

$$q_{A\pm}(x) = \left[e^{\pm i \frac{\pi x^2}{\lambda X F}} \text{ rect } (x/X) \right] * \sum_{n=-\infty}^{\infty} \delta(x - nX) \qquad (5)$$

where δ denotes the Dirac delta function. The phase P(x) for $q_{A-}(x) = e^{iP(x)}$ is shown in Fig. 2-5. It is well known that such a signal has a bandlimited uniform spectral density if the space bandwidth parameter $Q = X/(\lambda F) >> 10$ [17, 18]. If the maximum phase variation $(\pi Q)/4$ is not too large, the modulation $q_A(x)$ can be realized using a fly's eye lens array consisting of a train of positive or negative lenslets. It will be seen that it is advantageous to remove the discontinuity of $\frac{dP(x)}{dx}$ where the lenslets join by defining a new function

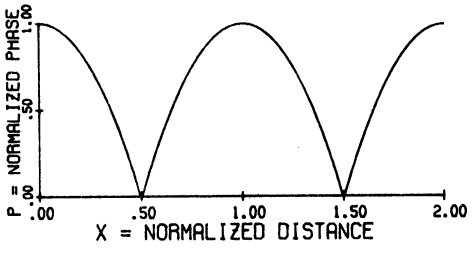

Figure 2-5. Phase for $q_{A-}(x)$

$$q_B(x) = \left[e^{\frac{i\pi Q}{4}} e^{-i\frac{\pi x^2}{\lambda XF}} \text{rect}\,(x/X) \right.$$

$$\left. + e^{-i\frac{\pi Q}{4}} e^{i\frac{\pi(x - X)^2}{\lambda XF}} \text{rect}\left(\frac{x - X}{X}\right) \right] * \sum_{n=-\infty}^{\infty} \delta(x - 2nX)$$

with alternating positive and negative lenslets as shown in Fig. 2-6.

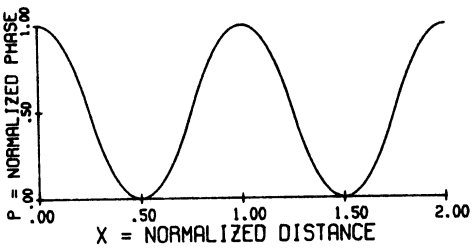

Figure 2-6. Phase for $q_B(x)$

Let $\hat{q}_{A-}(n/X)$ be the n-th complex Fourier series coefficient for $q_{A-}(x)$ if q_{A-} is periodic with period X. Figure 2-7 shows the dependence of $\left|\hat{q}_A(n/X)\right|^2$ and $\left|\text{FT}\{\text{rect}\,(x/X)q_A(x)\}\right|^2$ on Q.

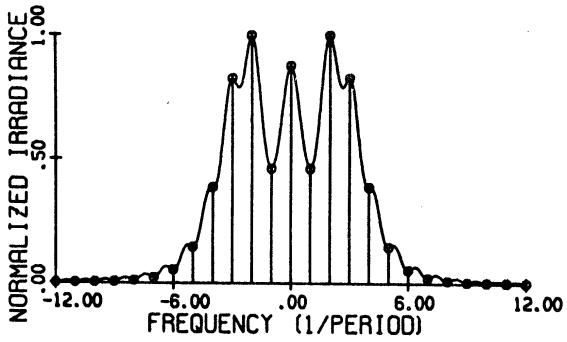

(a) Q = 10

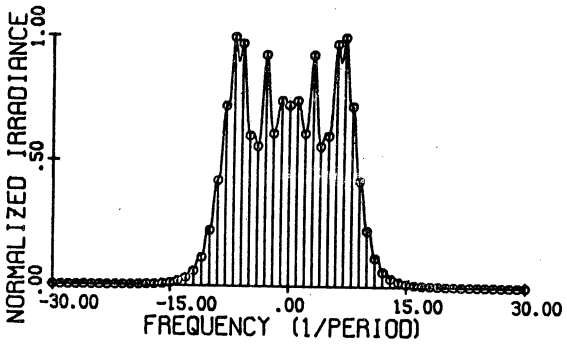

(b) Q = 21

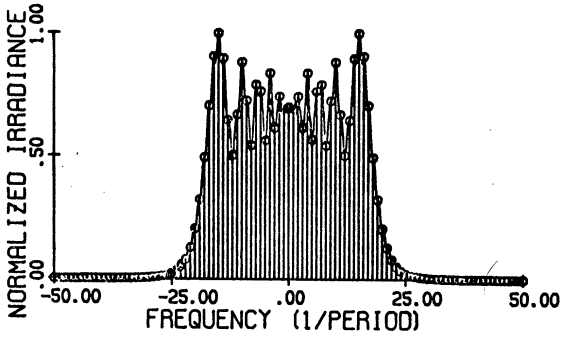

(c) Q = 41

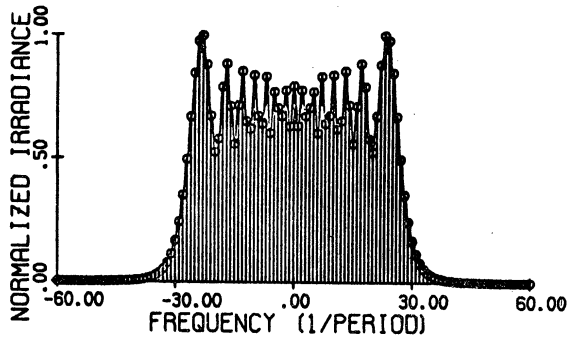

(d) Q = 60

Figure 2-7. Spectral Density of $q_A(x)$

The function $\hat{q}_{A-}(n/X)$ can be expressed in terms of Fresnel integrals. Let $L = -\sqrt{Q/2} + n\sqrt{2/Q}$ where $Q = X/(\lambda F)$ and define

$$x_L = \frac{\pi}{2}\left[\frac{Q}{2} + \frac{2n^2}{Q} - 2n\right]$$

and

$$x_U = \frac{\pi}{2}\left[\frac{Q}{2} + \frac{2n^2}{Q} + 2n\right]$$

Using the Fresnel integrals

$$C(x) = \int_0^{\sqrt{\frac{2}{\pi}x}} \cos\left(\frac{\pi}{2}u^2\right) du$$

and

$$S(x) = \int_0^{\sqrt{\frac{2}{\pi}x}} \sin\left(\frac{\pi}{2}u^2\right) du$$

$\hat{q}_{A-}(n/X)$ becomes

$$\hat{q}_{A-}(n/X) = \frac{Q^{-1/2}}{\sqrt{2}} e^{i\frac{\pi n^2}{Q}} f(x_U, x_L)$$

where $f(x_U, x_L) = [C(x_U) + C(x_L)] - i[S(x_U) + S(x_L)]$ if $L \leq 0$

and $f(x_U, x_L) = [C(x_U) - C(x_L)] - i[S(x_U) - S(x_L)]$ if $L \geq 0$

By taking the Fourier transform of the first convolution term in Eq. (5) and noting that the form is similar to Fraunhofer diffraction of a sinc function if $Q >> 10$, the envelope rect $(\lambda F f_x)$ is obtained for $\hat{q}_A(f_x)$. This implies that q_A has Q dominant orders when Q is very large. For negative lenslets $\hat{q}_{A+}(n/X) = \hat{q}_{A-}^*(n/X)$ since

q_A is even. If $\hat{q}_B(n/2X)$ represents the n-th complex Fourier series coefficient of $q_B(x)$, it can easily be shown using superposition that

$$\hat{q}_B(n/2X) = 2\ \mathrm{Re}\left\{e^{i\frac{\pi Q}{4}}\hat{q}_{A-}(n/2X)\right\} \quad \text{if n is even and}$$

$$= 2\ \mathrm{Im}\left\{e^{i\frac{\pi Q}{4}}\hat{q}_{A-}(n/2X)\right\} \quad \text{if n is odd.}$$

Re and Im denote the real and imaginary parts respectively of a complex number. Although Fig. 2-7 shows that $\left|\hat{q}_A(n/2X)\right|^2$ is almost constant for $|n| < Q$ when $Q >> 10$, it is not clear that $\left|\hat{q}_B(n/2X)\right|^2$ has this same property. It is clear that $\left|\hat{q}_B(n/2X)\right|^2 \le 4\left|\hat{q}_A(n/2X)\right|^2$ and this indicates that $\hat{q}_B$ may have a sharper cutoff than $\hat{q}_A$. As discussed earlier, the bandwidth of q_A and q_B is approximately Q/X if Q is large. In order to satisfy Condition (A), it is necessary that the bandwidth of the optical system exceed Q/X. Since q_A and q_B have periods of X and 2X respectively, the maximum number of dominant orders for $Q >> 10$ is approximately Q and 2Q respectively. In order to consider the spectral density uniformity of q_A and q_B, it is helpful to define the redundancy parameter

$$R_M \equiv \frac{\sum_{n=-N}^{N} |a_n|^2}{\max_n \left(\sum_{j=1}^{M} |a_{n+j}|^2\right)}$$

for periodic bandlimited functions $q(x) = \sum_{n=-N}^{N} a_n e^{in2\pi f_o x}$ with

bandwidth $2Nf_o$. The parameter R_M is directly related to G_α of Condition (B) by the equation $R_M = G_{M-1}$. Since the optical system must pass almost all the light diffracted by q_A or q_B if Condition (A) is to be satisfied, it is convenient to set N equal to infinity in order to remove the dependence of R_M on the system bandwidth. The parameter R_M thus becomes $\left[\max_n \left(\sum_{j=1}^{M} |a_{n+j}|^2 \right)\right]^{-1}$ since $\sum_{n=-\infty}^{\infty} |a_n|^2$ equals unity. Figure 2-8 shows R_M versus Q for q_A. Note that R_M must be bounded above by Q/M for Q >> 10, since q_A has Q dominant Fourier series coefficients.

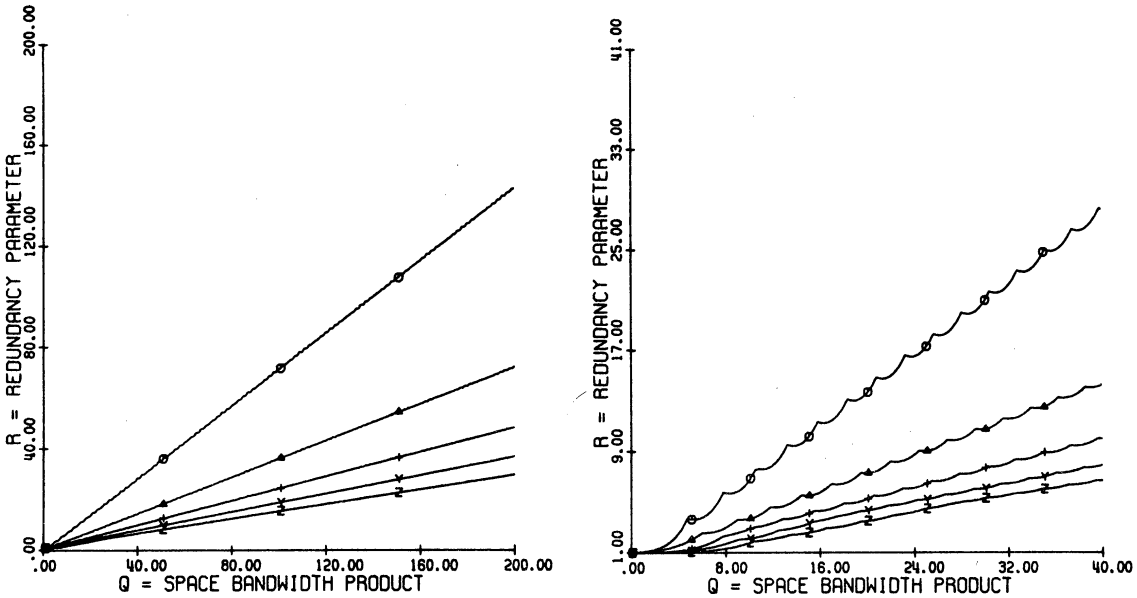

(a) (b)

Figure 2-8. Redundancy Characteristics for $q_A(x)$
The Symbols 0, Δ, +, Y, Z denote R_1, R_2, ... R_5 Respectively

Figure 2-9 shows R_M versus Q for $q_B(x)$. Since the period of q_B is 2X, R_M is now bounded above by the quantity (2Q)/M. To compare the redundancy characteristics of q_A and q_B, R_M of Fig. 2-8 should be compared with R_{2M} of Fig. 2-9. Figures 2-8 and 2-9 indicate that q_A and q_B both have rather uniform spectral densities for $Q >> 10$. Although q_A appears to have better spectral characteristics, it will be seen that q_B results in a much higher signal to noise ratio m^2/σ^2 (Condition A).

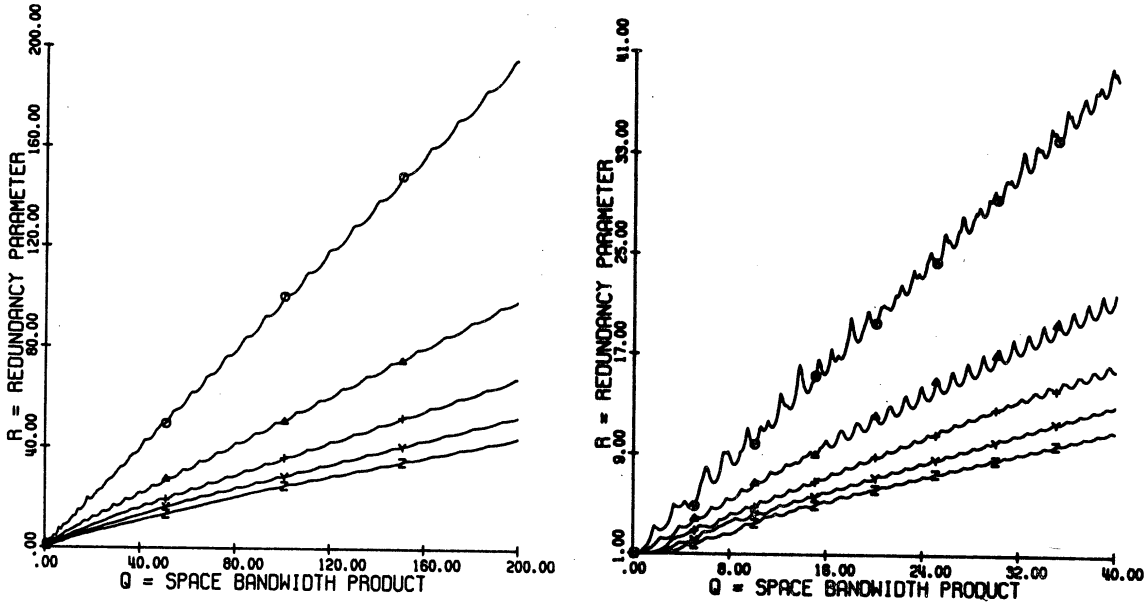

(a) (b)

Figure 2-9. Redundancy Characteristics for $q_B(x)$
The Symbols, 0, Δ, +, Y, Z denote R_1, R_2, ... R_5 Respectively

Condition (A) requires that the speckle noise from q be low. Let $\hat{h}(f_x) = \text{rect}\left(\frac{f_x X}{BQ}\right)$ be the frequency transfer function of the coherent system where $B \geq 1$. In order to achieve the best redundancy in the available system bandwidth

$$W = \frac{BQ}{X}$$

B should be almost unity. However, B must be greater than unity if m^2/σ^2 of Condition (A) is to be sufficiently high. A digital computer was used to examine

$$J(x) = |q(x) * h(x)|^2 * g_I(x)$$

of Condition (A) as a function of Q, W and the width of $g_I(x)$. Let

$$g_I(x) = \text{rect}\left[\frac{x}{\frac{A}{B}(X/Q)}\right]$$

This filtering operation is easily attained if a spatially noncoherent reference source is used to reconstruct a hologram. If A is greater than two, the filter g_I approximately increases the coherent resolution cell width by the factor A. Tables 2-1 and 2-2 give the characteristics of J(x) when q(x) equals q_A and q_B respectively. The variables given in these Tables are defined below.

m^2/σ^2 = the signal to noise ratio defined by Condition (A)

$M = 100\ \frac{\max\{J(x)\} - \min\{J(x)\}}{\max\{J(x)\}}$ and represents irradiance modulation due to speckle noise

$$R_M = \frac{\sum_{n=-N}^{N} |a_n|^2}{\max_n \left(\sum_{j=1}^{M} |a_{n+j}|^2 \right)}$$ where 2N+1 represents the total number of orders within the bandpass of the system

$E_s = 100 \sum_{n=-N}^{N} |a_n|^2$ and represents the percent of the light energy within the system bandpass

$W = (BQ)/X$ is the system bandwidth and equals $(2N)/X$ for q_A and N/X for q_B.

Table 2-1. Characteristics of J(x) and R_M for $q_A(x)$

Entry	Q	B	A	m^2/σ^2	M	E_s	R_1	R_2	R_4	R_6	2N+1
A	6.78	1.77	0	6.85	30.27	99.604	4.29	2.60			13
B	6.78	1.77	1	12.76	15.72						
C	10.	1.	0	2.43	67.33	97.052	6.53	3.57			11
D	10.	1.2	0	3.33	54.53	98.645	6.63	3.63			13
E	10.	1.4	0	4.37	44.27	99.288	6.68	3.65			15
F	10.	1.4	1	8.14	23.16						
G	10.	1.4	2	32.71	18.43						
H	10.	2.	0	7.88	26.92	99.825	6.72	3.67	2.12		21
I	20.	1.	0	1.79	78.1	97.321	13.25	7.09	4.20		21
J	20.	1.2	0	2.71	62.41	99.05	13.48	7.22	4.28		25
K	20.	1.4	0	3.76	49.65	99.566	13.55	7.26	4.30		29
L	20.	1.4	1	6.72	26.46						
M	20.	1.4	2	22.09	19.26						
N	20.	2.	0	7.31	27.74	99.914	13.60	7.28	4.32	2.95	41
O	20.	3.	0	14.61	16.04	99.994	13.61	7.29	4.32	2.95	61
P	20.	3.	1	24.85	8.96						
Q	40.	1.	0	1.43	85.06	97.738	27.73	13.96	7.71	5.83	41

Table 2-1. Characteristics of J(x) and R_M for $q_A(x)$ (continued)

Entry	Q	B	A	m^2/σ^2	M	E_s	R_1	R_2	R_4	R_6	2N+1
R	40.	1.2	0	2.40	66.94	99.405	28.21	14.19	7.84	5.93	49
S	40.	1.4	0	3.51	52.62	99.757	28.31	14.24	7.87	5.95	57
T	40.	2.	0	7.13	28.60	99.956	28.36	14.27	7.88	5.97	81
U	50.	1.	0	1.34	86.71	99.883	34.22	17.74	9.57	7.08	51
V	50.	1.2	0	2.33	67.89	99.499	34.79	18.03	9.73	7.20	59
W	50.	1.2	1	4.10	34.48						
X	50.	2.	0	7.10	28.82	99.964	34.95	18.12	9.77	7.23	101
Y	50.	2.	2	55.18	12.09						
AA	10.	3.	0	15.07	15.52						31
AB	10.	4.	0	23.73	9.87						41
AC	10.	6.	0	42.88	5.08						61
AD	10.	8.	0	63.93	3.18						81
AE	9.23	1.082	0	2.81	60.49	97.849	5.84	3.53			11
AF	9.23	1.082	1	5.21	34.75						11
AG	9.23	1.082	2	15.77	25.24						11
AH	9.23	1.30	0	3.81	48.03	98.973	5.91	3.57			13
AI	9.23	1.30	1	7.07	25.77						13
AJ	9.23	1.30	2	26.09	20.14						13

Table 2-2. Characteristics of J(x) and R_M for $q_B(x)$

Entry	Q	B	A	m^2/σ^2	M	E_s	R_2	R_4	R_8	R_{12}	$N+\frac{1}{2}$
A	10.	1.	0	3.08	51.21	98.379	6.42	4.12			10.5
B	10.	1.2	0	7.56	23.46	99.749	6.51	4.18			12.5
C	10.	1.4	0	17.92	10.59	99.954	6.53	4.19			14.5
D	19.	1.4	1	25.16	9.66						
E	10.	1.4	2	56.50	6.66						
F	10.	2.	0	116.89	2.62	99.998	6.53	4.19	2.31		20.5
G	20.	1.	0	2.42	53.30	98.661	12.05	6.99	4.29		20.5
H	20.	1.2	0	8.57	18.82	99.901	12.20	7.08	4.34	3.05	24.5
I	20.	1.4	0	26.24	7.22	99.988	12.21	7.09	4.34	3.05	28.5
J	20.	1.4	1	35.16	6.59						
K	20.	1.4	2	71.26	4.80						
L	20.	2.	0	224.92	1.40	99.9991	12.22	7.09	4.34	3.05	40.5
M	40.	1.	0	2.10	53.61	98.948	21.66	12.80	8.21	5.68	40.5
N	40.	1.2	0	12.57	12.91	99.971	21.88	12.93	8.30	5.74	48.5
O	40.	1.4	0	52.14	4.30	99.998	21.89	12.93	8.30	5.74	56.5
P	50	1.	0	2.10	54.69	99.04	25.96	15.80	9.73	7.13	50.5
Q	50.	1.2	0	15.28	11.25	99.990	26.20	15.95	9.82	7.19	60.5
R	50.	1.2	1	19.34	10.65						

The functions q_A and q_B can be compared in Tables 2-1 and 2-2 for identical values of Q. Since the period of q_B is 2X and the period of q_A is X, R_M should be compared with R_{2M} in Tables 2-1 and 2-2, respectively. Note that R_M is bounded above by (2N+1)/M. The function q_B has a much higher value of m^2/σ^2 than q_A if entries with the same Q, B, and A values are compared. Figures 2-10(a) and 2-11(a) show $J(x)/\max[J(x)]$ for entries V and Q in Tables 2-1 and 2-2, respectively. By comparing Figs. 2-10 and 2-11 with Figs. 2-5 and 2-6, it is seen that the principal place where diffuser noise occurs is the point at which lenslets join. Since $\frac{dP(x)}{dx}$ for q_B is continuous, Fig. 2-11 shows less speckle noise than Fig. 2-10.

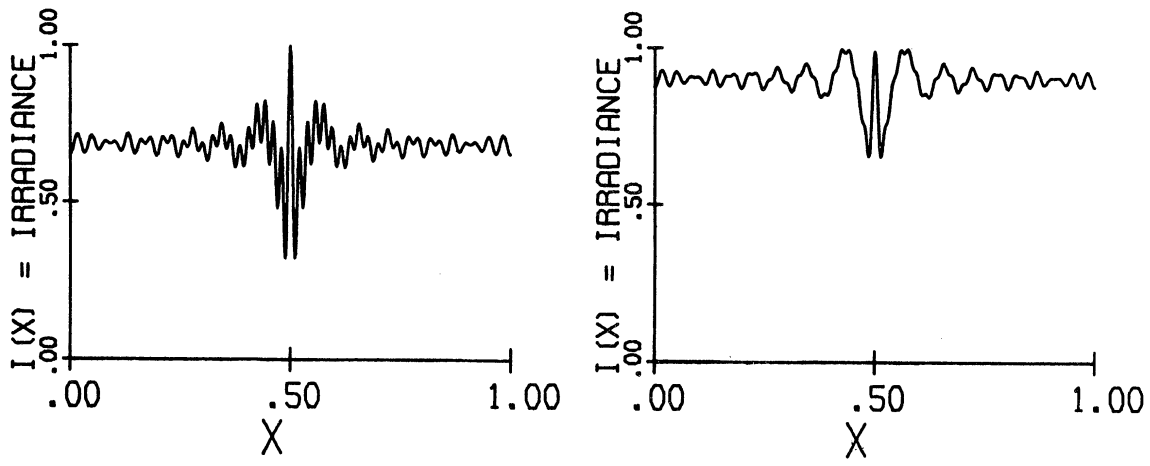

(a) (b)

Figure 2-10. (a) $I(x) = J(x)/\max\{J(x)\}$ for Entry V of Table 2-1, (b) I(x) for Entry W of Table 2-1

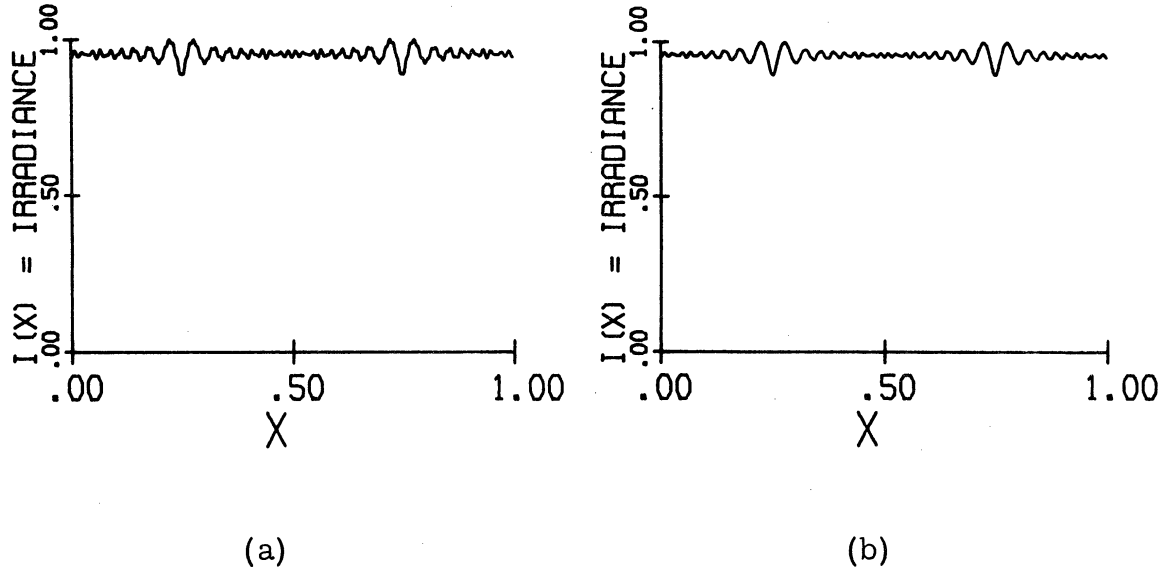

(a) (b)

Figure 2-11. (a) $I(x) = J(x)/\max\{J(x)\}$ for Entry Q of Table 2-2, (b) I(x) for Entry R of Table 2-2

For constant m^2/σ^2, Tables 2-1 and 2-2 show that q_B has better spectral density uniformity and thus higher redundancy. The redundancy properties of q_B are excellent for $Q >> 10$, since A and B are held constant, m^2/σ^2 increases rapidly as Q increases.

2.5.2. EXPERIMENTAL RESULTS

Experiments were performed which show the noise reduction characteristics of q_B in a coherent imaging system. Figure 2-12 shows a coherent imaging system where the function $q_B(y_1)$ was used to introduce redundancy along the y_1 coordinate; X, Q, and λ for $q_B(y_1)$ have values 0.5 mm, 142 and 0.6328 μ respectively. Since there exists no redundancy along the x_1 signal coordinate, two wires placed in Plane A parallel to the y_2 axis introduce dark diffraction patterns at the image plane as shown in Fig. 2-13(a). The maximum number of cycles per mm of the signal bar pattern is 7. However, when the two wires are placed parallel to the x_2

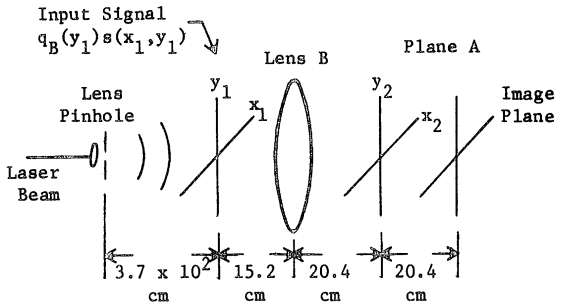

Figure 2-12. Coherent Imaging System, where Lens B has a Focal Length of 100 mm and a F-Number of 2.3. Two Wires each 0.23 mm in Diameter were Introduced at Plane A

axis, the wire diffraction patterns are highly attenuated as shown in Fig. 2-13(b). Figure 2-14 shows the irradiance at the back focal plane of Lens B. The function $q_B(y_1)$ had a spatial bandwidth of 284 cycles per mm.

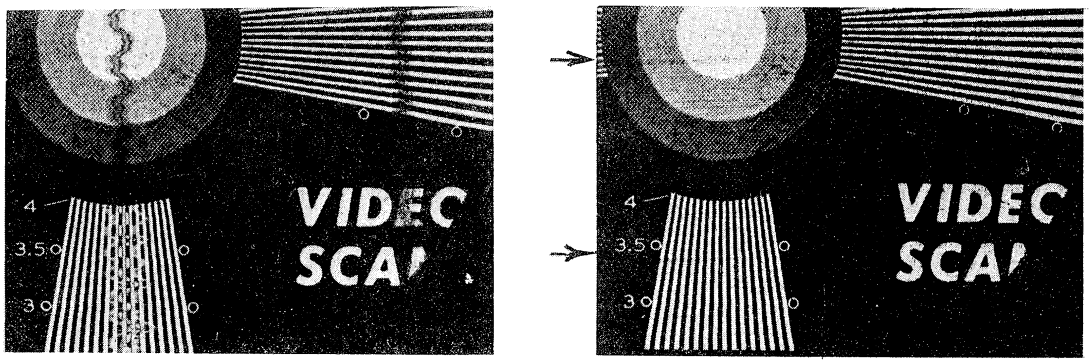

(a) (b)

Figure 2-13. (a) Image with Vertical Wires at Plane A of Fig. 2-12, (b) Image with Two Horizontal Wires at Plane A, whose Vertical Positions are Indicated with Arrows

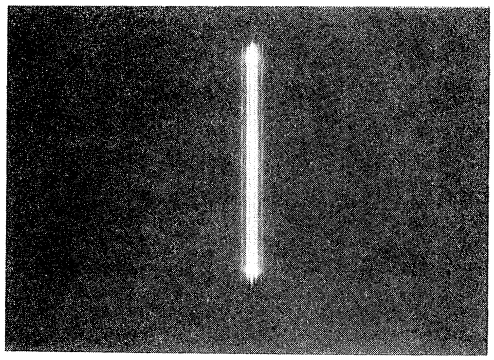

Figure 2-14. Irradiance Near the Back Focal Plane of Lens B

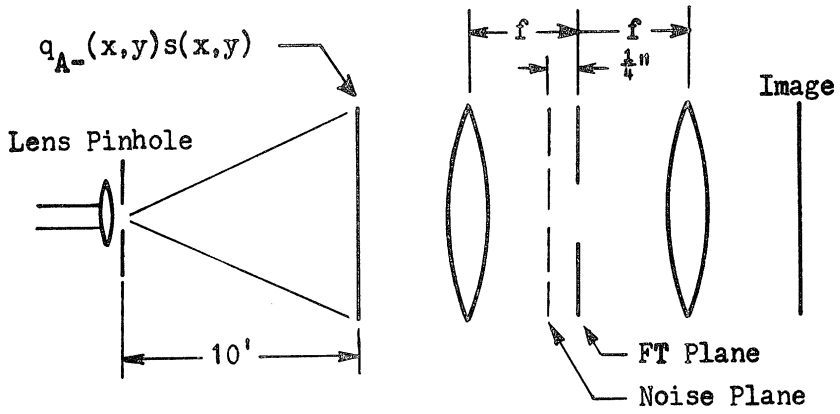

Figure 2-15. Coherent Imaging System

The optical system shown in Fig. 2-15 was used to test how $q_{A-}(x, y) = q_{A-}(x)q_{A-}(y)$ would perform in a near Fourier transform holographic storage system. Function q_{A-} corresponds to entry AE of Table 2-1 and consisted of positive lenslets with Q = 9.23 and X = 0.58 mm. A high quality lens array with a Q of 9.23 was obtained by glueing two lenticular gratings with their lines crossed rough side to rough side with a high index Kodak assembly cement. The bandwidth of q_{A-} was 15.9 cycles per mm and the system bandwidth was 18.2 cycles per mm. Figure 2-16(a) shows an image of a standard USAF resolution chart without any redundancy modulation. Element number 1 of group 1 represents two lines per mm. Figure 2-16(b) shows the same image if lens array q_{A-} is placed against the signal transparency. Note that the dust particle diffraction pattern which occurs at the top central region of the picture is multiply imaged and dispersed. This phenomenon will be discussed in the next section. Figure 2-17(a) shows how the image is affected by a system artifact in the near Fourier transform plane when the signal is illuminated with a uniform beam. The artifact consisted of a black letter "O" 0.8 mm high on a transparent glass plate. Figure 2-17(b) shows the image quality improvement when redundancy modulation q_{A-} is introduced.

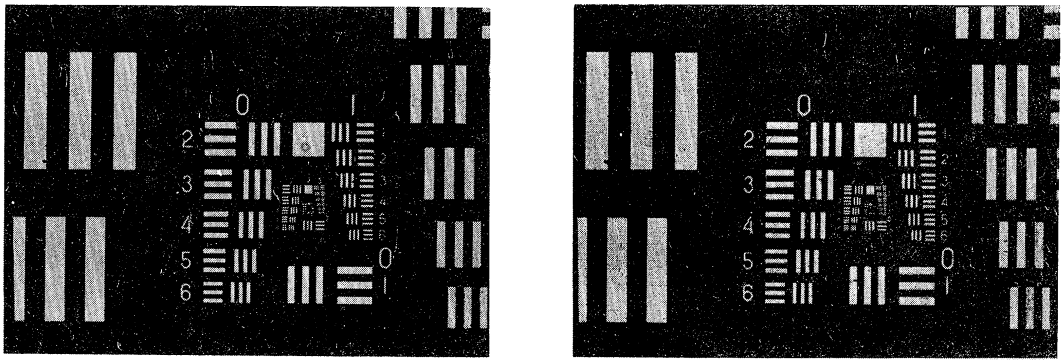

(a) (b)

Figure 2-16. (a) Image with Uniform Illumination, (b) Image with Quadratic Phase Modulation

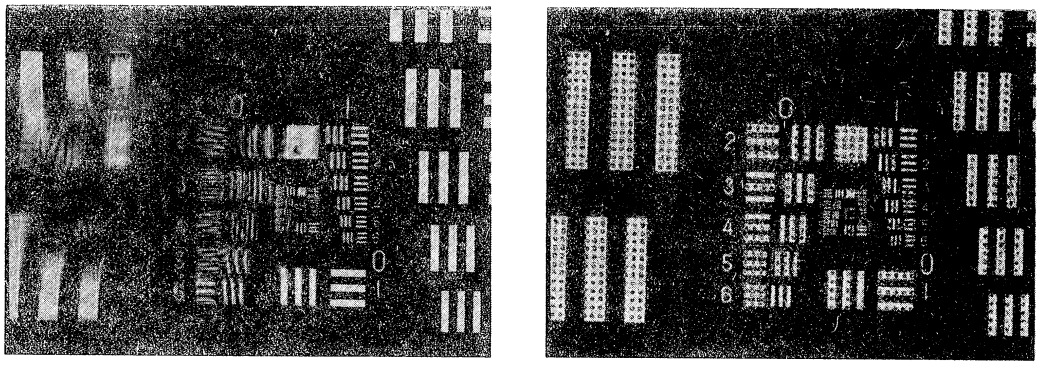

(a) (b)

Figure 2-17. Image of Fig. 2-16 with Artifact at Near Fourier Transform Plane. (a) No Redundancy, (b) Redundancy q_{A-}

Figure 2-18(a) shows $\left| FT\{s(x, y)q_{A-}(x, y)\} \right|^2$ at the Fourier transform plane of the system. Figure 2-18(b) shows both $\left|FT\{q_{A-}(x)\}\right|^2$ and $\left|FT\{\text{rect}\,(x/X)q_{A-}(x)\} \right|^2$ for Q = 9.23.

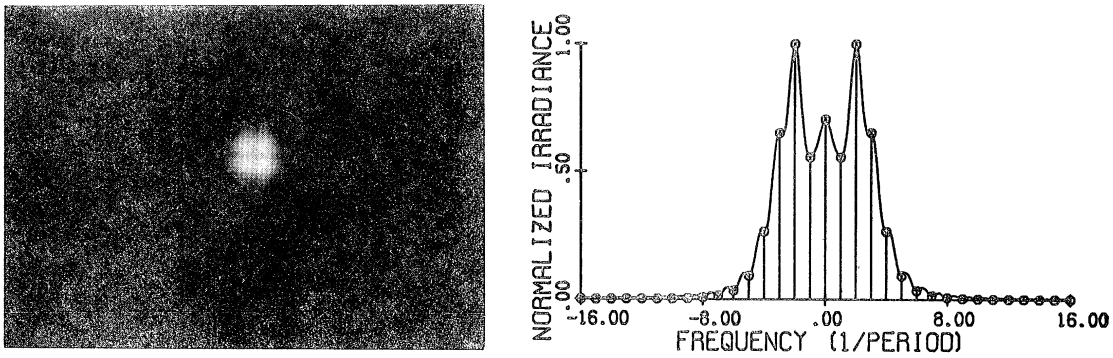

(a) (b)

Figure 2-18. (a) Irradiance at FT Plane of Fig. 2-15 with $q_{A-}(x, y)$ Present, (b) Spectral Density of q_{A-} for Q = 9.23

Although a lens array q_A can improve the image quality, it can be seen from entry AH of Table 2-1 that objectionable diffuser noise occurs where the lenslets join if B is near unity. It is also seen that R_1 is only one-half the maximum limit. A new class of redundancy modulation will be investigated in Chapter 4 which does not have these limitations.

2.5.3. OPTICAL NOISE DISPERSION

It was seen in Fig. 2-16 that a lens array can demagnify dust diffraction patterns. Geometrical optics or the direct correspondence between the signal space and the frequency space of q_A predicts this effect. Fig. 2-19 shows how a negative lenslet can demagnify a dust particle diffraction pattern. Geometrical optics

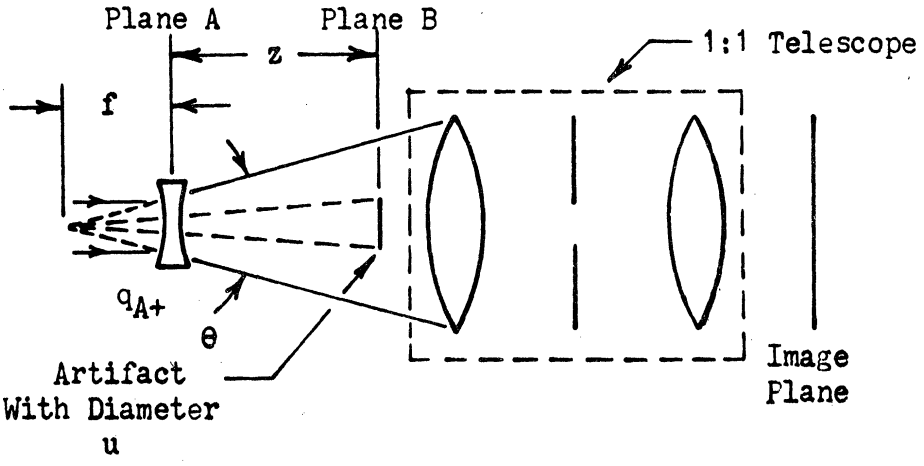

Figure 2-19. Coherent System Showing the Demagnification of Artifact Noise

predicts that the shadow of the particle at the image plane is $u[f/(f + z)]$. The number of images of the particle diffraction pattern at the image plane is $\theta(z + f)/X$ or approximately $(z + f)/f$ if θ is small. When diffraction theory predicts that the particle diffraction pattern will be significantly larger than $u[f/(f + z)]$, the local signal-to-noise ratio is improved. If

$$\frac{2u^2}{\lambda} \frac{f}{z(z + f)} < 1$$

it can be shown using stationary phase approximations developed in [19] that the particle diffraction amplitude becomes

$$d(x) \approx \exp\left(-ik \frac{x^2}{2z}\right) u\left[1 - i\, 0.65\, u^2 \frac{2}{\lambda} \frac{f}{z(z + f)}\right]^{-1/2}$$

$$\exp\left\{-\pi \frac{x^2}{\lambda^2 z^2}\, 0.65\, u^2 \left[1 - i\, 0.65\, u^2 \frac{2}{\lambda} \frac{f}{(z + f)z}\right]^{-1}\right\}$$

If

$$\frac{2u^2}{\lambda} \frac{f}{z(z + f)} << 1$$

the width of $|d(x)|^2$ reduces to approximately $(\lambda z)/u$. This becomes obvious if it is noted that the Fourier transform of the dust particle is formed at the back focal plane of the lenslet and has a width $(z + f)/u \approx (z/u)$ if $f << z$; and the above inequality is rewritten as

$$2u \left(\frac{f}{z + f}\right)\left(\frac{\lambda z}{u}\right)^{-1} << 1$$

When this condition holds and $(\lambda z)/u \geq X$, good dispersion of the noise will occur. If $(\lambda z)/u = X$ and $f << z$, the above inequalities require that

$$Q = X/(\lambda F) >> 2 \quad \text{and} \quad X << (uz)/(\lambda F)$$

If Q is large, the bandwidth of q_A is $1/(\lambda F)$ and Condition (B) is satisfied. For many practical display systems, the spatial bandwidth must be low, and the above inequalities cannot be met. Figure 2-20(a) shows the irradiance at the image plane of Fig. 2-19 when randomly placed black dots on a glass slide were introduced at Plane B. Figure 2-20(b) is the same picture when a lens array q_{A+} with 0.377×0.377 mm lenslets is placed at Plane A. The values for u, z, and f were 0.323 mm, 12.5 cm, and 3.35 cm, respectively. The demagnification factor $f/(f + z)$ was thus 0.211 and $\frac{2u^2}{\lambda} \frac{f}{z(z + f)}$ equaled 0.558.

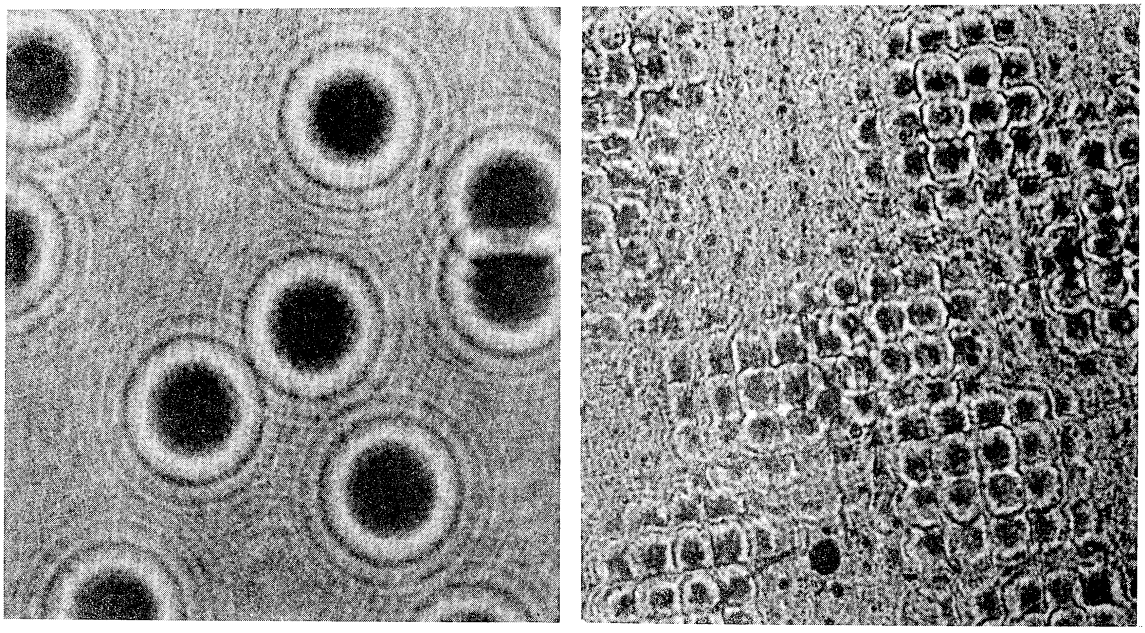

(a) (b)

Figure 2-20. (a) Irradiance at the Image Plane without q_{A+}, (b) Image when q_{A+} is Present

2.6. SUMMARY

In this chapter the redundancy requirements for suppressing optical noise in coherent systems was considered. The self-imaging property of gratings provides a convenient but not essential means for generating redundancy illumination. Constraints were established for the redundancy modulation needed to coherently image a continuous-tone transparency. It was seen that quadratic phase modulation can satisfy these constraints when the space bandwidth parameter Q is large. For some high density holographic storage systems, certain imaging constraints require that Q be small. In this case the spectral density of a lens array is no longer uniform, and a new class of functions must be considered.

3
REDUNDANCY REQUIREMENTS FOR HIGH DENSITY COHERENT STORAGE SYSTEMS

3.1. INTRODUCTION

Redundancy modulation for coherent imaging systems with very narrow spatial bandwidth will now be considered. One such system is Fourier transform holography, where a lens or converging wavefront is used to form the Fourier transform of an input signal near the hologram plane. Such a system has desirable properties for the high density storage of continuous-tone transparencies. Individual points on the hologram can record information concerning the entire image space. The storage of continuous-tone signals presents special difficulties since the dominant DC component of this class of signals makes the signal especially sensitive to artifact noise. For example, a small emulsion defect on the hologram may remove the DC portion of the signal. Special redundancy modulation will be investigated which can improve system performance and increase hologram diffraction efficiency by providing more uniform illumination at the hologram plane.

3.2. SYSTEM CONSTRAINTS

The resolution for a Fourier transform holographic system is inversely related to the size of the hologram. If a diffraction limited hologram with dimension D is recorded, the system resolution R_H is

$$R_H = \frac{\lambda f}{D}$$

where f and λ correspond to the focal length and wavelength respectively. To meet the system resolution requirements, the hologram width must exceed some lower limit D_R. Redundancy modulation should not require the hologram width to exceed D_R by more than a small factor such as two if a holographic system is to compete with present storage systems such as microfiche. The resolution of the eye and constraints on the use of an output enlarging lens place a lower bound on R_H. An output enlarging lens could increase this bound. However, the magnification of an enlarging lens is limited for a practical system since coherent noise suppression techniques are not effective for artifacts on an optical surface close to an image plane. Noncoherent noise suppression methods such as rotating the enlarging lens are too cumbersome to be helpful. Since Condition (B) of Chapter 2 limits the period X for quadratic phase modulation, this modulation cannot provide adequate redundancy for high density storage applications where the space bandwidth product XW and thus the parameter Q must be low. Consider Condition (B) for nonperiodic redundancy modulation q(x) when the space bandwidth product VW must be small. Since

$$S(f_x, V, x_o) = \left[e^{-i2\pi f_x x_o} \operatorname{sinc}(Vf_x) \right] * \hat{q}(f_x)$$

should be approximately equal to rect (f_x/W), the importance of the sinc term when VW is small makes it difficult to determine a function which satisfies Conditions (A) and (B). For periodic modulation with period X where L/X is greater than three or four, Condition (B) is satisfied if

$$\text{Envelope of } \left|\hat{q}(nf_o)\right| \approx \text{rect}\,(f_x/W)$$

where n is an integer. Since only discrete points must be considered,

the problem of synthesizing a function which satisfies Conditions (A) and (B) is more tractable. The parameter XW for periodic modulation represents the number of Fourier series components of q(x) recorded by the hologram. Since periodic phase modulation

$$q(x) = \sum_{n=-\infty}^{\infty} a_n e^{inwx}$$

requires that the number of non-zero orders be infinite and that $|a_n| \to 0$ as $n \to \infty$, this class of functions cannot provide maximum redundancy for systems with very limited spacial bandwidth.

3.3. BANDLIMITED PERIODIC REDUNDANCY MODULATION

To achieve high redundancy when VW << 100, consider periodic bandlimited redundancy modulation

$$q(x) = \sum_{n=-N}^{N} a_n e^{in2\pi f_o x} \qquad \text{where } 2N+1 < XW$$

Since this means the signal information will be placed on a multiplicity of carriers, the effect of the spatial frequency coordinates of each carrier on the system resolution will now be examined.

The Fourier transform of a real signal s(x) has the following property: If

$$\hat{s}(f_x) = \int_{-\infty}^{\infty} s(x)\, e^{i2\pi f_x x}\, dx$$

then

$$\hat{s}(-f_x) = \left[\hat{s}(f_x)\right]^*$$

This property means that the signal information can be recovered if a hologram records the DC term and only one sideband of the signal. Maximum resolution for a bandlimited system is achieved if only one sideband of the signal is recorded. Consider a bandlimited system such as Fig. 1-5, with frequency transfer function $\hat{h}(f_x, f_y) = \text{rect}\,(f_x/W)\ \text{rect}\,(f_y/W)$. Coordinates f_x and f_y are the Cartesian frequency plane coordinates. Figure 3-1 shows the image of a USAF resolution chart when plane wave illumination $e^{i2\pi(W/2)x}$ is incident on the signal. Since there was only single-sideband plus DC transmission along the horizontal x coordinate, higher frequency information was passed and the vertical bars are better resolved than the horizontal bars.

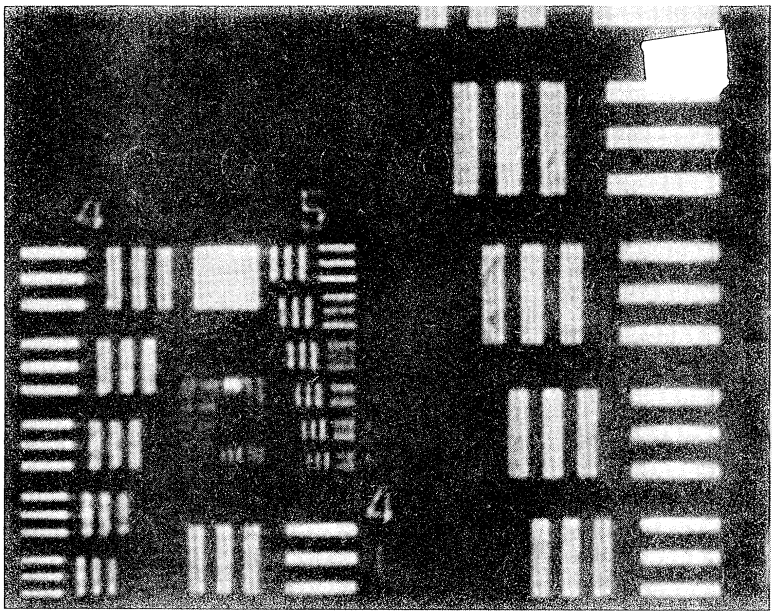

Figure 3-1. Image of USAF Resolution Chart with Single-Sideband Imaging for the Horizontal Coordinate

To account for the low contrast of the vertical bars, let the real signal

$$s(x) = \int_{-\infty}^{\infty} \hat{s}(f_x) e^{i2\pi f_x x} \, df_x$$

be written as

$$s(x) = s_o + s_1(x) + s_1(x)^*$$

where s_o is positive real constant and

$$s_1(x) = \int_{0^+}^{\infty} s(f_x) e^{i2\pi f_x x} \, df_x$$

For double-sideband imaging, the image irradiance is

$$s_o^2 + 4 \, \mathrm{Re}^2\{s_1\} + 4 s_o \, \mathrm{Re}\{s_1\}$$

and for single-sideband imaging the image irradiance becomes

$$s_o^2 + \mathrm{Re}^2\{s_1\} + \mathrm{Im}^2\{s_1\} + 2 s_o \, \mathrm{Re}\{s_1\}$$

The major effects of single-sideband imaging with a bandlimited optical system are to improve the resolution and to decrease the image contrast. For multicarrier imaging these effects must be averaged on an energy basis for each carrier. For example, an average channel bandwidth <W> is defined below where W_n represents the maximum single-sideband bandwidth for each carrier and

$$q(x) = \sum_{n=-N}^{N} a_n \, e^{in2\pi f_x x}$$

is the multicarrier illumination.

$$\langle W \rangle \equiv \frac{\sum_{n=-N}^{N} \left(|a_n|^2 W_n \right)}{\sum_{n=-N}^{N} |a_n|^2}$$

Additional complexities occur in using multicarrier illumination. Let s(x)q(x) be the input amplitude to a coherent imaging system with frequency transfer function

$$\hat{h}(f_x) = \text{rect}\,(f_x/W)$$

where s(x) is a real input signal and q(x) represents redundancy modulation. If the spectrum of s(x)q(x) falls completely within the system bandpass, the square-law detected output is simply

$$|s(x)|^2 |q(x)|^2$$

The example discussed below illustrates the case where the bandwidth of s(x)q(x) exceeds W. Consider the real signal

$$s(x) = s_o + s_1(x) + s_1(x)^*$$

and redundancy modulation

$$q(x) = \frac{e^{iw_1x} + e^{-iw_1x}}{\sqrt{2}}$$

consisting of two carriers at each edge of the system bandpass. The output irradiance $\left| [q(x)s(x)] * h(x) \right|^2$ becomes

$$\frac{1}{2}\left|(s_o + s_1)e^{-iw_1x} + (s_o + s_1^*)e^{iw_1x}\right|^2 = \left| s_o + s_1(x)\right|^2$$

$$+ s_o^2 \cos(2w_1x) + 2s_o \operatorname{Re}\left\{s_1(x)e^{-i2w_1x}\right\} + \operatorname{Re}\left\{s_1^2(x)e^{-i2w_1x}\right\}$$

The first term simply represents the output of a single-sideband system. The second term is the fringe pattern due to q(x) weighted by the DC component of the signal. Terms three and four represent interaction of the carriers with the signal. The last term is potentially dangerous; since if $s_1(x)$ has a dominant term $ce^{i(w+\epsilon)x}$, a low frequency moire fringe pattern occurs at the image plane if ϵ is small. This illustrates that caution is required if carriers are placed near the edge of the system bandpass.

It was seen in Chapter 2 that the frequency distribution of the image speckle resulting from coherent addition of the carriers limits the system resolution. Fortunately, classes of periodic bandlimited redundancy modulation which have no low frequency speckle exist and are presented in Chapter 4.

3.4. NOISE SUPPRESSION ANALYSIS

The noise suppression characteristics of periodic, bandlimited modulation will now be formulated in terms of a family of redundancy parameters. Dispersion of artifact noise uniformily over the image is the principle mechanism for improving the local signal-to-noise

ratio. If the density of artifacts is too high, coherent dispersion can no longer improve image quality. Consider the noise reduction for a single isolated artifact located at Planes 1 or 2 of Fig. 3-2.

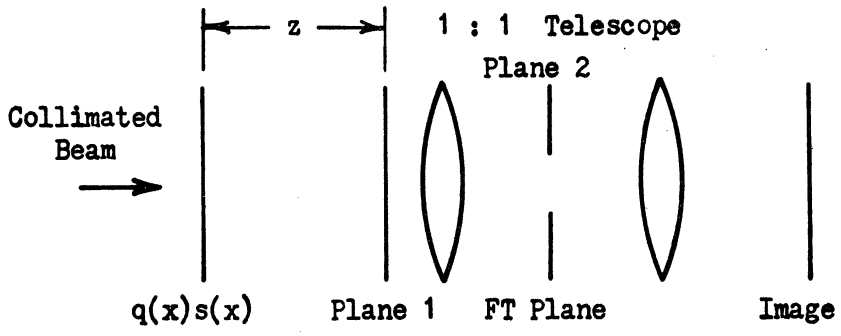

Figure 3-2. Coherent Imaging System

First to be considered is the effect of artifacts at Plane 1. Let h(x) be the impulse response of the system and 1 - n(x) represent the amplitude transmittance at Plane 1 where n(x) is zero if no artifacts are present. The propagation phenomenon may be regarded as a linear dispersive spatial filter [14]. For Fresnel diffraction the impulse response p(x) for this filter is

$$p(x) = \frac{e^{ikz}}{i\lambda z} \; e^{i\frac{k}{2z}x^2} \qquad \text{where } k = \frac{2\pi}{\lambda}$$

If z is constant, the z dependence will usually be ignored. The output image amplitude v(x) can be written

$$v(x) = v_1(x) + v_2(x)$$

where

$$v_1(x) = [q(x)s(x)] * h(x)$$

is the signal term and

$$v_2(x) = -\left[\{[q(x)s(x)] * p\}\, n(x)\right] * p^* * h(x)$$

is the noise term. If q has a rather uniform spectral density, the dispersive action of p will distribute the noise effects due to n(x) uniformly over a wider area of the image plane. The amount of dispersion is directly related to the distance z and the spectral width of q. The output irradiance is

$$|v(x)|^2 = |v_1|^2 + 2\,\mathrm{Re}\{v_1 v_2^*\} + |v_2|^2$$

If $v_2(x) \ll v_1(x)$ for all x, $|v(x)|^2 \approx |v_1|^2 + 2\,\mathrm{Re}\{v_1 v_2^*\}$. Although the redundancy modulation q(x) does not change the signal-to-noise ratio if the whole signal space is considered, it can improve the local S/N over a local region Λ of the image. One measure of the local signal-to-noise ratio $(S/N)_\Lambda$ is

$$(S/N)_\Lambda = \frac{\int_\Lambda |v_1(x)|^2\, dx}{\int_\Lambda \left[2\,\mathrm{Re}\{v_1 v_2^*\} + |v_2|^2\right] dx}$$

This measure will prove convenient since it can be expressed in terms of the redundancy parameter R_M. If periodic redundancy modulation

$$q(x) = \sum_{n=-N}^{N} a_n e^{inw_o x}$$

is considered and only the dominant DC component s_o of a continuous-tone signal is retained, $v_2(x)$ can be simplified. The expression

$$s_o q(x) * p(x, z) = s_o \sum_{n=-N}^{N} a_n e^{i2\pi \left[nf_o x + \frac{z}{\lambda}\sqrt{1-(\lambda n f_o)^2} \right]}$$

becomes

$$s_o \sum_{n=-N}^{N} a_n' e^{i2\pi(nf_o x)}$$

where

$$a_n' = a_n e^{i\pi\lambda z(nf_o)^2}$$

for Fresnel diffraction. The artifact function n(x) typically takes the form rect (x/u) for a dust particle with dimension u, hence v_2 becomes

$$v_2(x) = -s_o \sum_{n=-N}^{N} \left\{ a_n'(z) \left[e^{i2\pi n f_o x} \text{ rect } (x/u) \right] * e^{-i\frac{k}{2z}x^2} * h(x) \right\}$$

If u is several times larger than the period $1/f_o$, this expression predicts that multiple artifact diffraction patterns spaced $\lambda z f_o$ apart appear at the image plane. Noise suppression is dependent on the sequence $\left\{ |a_n|^2 \right\}_{n=-N}^{N}$. Since the irradiance of the n-th

artifact diffraction pattern is proportional to the coefficient $|a_n|^2$ of the plane wave that produced the image, noise suppression is maximum if all sequence terms are equal.

Consider the case where the main lobe of the multiple diffraction patterns do not overlap. Figure 3-3 below shows this condition for a small wire artifact when

$$q(x) = ie^{iw_o x} + 1 + ie^{-iw_o x}$$

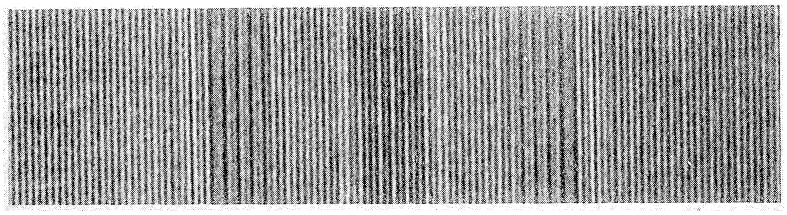

Figure 3-3. Image of Diffraction Pattern for a Small Wire Artifact ($w_o = 2\pi f_o$ and $f_o = 16$ cycles per mm)

If (S_o/N_o) is the local signal-to-noise ratio when $q(x) = 1$, the local signal-to-noise for the n-th artifact diffraction pattern is

$$(S/N)_{n\Lambda} = \frac{\sum_{n=-N}^{N} |a_n|^2}{|a_n|^2} (S_o/N_o)_{\Lambda}$$

It is necessary to maximize the minimum local signal-to-noise ratio. This is equivalent to maximizing the parameter

$$R_1 = \frac{\sum_{n=-N}^{N} |a_n|^2}{\max_n \left\{ |a_n|^2 \right\}}$$

since

$$\min_n \left\{ (S/N)_{n\Lambda} \right\} = R_1 (S_o/N_o)_\Lambda$$

Noting that

$$|a_n|^2 \leq \max \left\{ |a_n|^2 \right\}$$

it is seen that R_1 equals the maximum limit 2N+1 if all terms $|a_n|^2$ are equal. If the grating

$$q(x) = \sum_{n=-N}^{N} a_n e^{inw_o x}$$

which maximizes R_1 can be selected from the class of functions satisfying Condition (A) of Chapter 2, the optimization problem is over. However, what if P multiple noise diffraction patterns overlap and a grating with $R_1 = 2N+1$ cannot be found? In this case it it necessary to consider the redundancy parameter

$$R_P = \frac{\sum_{n=-N}^{N} |a_n|^2}{\max_n \left\{ \sum_{j=1}^{P} |a_{n+j}|^2 \right\}}$$

The sum in the denominator is maximized over the index N for $-N \le n \le N - P + 1$. The minimum local signal-to-noise ratio is now $R_P(S_o/N_o)_\Lambda$, and thus optimum redundancy is achieved if R_P is maximized.

A simple example will help illustrate the condition for no dust diffraction overlap. If the object plane is in the far field of a dust particle at Plane 1 of Fig. 3-2 and n(x) = rect (x/u), the diffraction pattern at the object plane is sinc $[(ux)/(\lambda z)]$ with main lobe width $(\lambda z)/u$. Let θ be the propagation angle of plane wave $e^{i2\pi f_o x}$ relative to the optical axis for a grating with period $X = 1/f_o$. Then the condition for no overlap is

$$\theta z \ge \frac{\lambda z}{u}$$

since $f_o \approx \theta/\lambda$ if $\theta << 1$, this implies

$$X \le u$$

The above inequality requires that the period of the grating be smaller than the artifact width. Thus if X is 1/5 mm, f_o must be greater than or equal to 5 cycles per mm if no overlap is to occur.

If the periodicity of the multiple wire diffraction patterns is examined in Fig. 3-3, it can be seen that the increased diffuser

noise that occurs is due to attenuation of one of the three coefficients a_{-1}, a_o, or a_1. The increase in the low frequency speckle noise due to a noise particle will be examined quantitatively for artifacts at Plane 2 of Fig. 3-2. This work will also be useful for estimating the low frequency speckle introduced by artifacts at Plane 1. Consider artifacts at Plane 2 of Fig. 3-2. For Fourier transform holography, Plane 2 represents the hologram plane. Let $\hat{h}(f_x)$ be the Fourier transform of the impulse response h(x) of the system. The output amplitude v(x) for amplitude transmittance $[1 - \hat{n}(f_x)]$ at Plane 2 is

$$v(x) = [q(x)s(x)] * h(x) - [q(x)s(x)] * h(x) * n(x)$$

If $\hat{h}(f_x) = \text{rect}\,(f_x/W)$ and $\hat{n}(f_x) = \text{rect}\left(\frac{f_x - f_c}{aW}\right)$ where $a << W$ and $|f_c| < W/2$, v(x) becomes

$$v(x) = W[q(x)s(x)] * \text{sinc}\,(Wx) - aW[q(x)s(x)] * \left[e^{i2\pi f_c x}\,\text{sinc}\,(aWx)\right]$$

Artifact noise at the Fourier transform plane affects the entire image space. If no redundancy modulation is employed, a small artifact could remove the DC component of the signal. Although periodic redundancy modulation q(x) with no low frequency speckle is determined in Chapter 4, the blockage of a spectral order of q(x) reduces m^2/σ^2 of Condition (A), since low frequency speckle is introduced at the image plane. This effect will now be formulated in terms of the redundancy parameter R_M. Since continuous-tone signals s(x) have a dominate DC component, only q(x) need be

considered in the following analysis. A small scratch or artifact attenuates one or more Fourier series components of q(x). Let (1 - B) be the attenuation factor due to such a noise term. If

$$\alpha_n = a_n e^{in2\pi f_o x}$$

then

$$\left|q(x)\right|^2 = \sum_{n,\, m=-N}^{N} \alpha_n \alpha_m^*$$

Let q_o represent q(x) after one order a_{n_o} is attenuated by the factor (1 - B). Then

$$q_o(x) = q(x) * [\delta(x) - n(x)]$$

$$= \left(\sum_{n=-N}^{N} \alpha_n \right) - B\alpha_{n_o}$$

and

$$\left| q_o(x) \right|^2 = \left| \sum_{n=-N}^{N} \alpha_n \right|^2 + \left| B \right|^2 \left| \alpha_{n_o} \right|^2$$

$$- 2 \left| \sum_{n=-N}^{N} \alpha_n \right| \left| \alpha_{n_o} \right| \left| B \right| \cos \left[\phi_1(x) - \phi_2(x) \right]$$

where

$$\phi_1(x) = \arg \left\{ q(x) \right\}$$

and

$$\phi_2(x) = \arg\left\{\alpha_{n_o} B\right\}$$

In Chapter 4 a class of even functions q(x) with no low frequency speckle are examined [20]. These functions have the characteristic

$$|q|^2 = \left| \sum_{n=-N}^{N} \alpha_n \right|^2$$

$$= 1 + D \cos (2\pi 2Nf_o x)$$

As R_1 increases, D becomes small relative to 1. For bandlimited phase modulation such as q_B of Chapter 2, D is essentially zero. If $D << 1$,

$$\left| \sum_{n=-N}^{N} \alpha_n \right| \approx 1 + (D/2) \cos (2\pi 2Nf_o x)$$

If $g_I(x) = [(2N)/X]\,\mathrm{rect}\,[(2Nx)/X]$ is the impulse response of a low-pass irradiance filter which removes the high frequency speckle term $\cos (2N2\pi f_o x)$,

$$|q_o(x)|^2 * g_I(x) = 1 + |B|^2 \frac{|a_{n_o}|^2}{\sum_{n=-N}^{N} |a_n|^2} - \frac{2|a_{n_o}||B|}{\left(\sum_{n=-N}^{N} |a_n|^2\right)^{1/2}}$$

$$\times \left\{ \left[1 + \frac{D}{2} \cos (2\pi 2Nf_o x) \right] \cos (\phi_1 - \phi_2) \right\} * g_I(x)$$

For small D the expression above is bounded above by

$$1 + \frac{|B|^2}{R_1} + \frac{2|B|}{\sqrt{R_1}}$$

and from below by

$$1 + \frac{|B|^2}{R_1} - \frac{2|B|}{\sqrt{R_1}}$$

thus

$$|q_o(x)|^2 * g_I(x) = 1 + \frac{|B|^2}{R_1} + \Delta(x)$$

where

$$|\Delta(x)| \leq \frac{2|B|}{\sqrt{R_1}}$$

Speckle modulation is thus very low if

$$\frac{2|B|}{\sqrt{R_1}} << 1$$

If an artifact is not at the Fourier transform plane, the effective B is often much less than one. Also, if R_1 is the redundancy for q(x), this same parameter has the value R_1^2 for two-dimensional modulation q(x)q(y).

A limit will now be established for the magnitude of Fourier

series coefficients of $|q_o|^2$ which are introduced by this type of artiface noise. If

$$|q|^2 = 1 + D \cos (2\pi 2Nf_o x)$$

attenuation of the complex coefficient a_{n_o} by the factor (1 - B) will introduce new irradiance frequency terms of the form

$$-2I_k \cos\left[2\pi k f_o x + \arg\left\{B^*\left(a^*_{n_o} a_{n_o+k} + a^*_{n_o-k} a_{n_o}\right)\right\}\right]$$

where

$$I_k = |B|\left|a^*_{n_o} a_{n_o+k} + a^*_{n_o-k} a_{n_o}\right|$$

Since

$$I_k \leq \frac{2|B| \max\left\{|a_n^2|\right\}}{\sum_{n=-N}^{N} |a_n|^2}$$

these new frequency coefficients are bounded by the inequality

$$2I_k \leq 4/R_1$$

As stated in Chapter 2, the frequency of the speckle noise is never lower than $f_o = 1/X$ for periodic functions, hence it is advantageous to keep the number of orders 2N + 1 or the space bandwidth parameter XW small.

3.5. SUMMARY

This chapter has considered the redundancy requirements of high density coherent storage systems for continuous-tone transparencies. Periodic functions appear to have the best characteristics for maximizing the redundancy in this type of system. The noise suppression characteristics of bandlimited periodic redundancy modulation were formulated in terms of a family of redundancy parameters. These parameters will prove useful in Chapter 4 in determining periodic modulation with optimum redundancy characteristics. Chapter 4 will show that uniform hologram illumination required for high diffraction efficiency in Fourier transform holography can be achieved by using periodic modulation in tandem with a coarse lens array. Experimental results presented indicate that this technique can improve noise suppression.

4
PERIODIC MODULATION WITH OPTIMUM REDUNDANCY CHARACTERISTICS

4.1. INTRODUCTION

In Chapter 3 the redundancy requirements of high density storage systems for continuous-tone transparencies were considered. There it was shown that periodic functions are the most promising class of redundancy modulation for systems where the space-bandwidth product $VW << 100$. Periodic modulation with optimum redundancy characteristics will now be investigated.

In order to satisfy Condition A of Chapter 2, redundancy modulation $q(x)$ should have no low frequency speckle noise. It is well known that a grating which generates three orders can produce a diffraction pattern which is twice as fine as the grating period [21]. Gabor [20] generalized this property by showing that it is possible for a grating with $2N + 1$ orders to produce a fringe pattern that is $2N$ times as fine as the grating period. Consider the class of bandlimited functions

$$q(x) = \sum_{n=-N}^{N} a_n e^{i2\pi n f_0 x}$$

having $2N + 1$ orders. The irradiance

$$I(x) = \left| q(x) \right|^2$$

thus becomes

$$I(x) = I_0 + 2 \sum_{n=1}^{2N} I_n \cos (2\pi n f_0 x - \phi_n)$$

If

$$c_k \equiv \sum_{n=-N}^{N-k} a_n a^*_{n+k}$$

then

$$I_k = |c_k| \qquad \text{and} \qquad \phi_k = \arg \{c_k\}$$

where arg $\{\cdot\}$ denotes the angle of a complex number. Low frequency speckle modulation is eliminated if the system of nonlinear equations given below is satisfied.

$$\sum_{n=-N}^{N-k} a_n a^*_{n+k} = 0 \quad \text{for } k = 1, 2, \ldots, 2N-2, 2N-1 \qquad (6)$$

Since only relative values of the coefficients $\{a_n\}_{n=-N}^{N}$ are of interest, let $a_N = i$. Assuming that only even functions are of interest, $a_{-n} = a_n$, and the system of Eqs.(6) above reduces to 2N-1 equations and 2N unknowns. This leaves one free parameter which can be varied to maximize the redundancy parameter

$$R_M \equiv \frac{\sum_{n=-N}^{N} |a_n|^2}{\max_n \left\{ \sum_{j=1}^{M} |a_{n+j}|^2 \right\}}$$

in order to obtain a grating with the best spectral uniformity. The irradiance I(x) can be written as

$$I(x) = \left[2 + \sum_{n=-(N-1)}^{N-1} |a_n|^2 \right] + 2 \cos (2\pi 2Nf_o x)$$

Thus if q(x) has a rather uniform spectral density, it is clear that as $N \to \infty$ that

$$\frac{\text{Var}\{I(x)\}}{E^2\{I(x)\}} \to 0 \quad \text{and thus} \quad q(x) \to e^{i\alpha(x)}$$

For fixed N, the free parameter value could be selected to make $\frac{\text{Var}\{I(x)\}}{E^2\{I(x)\}}$ small rather than simply maximizing R_M. In this case redundancy would be sacrificed in order to achieve diffraction limited resolution performance.

4.2. GABOR'S SOLUTIONS

Gabor obtained even function solutions to equation system (6). Noting the solution pattern that developed, he attempted to derive a recurrence relation which would yield a higher order solution sequence $\{a_n\}_{n=-(N+1)}^{N+1}$ from the solution sequence $\{a_n\}_{n=-N}^{N}$. The recurrence relation was formed by considering the new terms introduced for equations $I_1 = 0$ and $I_2 = 0$ when the number of grating orders increases from 2N+1 to 2(N+1)+1. It appeared that to obtain a solution

$$\left\{ \underline{a}_{-(N+1)}, \underline{a}_{-N}, \cdots \underline{a}_{-1}, \underline{a}_0, \underline{a}_1, \cdots \underline{a}_{N+1} \right\}$$

from the lower order solution sequence $\{a_{-N}, a_{-(N-1)}, \ldots, a_N\}$, it was only necessary to calculate a new DC term $\underline{a}_0$ from terms a_0 and a_1 and let $\underline{a}_1 = a_0$ and $\underline{a}_{n+1} = a_n$ for $n \geq 1$. The recurrence relation obtained can be written as

$$\underline{a}_0 = ia_0 \frac{|a_0|^2 - |a_1|^2}{2\mathrm{Im}\{a_0 a_1^*\}} \tag{7}$$

where $\mathrm{Im}\{\cdot\}$ denotes the imaginary part of a complex number. Solutions given by Gabor are listed below [20]. Note that a_N was set equal to 1 instead of i.

N	$\{a_n\}_{n=-N}^{0}$, (Note $a_{-n} = a_n$ for $\{a_n\}_{n=-N}^{N}$)			
1			1	ik
2		1	ik	$-\frac{1}{2}k^2$
3	1	ik	$-\frac{1}{2}k^2$	$-\frac{1}{8}ik(k^2 - 4)$
4	1	ik	$-\frac{1}{2}k^2$	$-\frac{1}{8}ik(k^2 - 4)$ $\quad \frac{1}{64}(k^4 - 24k^2 + 16)$

k is a real free parameter.

Solution sequences for N = 3 and 4 were obtained using recurrence relation (7). If the above solution sequences are checked in Eqs. (6), it is found that although $\{a_n\}_{n=-3}^{3}$ given above satisfies Eqs. (6), $\{a_n\}_{n=-4}^{4}$ <u>does not</u>. For N = 4, the frequency coefficient I_4 of $|q|^2$ is

$$I_4 = \frac{1}{32}(k^4 + 8k^2 + 16)$$

$$\neq 0 \text{ for real } k$$

The class of solutions obtained by Gabor possess the 90 degree phase property, $\arg\{a_n a^*_{n+1}\} = \pm\pi/2$. Although recurrence relation (7) does not yield a solution sequence for $N > 3$, solutions for $N > 3$ do exist and will be determined in Sections 4.4 and 4.5.

Before obtaining even function solutions to Eqs. (6), let us regress a step and consider two-dimensional redundancy modulation and one-dimensional solutions where $a_{-n} \neq a_n$.

4.3. TWO-DIMENSIONAL REDUNDANCY MODULATION

Let x and y be Cartesian coordinates. Two-dimensional redundancy modulation $q_2(x, y)$ can easily be attained by forming the separable function $q_2(x, y) = q(x)q(y)$. The redundancy R_M for q_2 is then simply equal to the square of the redundancy for the one-dimensional case. If $q_2(x, y)$ is not separable, the problem of selecting q_2 such that $|q_2|^2$ has no low frequency speckle is much more difficult. However, it is natural to ask if nonseparable functions can be found with better redundancy characteristics than separable functions. Consider the function

$$q_2(x, y) = \sum_{n,m=-N}^{N}\sum a_{nm} e^{i(nwx+mwy)}$$

Suppose a function $q_2(x, y)$ exists with the following characteristic: All of the Fourier series coefficients of $|q_2|^2$ are zero except the DC term and the terms due to the interference of the two orders $a_{-N,N}$ and $a_{N,-N}$ and the two orders $a_{-N,-N}$ and $a_{N,N}$. This characteristic makes the spatial frequency of the diffuser noise a

factor $\sqrt{2}$ greater than that attained with separable solutions. Imposing this condition requires more equations than unknowns. For example, such a condition results in 20 equations and 16 unknowns for N = 1, and 60 equations and 48 unknowns for N = 2 if no assumptions about symmetry are made. It is therefore doubtful that a nontrivial solution exists. Trivial solutions such as

$$\{a_{-1,-1},\ a_{-1,1},\ a_{1,1},\ a_{1,-1}\} = \{1,\ i,\ 1,\ i\}$$

and all other $a_{n,m} = 0$ can, of course, satisfy the above conditions. If the frequency condition attained using separable functions is imposed for N = 1, this results in a nonlinear system of 16 equations and 16 unknowns. If these conditions are relaxed, the number of free parameters increases rapidly as N increases. Because of the above difficulties, only separable functions will be considered in the next section. Fortunately, there are also practical reasons for considering separable functions since they are easily synthesized by using two one-dimensional gratings in tandem with their lines crossed.

4.4. GENERAL SOLUTIONS TO EQUATIONS (6)

Appendix I investigates general solutions to Eq. (6). It is shown that considerable effort is required to obtain solutions for even small values of N. For N equal to two, a two-dimensional solution space results and a nonlinear system of equations must be solved using numerical algorithms which require an initial guess. Fortunately, one-dimensional even functions are easier to synthesize; and it will be seen that with a modest computer effort an even solution sequence with R_1 near the maximum limit 2N+1 can be found for N = 4.

4.5. EVEN FUNCTION SOLUTIONS TO EQUATIONS (6)

With the even function assumption, $a_{-n} = a_n$ and the problem of maximizing the redundancy parameter R_M becomes tractable.

4.5.1. SOLUTIONS WHERE $\arg\{a_n a^*_{n+1}\} = \pm\pi/2$

First to be considered are the class of even function solutions, with the 90 degree phase property $\arg\{a_n a^*_{n+1}\} = \pm\pi/2$. The 90 degree phase property makes each of Eqs. (6) represent the addition of collinear vectors. This together with the symmetry condition $a_{-n} = a_n$ greatly simplifies these equations. Since the solutions given by Gabor are correct for N = 1, 2 and 3, these solutions will simply be listed below. These solutions differ by a multiplicative factor i from those listed earlier, since a_{-N} is set arbitrarily equal to i for the new solutions to be developed in this chapter.

N	$\{a_n\}_{n=-N}^{N}$ (where $a_{-n} = a_n$ and $\arg\{a_n a^*_{n+1}\} = \pm\pi/2$)
1	$\{i,\ b_R,\ .\}$
2	$\{i,\ b_R,\ -i\ 0.5b_R^2,\ ..\}$
3	$\{i,\ b_R,\ -i\ 0.5b_R^2,\ -0.125b_R(b_R^2 - 4),\ ...\}$

b_R is a real number and represents the free parameter discussed earlier

Solutions will now be obtained for N = 4, 5 and 6. As a shorthand notation, let Eq. (N, k) denote equation

$$\sum_{n=-N}^{N-k} a_n a^*_{n+k} = 0$$

of the 2N - 1 Eqs. (6). Relation (C) is defined below in order to

reduce the work required for higher order solutions. In general,

Eqs. (N, 2N-1), (N, 2N-2), ... (N, N+1) are equivalent to Eqs. (1, 1), (2, 2), ... (N-1, N-1) (C)

Equations (6) will now be solved for N = 4. Using Relation (C) $\{a_n\}_{n=-4}^{4}$ becomes

$$\{i,\ b_R,\ -i\ 0.5 b_R^2,\ d_R,\ i\ e_I,\ \ldots.\}$$

All variables such as b_R, d_R, and e_I are understood to be real in the ensuing discussion.

$$\text{Eq. } (4,4) \Rightarrow e_I = -b_R d_R - 0.125\, b_R^4$$

Eq. (4, 3) is satisfied because of symmetry conditions.

$$\text{Eq. } (4,2) \Rightarrow d_R^2 + 2 b_R d_R - b_R^2 e_I - b_R^2 = 0$$

Solving Eqs. (4, 4) and (4, 2), d_R and e_R become

$$d_R(b_R) = (-1 \pm 2^{1/2}) b_R + 0.5(-1 \pm 2^{-1/2}) b_R^3$$

$$e_I(b_R) = (1 \mp 2^{1/2}) b_R^2 + 0.5(0.75 \mp 2^{-1/2}) b_R^4$$

The solution sequence for N = 4 is thus

$$\{i,\ b_R,\ -i 0.5\ b_R^2,\ d_R(b_R),\ i e_I(b_R), \ldots.\}$$

Next to be considered, is the solution sequence

$$\{a_n\}_{n=-5}^{5} = \{a,\ b,\ c,\ d,\ e,\ f,\ e,\ d,\ c,\ b,\ a\}$$

Let the subscripts R and I denote the real part and the imaginary part respectively of a complex sequence term. Using Relation (C), $\{a_n\}_{n=-5}^{5}$ becomes

$$\{i,\ b_R,\ -i\ 0.5\ b_R^2,\ d_R,\ -i(b_R d_R + 0.125\ b_R^4),\ f_R,\ \ldots\ldots\}$$

Equations (5, 5), (5, 3), and (5, 1) are satisfied because of symmetry conditions.

$$\text{Eq. (5, 4)} \Longrightarrow -2(b_R d_R + 0.125\ b_R^4) + 2b_R f_R$$

$$+ b_R^2(b_R d_R + 0.125\ b_R^4) + d_R^2 = 0$$

After simplifying the above two equations, d_R and f_R can be obtained as a function of b_R by solving the equations below.

$$d_R^3 - 2b_R d_R^2 - b_R^2(2 + 1.25\ b_R^2 + 0.125\ b_R^4)d_R$$

$$- b_R^3(-1 + 0.125\ b_R^4 + b_R^6/64) = 0$$

$$f_R = -0.5\ b_R^{-1} d_R^2 + (1 - 0.5\ b_R^2)d_R + (b_R^3/16)(2 - b_R^2)$$

It is seen that the amount of work required to obtain a solution increases rapidly as N increases. Finally, the solution

sequence $\{a_n\}_{n=-N}^{N}$ will be considered for N = 6. After applying Relation (C), this sequence becomes

$$\{i,\ b_R,\ -i\ 0.5\ b_R^{\ 2},\ d_R,\ -i(b_R d_R + 0.125\ b_R^{\ 4}),\ f_R,\ i\ g_I, \ldots\ldots\}$$

After considerable work, the equations below which express the sequence terms as functions of b_R are obtained. Let

$$c_0 = b_R^{\ 3}\left(\frac{9}{4096}\,b_R^{\ 12} + \frac{3}{128}\,b_R^{\ 10} + \frac{27}{128}\,b_R^{\ 8} + \frac{5}{8}\,b_R^{\ 6} - \frac{7}{16}\,b_R^{\ 4} - 4b_R^{\ 2} - 4\right)$$

$$c_1 = b_R^{\ 4}\left(\frac{3}{64}\,b_R^{\ 8} + \frac{9}{32}\,b_R^{\ 6} + \frac{21}{8}\,b_R^{\ 4} + 9.5\,b_R^{\ 2} + 10\right)$$

$$c_2 = b_R\left(\frac{27}{64}\,b_R^{\ 8} + \frac{15}{16}\,b_R^{\ 6} + 8.25\,b_R^{\ 4} + 29\,b_R^{\ 2} + 24\right)$$

$$c_3 = 2b_R^{\ 6} + b_R^{\ 4} + 4b_R^{\ 2} + 16$$

$$c_4 = b_R\left(2 + \frac{19}{4}\,b_R^{\ 2}\right)$$

$$c_5 = 4$$

Then solutions for d_R can be obtained by solving the polynomial

$$\sum_{n=0}^{5} c_n\, d_R^{\ n} = 0$$

Then if $2d_R + b_R(2 + b_R^2) \neq 0$,

$$f_R = \frac{(-1.5\, b_R^2)d_R^2 + b_R(2 - 0.75\, b_R^4)d_R + b_R^4\left[0.25 - (5/64)b_R^4\right]}{2d_R + b_R(2 + b_R^2)}$$

$$g_I = -b_R f_R - 0.5\, b_R^2(b_R d_R + 0.125\, b_R^4) - 0.5\, d_R^2$$

No solution exists if $2d_R + b_R(2 + b_R^2) = 0$.

It was shown in Chapter 3 that the redundancy parameter

$$R_M \equiv \frac{\sum_{n=-N}^{N} |a_n|^2}{\max_n \left\{ \sum_{j=1}^{M} |a_{n+j}|^2 \right\}} \quad \text{where } M = 1, 2, \ldots$$

is a useful measure of the spectral density uniformity of periodic functions. The parameter $M = 100\, I_{max}^{-1}(I_{max} - I_{min})$ where $I(x) = |q(x)|^2$ is a measure of the high frequency fringe modulation term. The percent modulation $A = 100\,(I_{max} + I_{min})^{-1}(I_{max} - I_{min})$ equals $M(2 - M)^{-1}$ for sinusoidal modulation. The redundancy parameters $R_1, R_2, \ldots, R_{[N/2]+1}$ and the modulation parameter M were plotted in Figs. 4-1 through 4-5 as a function of $BR = b_R$ for each of the solutions above using a digital computer. The redundancy and corresponding modulation characteristics are adjacent to one another. The parameter b_R was varied from -4 to 4 in 0.01 increment steps. The computer program which plotted

these characteristics also determined the solution sequence $\{a_n\}_{n=-N}^{N}$ which maximized R_1. These results are tabulated in Section 4.5.3. It is not necessary to vary b_R over a very large interval in order to determine which values maximize R_M. For example, since $|a_{-N}| = 1$ and $a_{-N+1} = b_R$, R_1 can never exceed $2N - 0.875$ if $|b_R| > 4$. It is sometimes necessary to examine the functional dependence of the sequence coefficients in order to minimize this interval, however. The K roots from solutions involving K-th order polynomials were stored in K different storage arrays. The discontinuities and lack of symmetry for some of these figures is due to a cross over of roots during array assignment. Arrays with very low redundancy were not plotted. Since the functional relationship of the sequence coefficients reveal that R_M and M are even functions of b_R, negative values of b_R could have been omitted. The next section shows that it can be advantageous not to retain the functional relationship of the coefficients. Since Figs. 4-1 through 4-5 show that R_1 is well below the maximum limit $2N + 1$ for $N = 2, 3, \ldots 6$, the condition $\arg\{a_n a^*_{n+1}\} = \pm\pi/2$ will be removed in order to see if R_1 can be increased. It will be seen later, however, that functions with the 90 degree phase property are somewhat easier to synthesize.

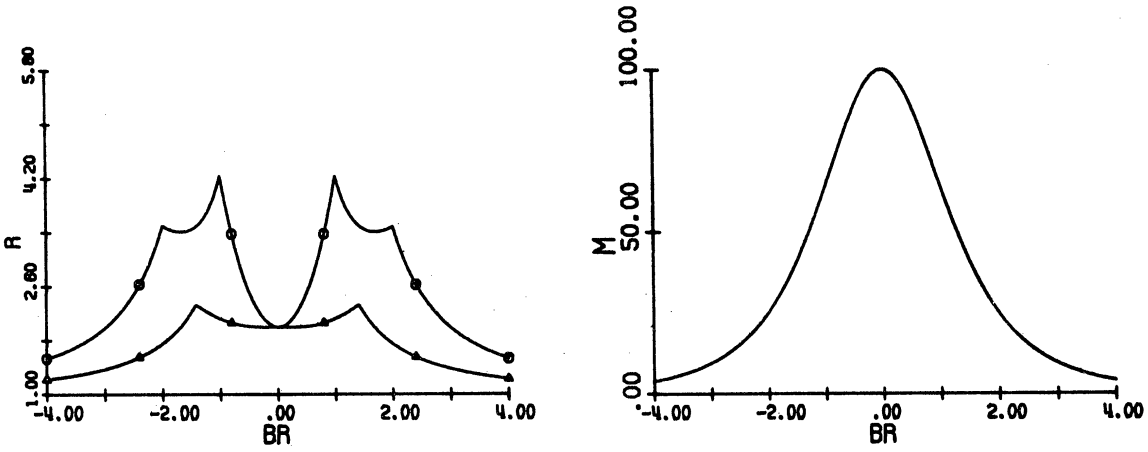

Figure 4-1. Redundancy and Modulation Characteristics for N = 2. The Symbols 0 and Δ Denote R_1 and R_2 Respectively.

$$M = 100(I_{max} - I_{min})I_{max}^{-1}$$

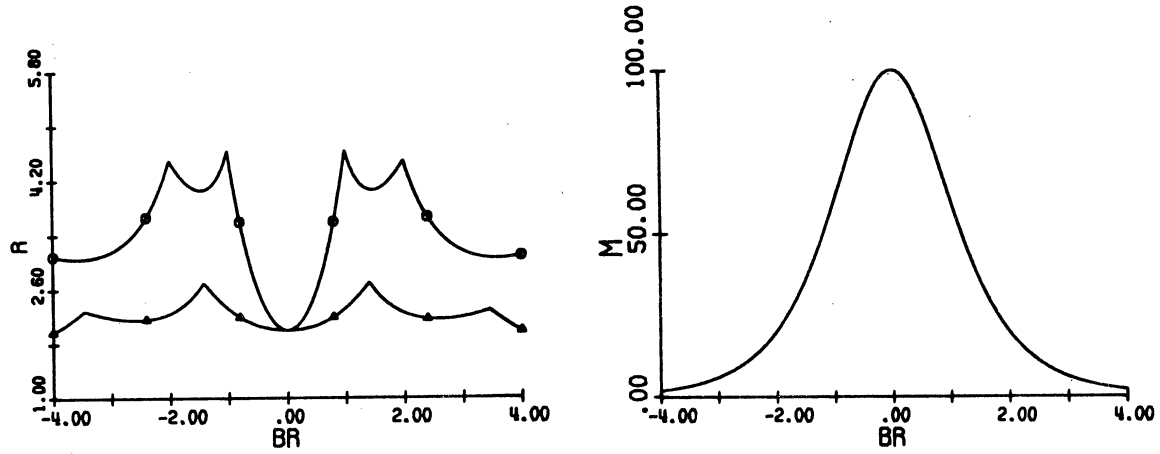

Figure 4-2. Redundancy and Modulation Characteristics for N = 3. The Symbols 0 and Δ Denote R_1 and R_2 Respectively.

$$M = 100(I_{max} - I_{min})I_{max}^{-1}$$

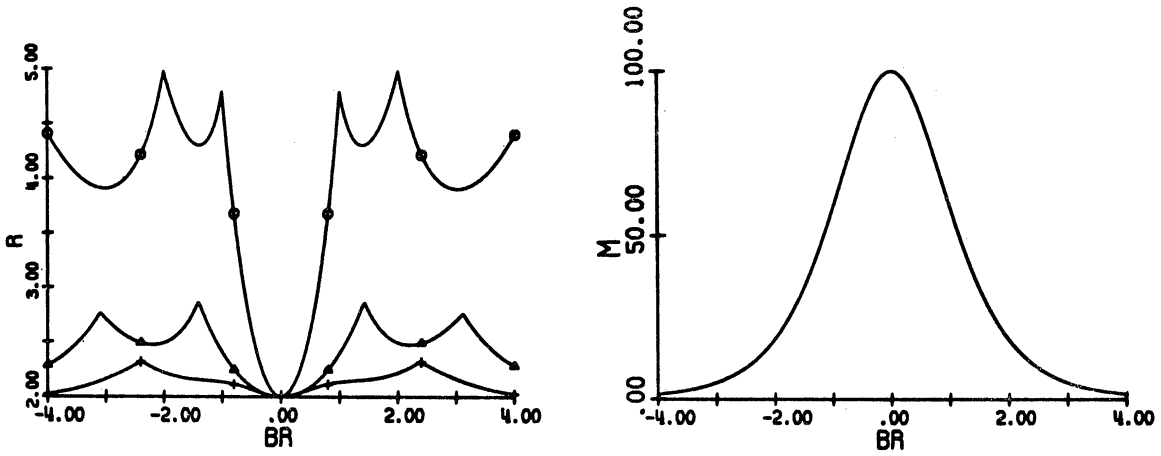

(a)

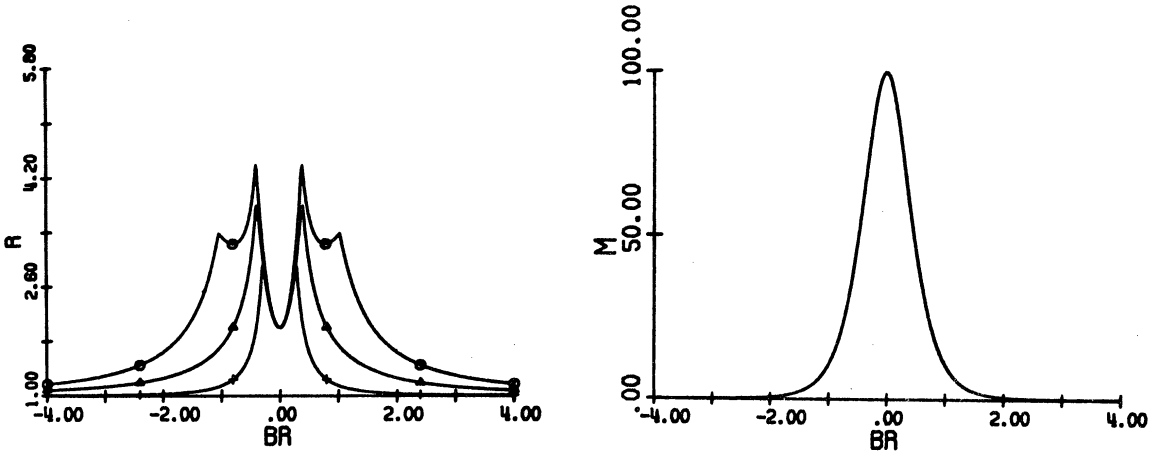

(b)

Figure 4-3. Redundancy and Modulation Characteristics for N = 4. The Symbols 0, Δ, and + Denote R_1, R_2, and R_3 Respectively.

$$M = 100(I_{max} - I_{min})I_{max}^{-1}$$

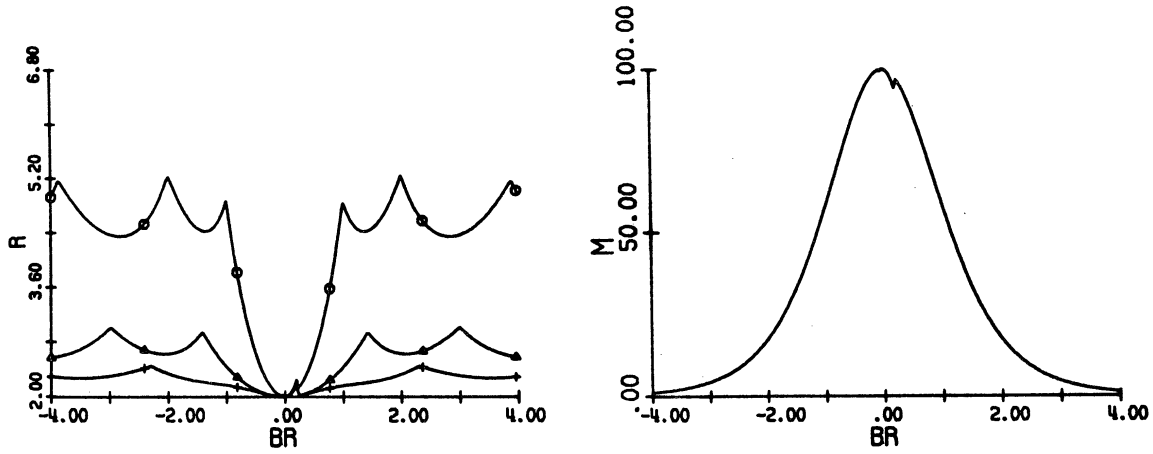

(a)

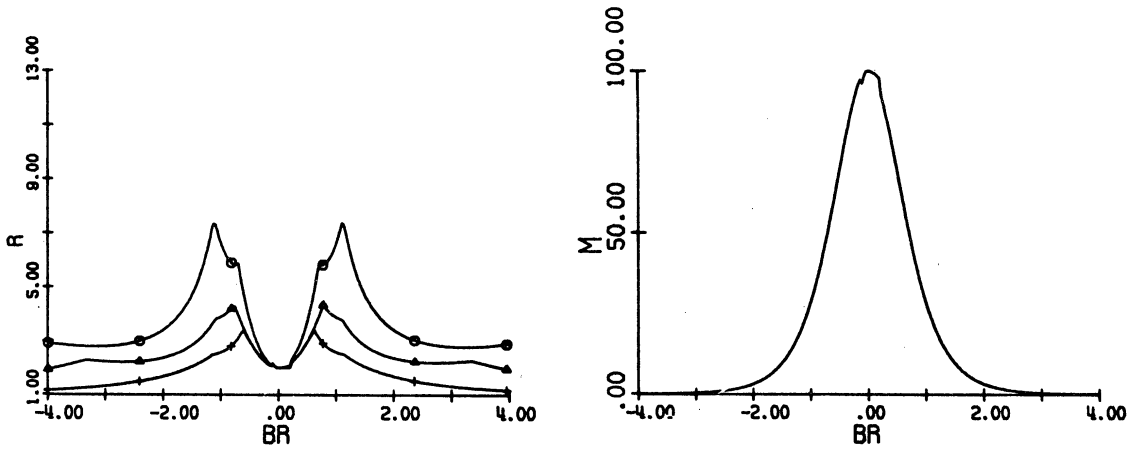

(b)

Figure 4-4. Redundancy and Modulation Characteristics for N = 5. The Symbols 0, Δ, and + Denote R_1, R_2, and R_3 Respectively.

$$M = 100(I_{max} - I_{min})I_{max}^{-1}$$

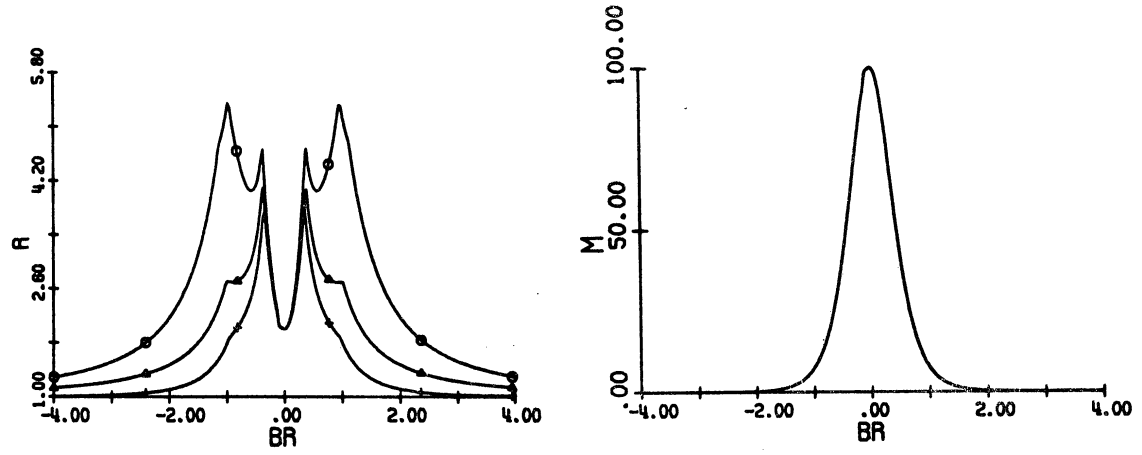

(c)

Figure 4-4. Redundancy and Modulation Characteristics for N = 5. The Symbols 0, Δ, and + Denote R_1, R_2, and R_3 Respectively.

$$M = 100(I_{max} - I_{min})I_{max}^{-1}$$ (continued)

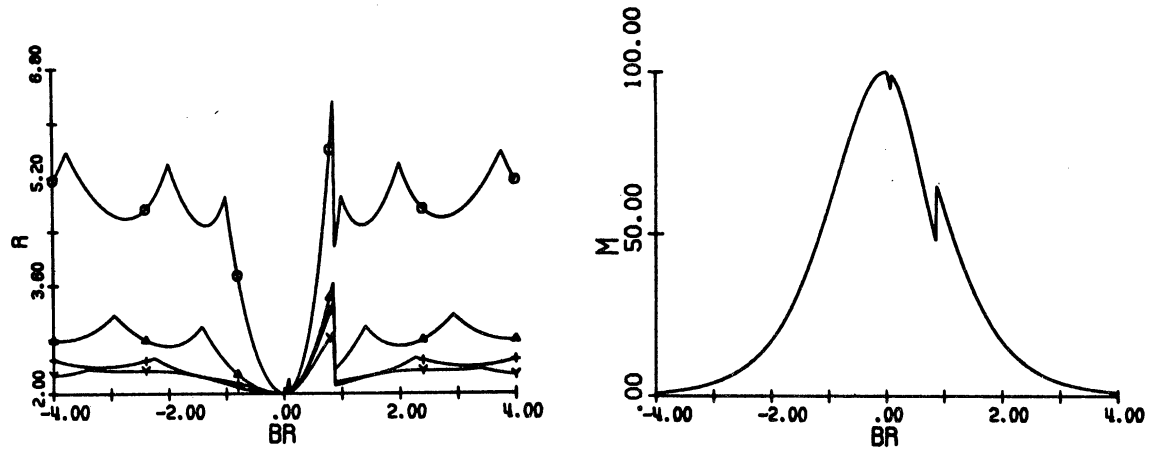

(a)

Figure 4-5. Redundancy and Modulation Characteristics for N = 6. The Symbols 0, Δ, +, and Y Denote R_1, R_2, R_3, and R_4 Respectively.

$$M = 100(I_{max} - I_{min})I_{max}^{-1}$$

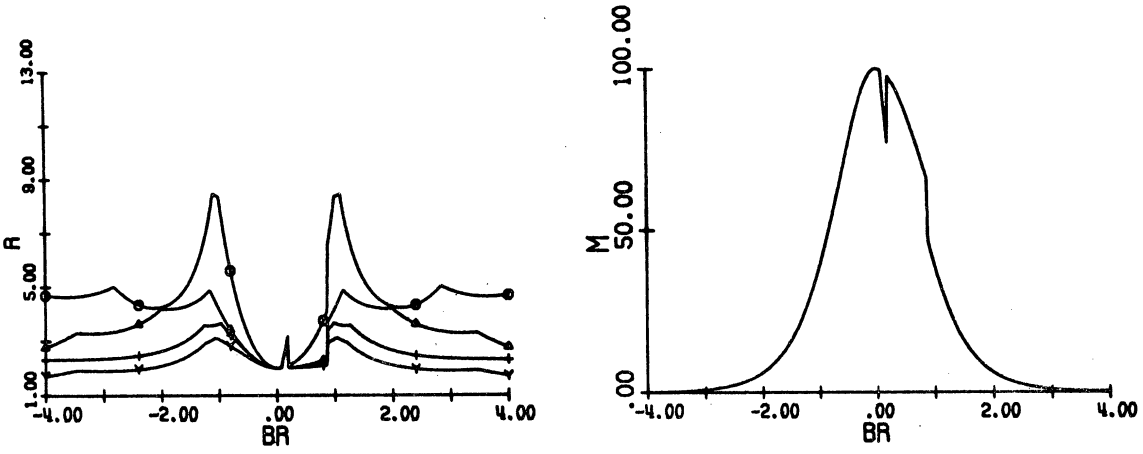

(b)

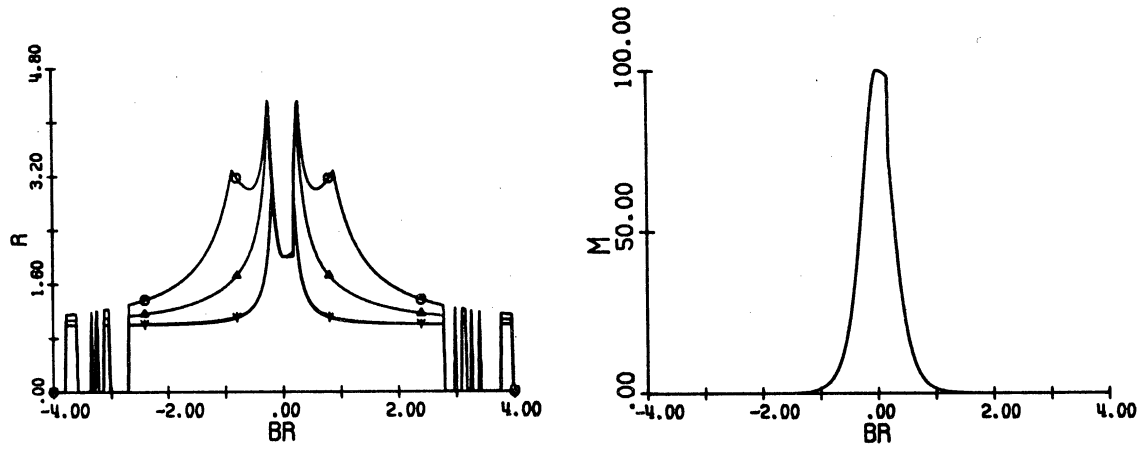

(c)

Figure 4-5. Redundancy and Modulation Characteristics for N = 6. The Symbols 0, Δ, +, and Y Denote R_1, R_2, R_3, and R_4 Respectively.

$M = 100(I_{max} - I_{min})I_{max}^{-1}$ (continued)

4.5.2. GENERAL EVEN FUNCTION SOLUTIONS

Although added complexity results if the 90 degree phase condition is not imposed, significantly higher redundancy can be attained.

Let subscripts R and I again denote the real and imaginary parts respectively of a complex sequence term. Again consider the solution sequence $\{a_n\}_{n=-N}^{N}$ to Eqs. (6), where $a_{-n} = a_n$ and $a_{-N} = i$. For N = 1, if $\{a_n\}_{n=-1}^{1} = \{i, b, i\}$, Eq. (1, 1) $\Longrightarrow b_I = 0$. For N = 2, after applying Relation (C) the solution sequence becomes $\{i, b_R, c, b_R, i\}$. Eq. (2, 2) $\Longrightarrow c_I = -0.5\, b_R^2$, and Eq. (2, 1) $\Longrightarrow c_R = 0$ if $b_R \neq 0$. This is the same solution as before, since $\arg\{a_n a^*_{n+1}\} = \pm(\pi/2)$. For N = 3 the solution sequence simplifies to $\{i, b_R, c_R - i\,0.5\, b_R^2, d, \ldots\}$ if Relation (C) is employed. Eq. (3, 3) $\Longrightarrow d_I = -b_R c_R$. This result together with Eq. (3, 1) yield the solution sequence

$$\{a_n\}_{n=-3}^{3} = \Big\{ i,\ b_R, \pm 3^{1/2} b_R (1 + 0.25\, b_R^2)^{1/2}$$

$$- i\,0.5\, b_R^2, - b_R (1 + 0.5\, b_R^2)$$

$$\mp i\, 3^{1/2} b_R^2 (1 + 0.25\, b_R^2)^{1/2}, \ldots \Big\} \quad \text{where } a_{-n} = a_n$$

For N = 4, Relation (C) reduces the solution sequence to

$$\{a_n\}_{n=-4}^{4} = \{i,\ b_R,\ c_R - i\,0.5\, b_R^2,\ d_R - i\, b_R c_R,\ e, \ldots.\}$$

Appendix II explains the manner in which the remaining equations were solved. A function labeling technique incorporated into the computer program eliminated some very tedious algebra. A computer search which maximized R_1 resulted in a solution sequence with an R_1 of 8.49. Since R_1 is bounded above by 9 when N = 4, this is a very encouraging result. A grating with 9 orders should be quite suitable for a high density storage system since Chapter 3 showed that the number of orders must be limited for this type of system.

The redundancy characteristics for the principle roots to Eqs. (6) for N = 3 and 4 are given in Figs. 4-6 and 4-7. Removing the 90 degree phase condition increased the maximum value of R_1 from 4.64 to 5.3 for N = 3, and from 4.99 to 8.49 for N = 4. The upper bound for R_1 is 2N + 1. Note that $\frac{\max\{R_1\}}{2N+1}$ increased from 0.75 to 0.94 when N increased from 3 to 4. It is logical to ask if $\frac{\max\{R_1\}}{2N+1}$ will approach unity as N is further increased. Appendix III shows that maximizing R_1 for N > 4 is a very difficult task.

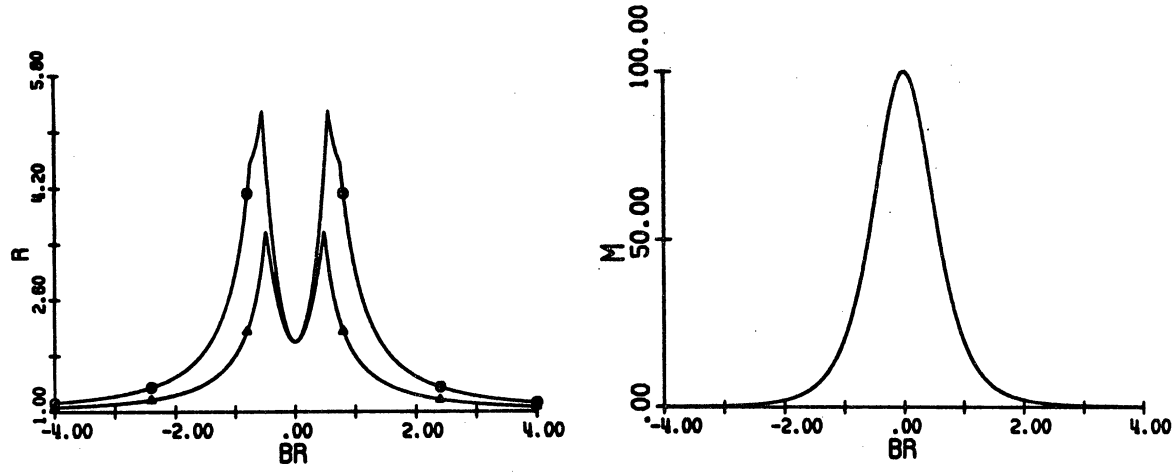

Figure 4-6. Redundancy and Modulation Characteristics for N = 3. The Symbols 0 and Δ Denote R_1 and R_2 Respectively.

$$M = 100(I_{max} - I_{min})I_{max}^{-1}$$

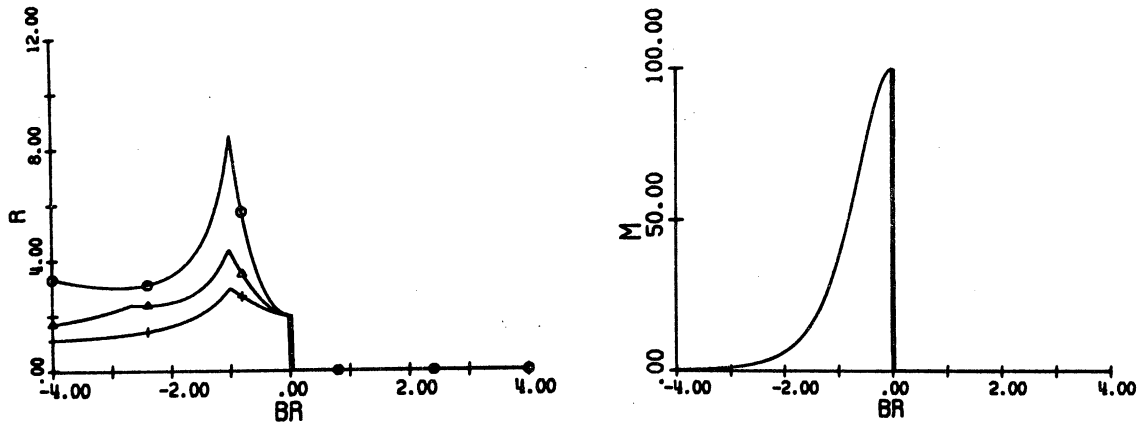

(a)

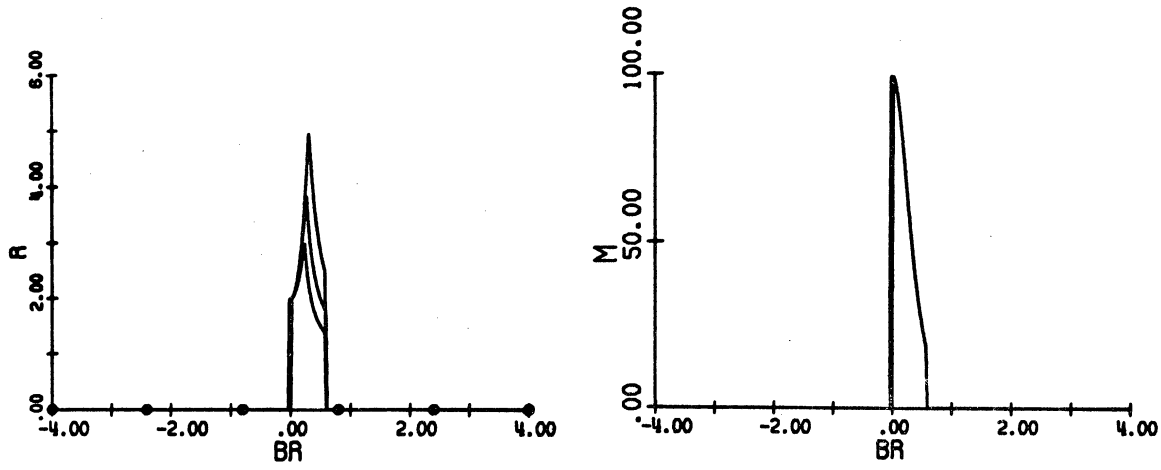

(b)

Figure 4-7. Redundancy and Modulation Characteristics for N = 4. The Symbols 0, Δ, and + Denote R_1, R_2, and R_3 Respectively.

$$M = 100(I_{max} - I_{min})I_{max}^{-1}$$

4.5.3. SOLUTION SUMMARY

Table 4-1 lists even function solutions $\{a_n\}_{n=-N}^{N}$ to Eqs. (6) which maximize the redundancy parameter R_1.

Let $FT\{\bullet\}$ denote the Fourier transform operation. Figs. 4-8(a) to 4-8(g) show the coefficients $|\hat{q}(n/X)|^2 = |a_n|^2$ and the envelope $|FT\{rect(x/X)q(x)\}|^2$ for entries B through H of Table 4-1. Figure 4-8(h) shows the spectral density corresponding to point BR = 1 of Fig. 4-4(c). In this example R_1 is not maximum, but the modulation parameter M is quite small.

Table 4-1. Solution Summary

Entry	Assumption $\arg\{a_n a^*_{n+1}\} = \pm\pi/2$	N	R_1	$\lvert q(x)\rvert^2$ where $w = \frac{2\pi}{X}$	$\{a_n\}_{n=-N}^{N}$ where $a_{-n} = a_n$
A		1	3	1. + 0.66 cos 2wx	{i, 1, i}
B		2	4.25	1. + 0.47055 cos (4wx)	{i, 1.00007, -i0.50007, . .}
C	*	3	4.64	1. + 0.43094 cos (6wx)	{i, 1.00007, -i0.500007, 0.375009, . . .}
D		3	5.3	1. + 0.37734 cos (6wx)	{i, 0.550074, 0.988133 -i0.151290, -0.633294 -i0.543546, . . .}
E	*	4	4.99	1. + 0.10022 cos (8wx)	{i, -1.999953, -i1.999907, 0.343029, -i1.312095, ...}
F		4	8.49	1. + 0.23231 cos (8wx)	{i, -0.999931, 0.792831 -i0.499931, 0.621247 +i0.792776, 0.889049 +i0.181948, ...}
G	*	5	7.40	1. + 0.13162 cos (10 wx)	{i, 1.100068, -i0.605075, -1.432878, i1.393206, -1.433349, ...}
H	*	6	8.47	1. + 0.19489 cos (12 wx)	{i, -1.099933, -i0.604926, 0.799482, i0.696409, 0.908429, i1.100901, ...}

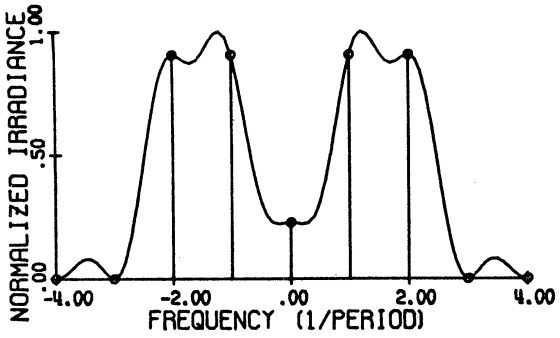

(a) Entry B of Table 4-1

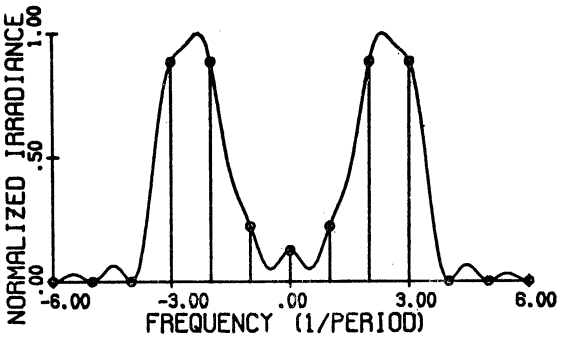

(b) Entry C of Table 4-1

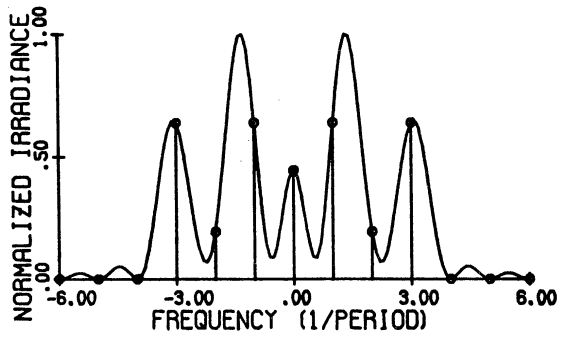

(c) Entry D of Table 4-1

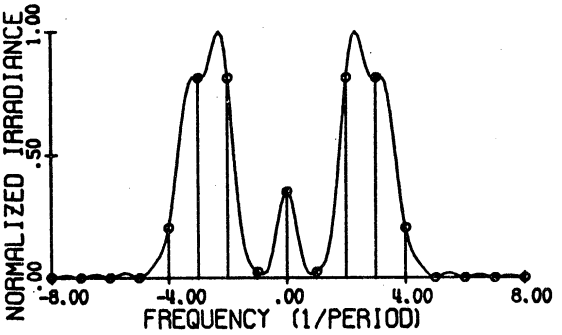

(d) Entry E of Table 4-1

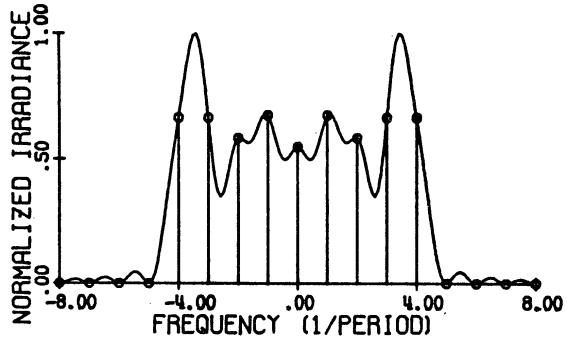

(e) Entry F of Table 4-1

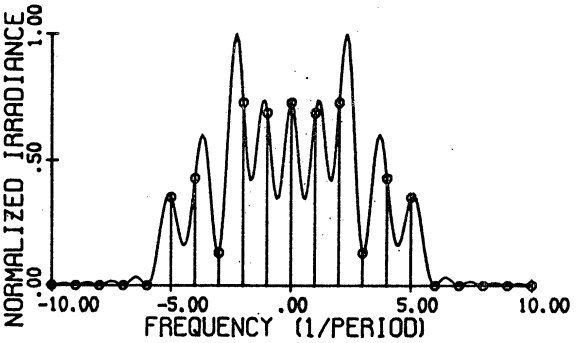

(f) Entry G of Table 4-1

Figure 4-8. Spectral Density Characteristics

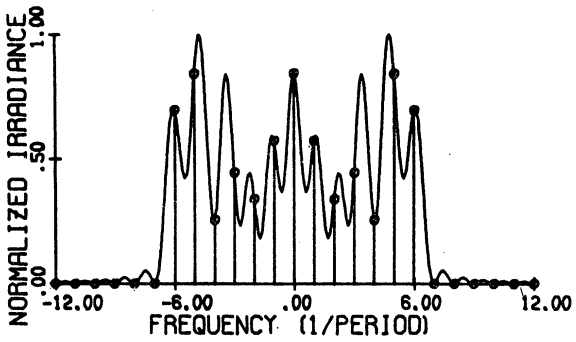

(g) Entry H of Table 4-1.

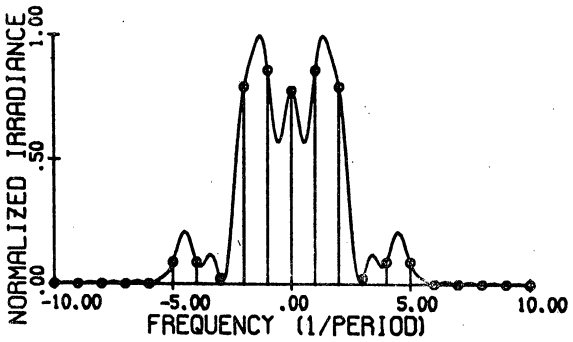

(h) Point BR = 1 of Fig. 4-4(c)

Figure 4-8. Spectral Density Characteristics (continued)

4.6. SYNTHESIS OF PERIODIC MODULATION WITH OPTIMUM REDUNDANCY CHARACTERISTICS

The first method of synthesis to be considered is that suggested by Gabor [20]. Here, the complex modulation q(x) is synthesized by constructing a special filter with an amplitude transmittance proportional to

$$q(x) = \sum_{n=-N}^{N} a_n e^{i2\pi n f_o x}$$

Such a filter is constructed using two distinct filters with amplitude transmittances of $t_1(x)$ and $t_2(x)$ respectively. These functions are defined below:

$$t_1(x) = \left| \sum_{n=-N}^{N} a_n e^{i2\pi n f_o x} \right|$$

$$= \left[2 + \sum_{n=-(N-1)}^{N-1} |a_n|^2 + 2 \cos (2\pi 2N f_o x) \right]^{1/2}$$

and

$$t_2(x) = e^{iP(x)}$$

where

$$P(x) = \arg \left\{ \sum_{n=-N}^{N} a_n e^{i2\pi n f_o} \right\}$$

Two such filters in tandem produce the complex amplitude transmittance $q = t_1 t_2$. The first filter has a real amplitude transmittance and can be produced photographically. The second filter is a pure phase function with a period 2N times as coarse as that of t_1, and can be produced using a ruling engine. New technologies being developed, such as electron beam thermoplastic recorders, may provide other means of synthesizing t_2.

The self-imaging characteristics of periodic modulation make it unnecessary to place the two filters in contact with one another. This property should also prove useful when two such filters are crossed at right angles to provide two-dimensional redundancy. The phase profiles for t_2 representing entries B through H of Table 4-1 are given in Figs. 4-9(a) to 4-9(g). Computer program logic produced a smooth curve for P(x) instead of P(x) modulo 2π. The

Fast Fourier Transform algorithm [22] was used to perform the complex summation $\sum_{n=-N}^{N} a_n e^{i2\pi n f_o x}$ efficiently for a large number of points. Figure 4-9(h) represents the phase profile for the solution sequence whose spectral density is shown in Fig. 4-8(h). For this particular example, R_1 is not maximum but the fringe modulation M is only 3 percent. The triangular profile shown in Fig. 4-9(d) should be one of the simplest to fabricate.

The second synthesis technique to be considered requires optical spatial filtering, and is most applicable for solution sequences with the property $\arg\{a_n a^*_{n+1}\} = \pm\pi/2$. Some special properties of this class of solutions will now be given. Consider functions of the form $q(x) = \sum_{n=-N}^{N} a_n e^{i2\pi n f_o x}$ with period $X = 1/f_o$, and let $|q(x)| = m(x)$ and $\arg\{q(x)\} = P(x)$. If $q(x)$ is even and $\{a_n\}_{n=-N}^{N}$ satisfies Eqs. (6), then $m(x)$ and $P(x)$ are both even and $m(x)$ has a period of length $X/(2N)$. Let $a_n = f_R(n) + i f_I(n)$ and suppose $P(x + X/2) = -P(x)$. Since

$$m(x + X/2) \cos [P(x + X/2)] = m(x) \cos [P(x)]$$

and

$$m(x + X/2) \sin [P(x + X/2)] = -m(x) \sin [P(x)]$$

$$f_R(n) = 0 \text{ for } n \text{ odd and}$$

$$f_I(n) = 0 \text{ for } n \text{ even or zero}$$

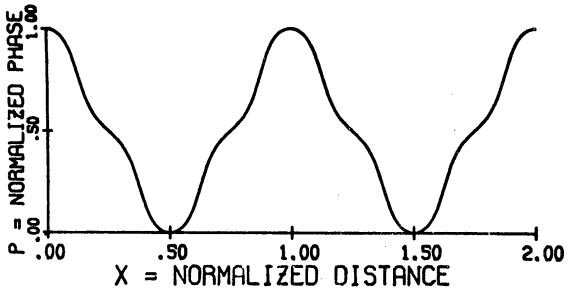

(a) Entry B, $P_{max} = 0.7048\ \lambda$

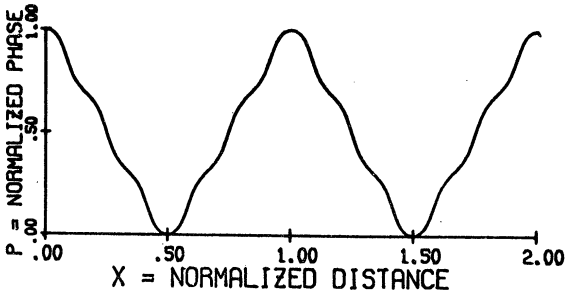

(b) Entry C, $P_{max} = 1.1268\ \lambda$

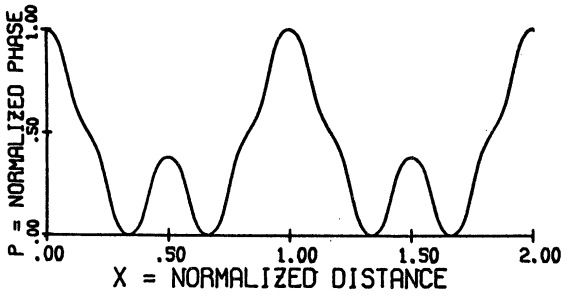

(c) Entry D, $P_{max} = 0.6719\ \lambda$

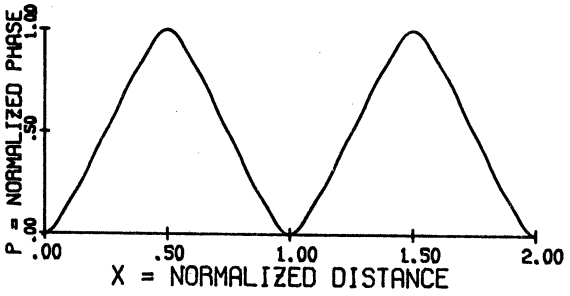

(d) Entry E, $P_{max} = 1.2501\ \lambda$

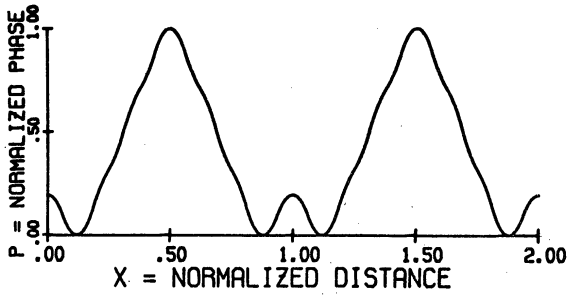

(e) Entry F, $P_{max} = 1.0152\ \lambda$

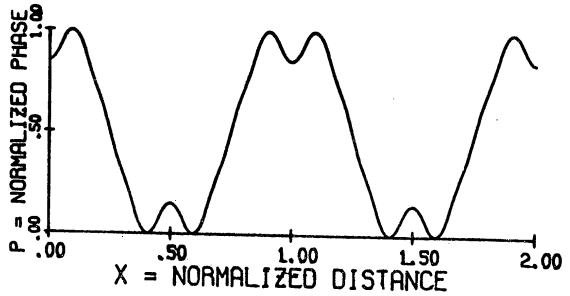

(f) Entry G, $P_{max} = 0.9542\ \lambda$

Figure 4-9. Phase Profiles for Entries B through H of Table 4-1 and the Point BR = 1 of Fig. 4-4(c). The Parameters P_{max} and λ Represent the Maximum Phase Variation and 2π Radians Respectively

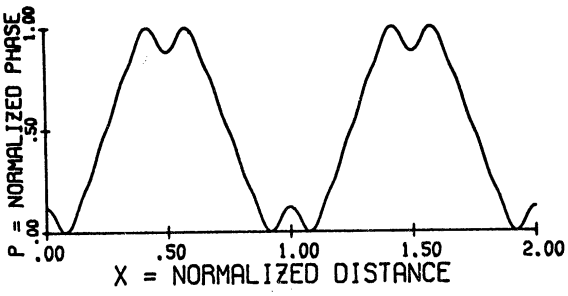

(g) Entry H, $P_{max} = 1.4655\lambda$

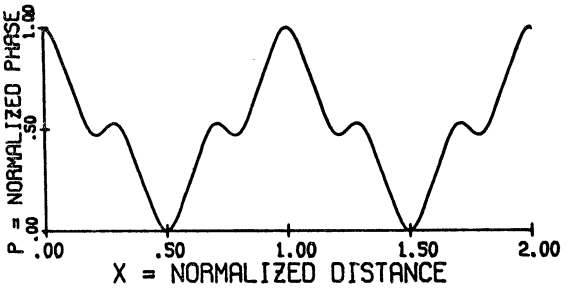

(h) Point BR = 1 of Fig. 4-4(c) $P_{max} = 0.7425\ \lambda$

Figure 4-9. Phase Profiles for Entries B through H of Table 4-1 and the Point BR = 1 of Fig. 4-4(c). The Parameters P_{max} and λ Represent the Maximum Phase Variation and 2π Radians Respectively (continued)

It is thus clear that q(x) or $e^{i\theta_o} q(x)$ has the property $\arg\{a_n a^*_{n+1}\} = \pm\pi/2$ if θ_o is a constant. Note that the phase plots in Fig. 4-9 satisfy the equation

$$\alpha(x + X/2) = -\alpha(x)$$

where

$$\alpha(x) = P(x) - (1/X) \int_{-X/2}^{X/2} P(x)\, dx$$

The sinusoidal phase function $e^{iA\cos(wx)}$ also has this 90 degree phase property and can be fabricated rather easily using photographic bleaching techniques. Thus, some of the solutions to Eqs. (6) can be formed by using a simple discrete optical filter to properly weight the Fourier series coefficients of a sinusoidal phase grating. As a

simple example, consider the function $e^{iA \cos (wx)}$ where the constant A is chosen so that the lower order Fourier series terms are

$$a_1(x) = -0.097 + i\, 0.942 \cos (wx) - 0.92 \cos (2wx) - i\, 0.47 \cos (3wx)$$

The DC term of $a_1(x)$ can be removed by spatial filtering to yield

$$a_2(x) = a_1(x) + 0.097$$

and hence,

$$\left|a_2(x)\right|^2 = 0.977 + 0.001 \cos (2wx) - 0.02 \cos (4wx) + 0.11 \cos (6wx)$$

This particular example was achieved experimentally.

A third method of synthesis for functions $q(x) = \sum_{n=-N}^{N} a_n e^{inwx}$ with the property $\arg\{a_n a^*_{n+1}\} = \pm \pi/2$ becomes evident if the Fresnel free space transfer function $H(f_x, f_y)$ is examined.

$$H(f_x, f_y) = e^{ikz} e^{-i\pi\lambda z(f_x^2 + f_y^2)}$$

where f_x and f_y are spatial frequencies for the x and y coordinates respectively of a Cartesian coordinate system. For separable functions only a one-dimensional transfer function need be considered. For

periodic functions with period $X = 1/f_o$, $f_x = nf_o$ and H becomes

$$H(nf_o) = e^{ikz} e^{-i\pi\lambda z f_o^2 n^2}$$

Now if $\pi\lambda z_o f_o^2 = 2\pi J - \pi/2$ where J is an integer,

$$e^{-ikz_o} H(nf_o) = -i \qquad \text{if n is odd}$$
$$= 1 \qquad \text{if n is even or zero}$$

The Fresnel diffraction pattern at a distance z_o from q(x) becomes

$$q(x, z_o) = \sum_{n=-N}^{N} a_n H(nf_o) e^{in2\pi f_o x}$$
$$= e^{i\theta_o} f(x)$$

where f(x) is a real function and $e^{i\theta_o}$ is a complex constant. Since f(x) is real, a filter with amplitude transmittance

$$t(x) = \frac{f(x) - \min\{f(x)\}}{\max\{f(x)\} - \min\{f(x)\}}$$

can be fabricated photographically. Then if an optical filter is used to remove the bias term $-\min\{f(x)\}\left[\max\{f(x)\} - \min\{f(x)\}\right]^{-1}$, the complex modulation q(x) is achieved by imaging a plane a distance z_o from the filter.

Optical filtering noise will limit the quality of the illumination obtained by the second and third synthesis methods.

4.7. DIFFRACTION EFFICIENCY CONSIDERATIONS

In order to record holograms with high diffraction efficiency in Fourier transform holography, it is necessary that $\left| FT\{q(x)\} \right|^2$ be rather uniform. This condition can be met if the solutions given in Table 4-1 are used in tandem with a coarse lens array to obtain a new modulation function $q(x) = q_1(x)q_2(x)$; where $q_1(x)$ is a solution to Eqs. (6) such as Entry F of Table 4-1, and $q_2(x)$ is a lens array with a period X_2 large enough to satisfy the equations given below.

$$FT\{q_1(x)\} = \sum_{n=-N}^{N} a_n \delta\left(f_x - \frac{n}{X_1} \right)$$

f_x is a spatial frequency variable. If

$$FT\{q_2(x)\} \approx \text{rect}\,(X_1 f_x)$$

then

$$\left| FT\{q_1(x)q_2(x)\} \right|^2 \approx \text{rect}\left(\frac{X_1 f_x}{2N+1} \right)$$

An experiment illustrating this concept was performed using the parameters listed below

$$q_1(x) = \sum_{n=-1}^{1} a_n e^{i\frac{2\pi n x}{X_1}}, \text{ where } \{a_n\}_{n=-1}^{1} = \{i,\ 1,\ i\} \text{ and}$$

$$X_1 = 1/(16) \text{ mm}$$

$q_2(x) = q_A(x)$ of Chapter 2 where $X_2 = 0.58$ mm and $Q = 9.28$.

Figures 4-10(a) and 4-10(b) show $\left|FT\{q_1\}\right|^2$ and $\left|FT\{q_1 q_2\}\right|^2$ respectively at the Fourier transform plane of a bandlimited coherent imaging system. The imaging system was the same as that shown in Fig. 3-2 and had bandwidth $(4 - \epsilon)/X_1$ where $\epsilon << 1$. Figures 4-11(a) through 4-11(d) show the image plane of the system when q(x) equals 1, $q_2(x)$, $q_1(x)$, and $q_1(x)q_2(x)$ respectively. In each of these figures, two wires were placed between the imaging system and image plane. These two wires introduce two dark horizontal lines when q(x) = 1. The upper and lower wires were 0.235 mm and 0.112 mm respectively in diameter, and were placed at the respective distances 5.5 cm and 10.0 cm from the image plane.

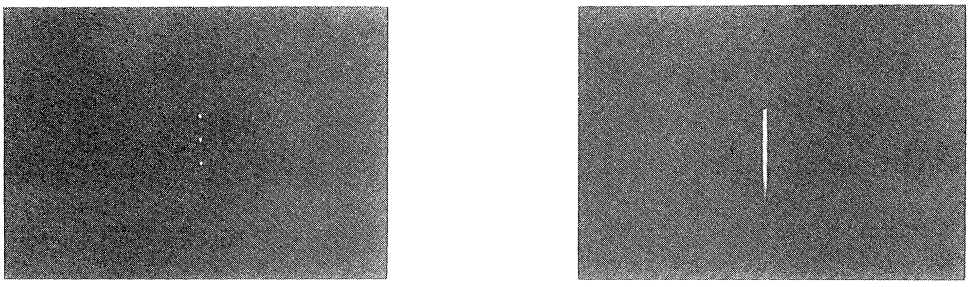

(a) Spectral Density of q_1 (b) Spectral Density of $q_1 q_2$

Figure 4-10. Irradiance at System Fourier Transform Plane

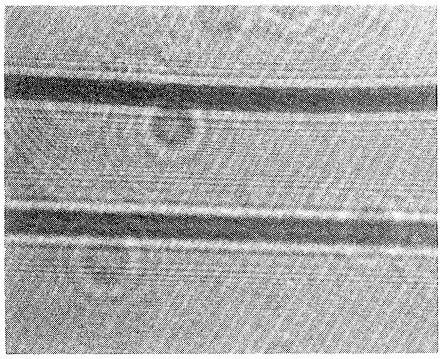

(a) $q(x) = 1$

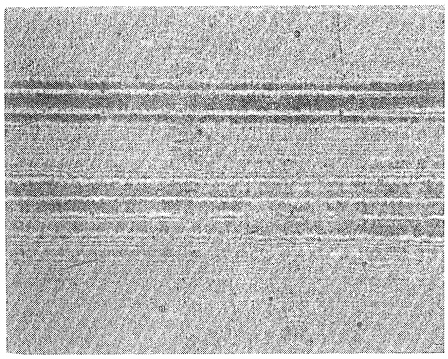

(b) $q(x) = q_2(x)$

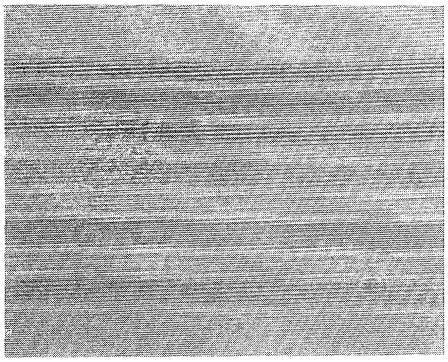

(c) $q(x) = q_1(x)$

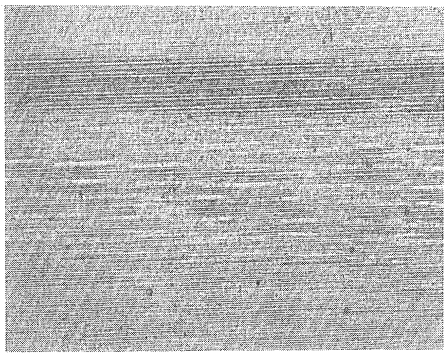

(d) $q(x) = q_1(x)q_2(x)$

Figure 4-11. Irradiance at the Image Plane with Two Wires Introduced as Artifacts

Figures 4-11(c) and 4-11(d) show that the addition of a coarse lens array can increase noise dispersion uniformity and thus aid the noise suppression process if the focal length of each lenslet is small relative to the scatterer to image distance. If the period of the lens array is chosen sufficiently large, its self-imaging distance will be large relative to the optical system dimensions. Geometrical optics predicts that a choice of negative lenslets for q_2 is sometimes necessary to assure that q_2 does not reduce noise suppression at some points in the system.

4.8. INCREASING THE REDUNDANCY OF PERIODIC MODULATION BY REDUCING THE SPECKLE FREQUENCY REQUIREMENTS

In the previous sections the low frequency speckle noise was minimized by imposing Eqs. (6) which require that each of the low frequency coefficients $I_1, I_2, \ldots I_{2N-1}$ be zero for a grating with $2N + 1$ orders. Solutions were then found which optimized the spectral density uniformity. It was seen that solutions with good spectral uniformity exist.

For cases where solutions with good redundancy characteristics do not exist, it is logical to increase the dimension of the solution space to J by requiring that only the first $2N - J$ of the coefficients $\{I_n\}_{n=1}^{2N-1}$ be zero, where $J > 1$. Of course, if J is not small relative to 2N, the storage density of an optical system will be significantly reduced. An alternative approach is to impose spectral uniformity by requiring that R_1 equal $2N + 1$. Equations (6) can then be studied to see if J can be made small. A group at RCA reported work which is related to this latter approach [23]. They examined the Fresnel diffraction pattern generated by a pinhole array. The characteristics of a one-dimensional pinhole array are derived in Appendix IV. Computer calculations reported in this appendix show that the redundancy characteristics of a pinhole array are not optimum for high density storage systems.

5
CONCLUSIONS

Chapter 1 investigated the limitations that laser speckle places on the image quality and resolution of coherent imaging systems. Mixed-integration processing which reduces the speckle fluctuation can improve image contrast. Mixed integration can be achieved efficiently using a spinning lens array. An important result given in Section 1.3.2 was the equivalence between noncoherent techniques which continuously sample a signal's spectrum and a simple irradiance filter. This result helps clarify what performance can be expected from various mixed integration methods. An analysis of speckle reduction techniques led to the moving grating method which proved to be an effective means for introducing redundancy into coherent spatial filtering systems. Since optical artifact noise can be suppressed in coherent optical filtering systems by reducing the source coherence, it is advantageous that the source coherence not exceed the system requirements.

Most noncoherent noise suppression techniques are not useful for diffraction limited holographic storage systems. In order to coherently image continuous-tone transparencies, special types of bandlimited redundancy modulation must be considered. Redundancy modulation must satisfy two constraints. First, the modulation must be free of low frequency speckle. Second, the spectral density of the modulation must be rather uniform. There exist two mechanisms for optical noise suppression. One mechanism is to increase the spatial bandwidth of the noise irradiance. The principle mechanism for noise suppression is to disperse optical noise

more uniformily at the image plane. Quadratic phase modulation has good redundancy characteristics if the space bandwidth parameter Q is much greater than ten. Computer results and experimental evidence were presented which show the redundancy characteristics of quadratic phase modulation as a function of Q.

Periodic functions are the most promising form of redundancy modulation for the high density storage of continuous-tone transparencies. The noise suppression performance of this class of functions was analyzed in terms of a family of redundancy parameters. When speckle-free periodic redundancy illumination is perturbed by a system artifact, some low frequency speckle is introduced. Limits on the low frequency speckle modulation were established which show how speckle modulation is related to the spectral uniformity of the redundancy illumination. Recently a system was described in the literature which used a pinhole array filter to generate redundancy illumination [23]. Appendix IV discusses the redundancy characteristics of a pinhole array illumination and shows that this type of modulation is not optimum for the high density storage of continuous-tone transparencies. A computer program developed to investigate self-imaging characteristics on an arbitrary periodic function from its complex Fourier series coefficients was used in this analysis.

A system of nonlinear equations must be solved in order to determine periodic modulation which is free of low frequency speckle. For the class of even function solutions obtained by Gabor, a 90 degree phase difference existed between adjacent Fourier series coefficients. The recurrence relationship given by Gabor to generate higher order solutions is not valid for a function with more than 7 nonzero Fourier coefficients. Solutions do exist, however, and have been calculated for functions with up to 13 nonzero orders. Numerical techniques were required to solve these equations. The spectral characteristics of the solutions considered can be predicted from

the redundancy parameter plots. Although even function solutions without the 90 degree phase condition are more difficult to obtain, more general solutions have better spectral uniformity and thus higher redundancy. In particular, a 9 order grating defined by entry F of Table 4-1 appears to meet quite well the redundancy requirements of holographic microfiche systems which store continuous-tone transparencies. One method of synthesizing these solutions is to directly fabricate a filter with the proper complex amplitude transmittance. A computer program was developed to plot the continuous phase function for a particular solution from its Fourier series coefficients. For solutions with a 90 degree phase difference between adjacent complex Fourier coefficients, two indirect synthesis methods requiring a spatial filtering operation were presented.

Redundancy modulation with good diffraction efficiency characteristics can be obtained by using a coarse lens array in tandem with a periodic grating solution. Experimental results demonstrated that the addition of a lens array can improve the noise suppression characteristics of this class of functions.

REFERENCES

1. L. I. Goldfisher, J. Opt. Soc. Am., 55, 247 (1965).
2. R. W. Lewis, "Mixed-Integration Processing of Synthetic Aperture Radar Data," Technical Report AFAL-TR-72-215, Air Force Avionics Laboratory, Air Force Systems Command, Wright-Patterson Air Force Base, Ohio, August 1972.
3. L. J. Porcello, N. G. Massey, R. B. Innes, and J. M. Marks, "Diversity and Mixed-Integration Processing in Synthetic Aperture Radar (U)," Fourteenth Annual Tri-Service Radar Symposium Record (U), Vol. II, Willow Run Laboratories of the Institute of Science and Technology, The University of Michigan, Ann Arbor, July 1968, pp. 114-142 (SECRET).
4. L. H. Enloe, Bell Sys. Tech. J., 46, 1479 (1967).
5. J. I. Marcum and P. Swerling, Special Monograph Issue, IRE Trans. Inform. Theory, IT-6 (1961).
6. A. Kozma, E. N. Leith, and N. G. Massey, Appl. Opt., 11, 1766 (1972).
7. C. E. Thomas, Appl. Opt., 7, 517 (1968).
8. J. Upatnieks and R. Lewis, Opt. Soc. Am. Meeting Program, Oct., M13 (1972).
9. G. B. Brandt, Opt. Soc. Am. Meeting Program, Oct., B16 (1972).
10. G. B. Brandt, U. S. Patent 3620598.
11. M. Elbaum, M. Greenebaum, and M. King, Opt. Commun., 5, 171 (1972).
12. E. N. Leith and J. Upatnieks, Appl. Opt., 10, 2085 (1968).
13. F. Talbot, Phil. Mag., 9, 401 (1836).
14. J. W. Goodman, Introduction to Fourier Optics, McGraw-Hill Book Co., Inc., New York, 1968.
15. M. Born and E. Wolf, Principles of Optics, Pergamon Press, London, 1965.
16. J. Upatnieks, Appl. Opt., 6, 1905 (1967).
17. J. R. Klauder, A. C. Price, S. Darlington, and W. J. Albersheim, Bell Sys. Tech. J., 39, 745 (1960).
18. E. N. Fowle, IEEE Trans., IT-10, 61 (1964).

19. S. S. Hsiao, "Analysis on Information Reduction and Beam-width Reduction in Holography," Ph. D. Dissertation, University of Michigan, Ann Arbor, Michigan, p. 198, 1972.

20. D. Gabor, IBM J. Res. Develop., 14, 509 (1970).

21. F. Zernike, J. Opt. Soc. Am., 40, 326 (1950).

22. J. W. Cooley and J. W. Tukey, Math. Comput., 19, 297, (1965).

23. A. H. Firester, E. C. Fox, J. Gayeski, W. J. Hannan, and M. Lurie, RCA Review, 33, 131 (1972).

24. H. J. Gerritsen, W. J. Hannan, and E. G. Ramberg, Appl. Opt., 7, 2301 (1968).

APPENDIX I
GENERAL SOLUTIONS TO EQUATIONS (6)

Consider a solution sequence $\{a_n\}_{n=-N}^{N}$ to Eqs. (6) of Chapter 4 when $a_{-n} \neq a_n$ and $N = 1$. If

$$\{a_n\}_{n=-1}^{1} = \{i,\ a,\ b\}$$

Eqs. (6) imply that

$$b = i\frac{a}{a^*}$$

Thus if

$$a = |a|e^{i\theta_a}$$

the solution sequence

$$\{a_n\}_{n=-1}^{1} = \left\{ i,\ |a|e^{i\theta_a},\ ie^{i2\theta_a} \right\}$$

is obtained. When the two free parameters θ_a and $|a|$ are set equal to zero and one respectively, the sequence

$$\{a_n\}_{n=1}^{1} \text{ becomes } \{i,\ 1,\ i\}$$

This particular sequence is an even function solution and can be generated efficiently using the first three orders of a sinusoidal phase grating [24].

Next, consider a grating for N = 3, which has four nonzero coefficients. If $\{a_n\}_{n=-3}^{3} = \{b_1, 0, b_2, 0, b_3, 0, b_4\}$, the maximum limit for R_1 is 4. Since b_2 can be set arbitrarily equal to 1, equations system (6) consists of 4 equations and 6 unknowns. The solution sequence

$$\left\{ -\frac{b_3^*}{1 - |b_3|^2},\ 0,\ 1,\ 0,\ b_3,\ 0,\ \frac{b_3^{\ 2}}{1 - |b_3|^2} \right\}$$

for these equations has two free parameters: $|b_3|$ and arg $\{b_3\}$. It is clear that the maximum limit for R_1 cannot be attained since $|b_3| = 1$ implies that $|b_1|$ and $|b_4|$ are equal to infinity.

Finally, consider the solution sequence $\{b_1, b_2, b_3, b_4, b_5\}$ for N = 2. By setting b_1 equal to 1 and by reducing equation system (6) to 4 unknowns and 2 equations, this sequence becomes

$$\left\{ 1,\ b_2,\ b_3,\ \frac{b_2^* b_3}{b_3^* - b_2^{*2}},\ \frac{-b_3}{b_3^* - b_2^{*2}} \right\}$$

where b_2 and b_3 must satisfy the complex equation

$$b_2^* + b_2 b_3^* + \frac{|b_3|^2 b_2}{(b_3 - b_2^{\ 2})} - \frac{|b_3|^2 b_2^*}{|b_3 - b_2^{\ 2}|^2} = 0 \qquad (8)$$

Suppose $b_2 = 1 + i$. After reducing Eq. (8) to a cubic equation, the following roots are obtained:

$$b_3 = i,\ i(2 + 2\sqrt{2}),\ i(2 - 2\sqrt{2})$$

One possible solution sequence is

$$\{a_n\}_{n=-2}^{2} = \{1,\ 1+i,\ i,\ 1-i,\ -1\} \quad \text{where } a_n \equiv b_{n+3}$$

The value of R_1 for this sequence is 3.5. It will now be established that no solution exists with R_1 equal to the maximum limit 5.

Suppose $R_1 = 5$. Then $|b_2| = |b_3| = 1$, and the solution sequence becomes

$$\left\{ 1,\ e^{i\theta_2},\ e^{i\theta_3},\ \frac{e^{i(\theta_3-\theta_2)}}{e^{-i\theta_3}\left[1 - e^{i(\theta_3 - 2\theta_2}\right]},\ \frac{e^{i\theta_3}}{e^{-i\theta_3}\left[1 - e^{i(\theta_3-2\theta_2)}\right]} \right\}$$

Since $|b_4|$ and $|b_5|$ also must be unity, this requires that

$$(\theta_3 - 2\theta_2) = \pm\frac{\pi}{3}$$

It can be shown using Eq. (8) that this implies

$$2\cos\ (\theta_2 \pm \pi/3) = \cos\theta_2$$

and

$$2\sin\ (\theta_2 \pm \pi/3) = \sin\theta_2$$

A contradiction is now apparent since these equations imply $1 = 4$. The above examples have shown that obtaining general solutions to Eqs. (6) is difficult even if N is small. A computer search to maximize R_M must be over a two-dimensional parameter space. The system of nonlinear equations differs for each point in the

parameter space; and algorithms to solve these equations require an initial guess. Fortunately, it will be seen that if $a_{-n} = a_n$, a more modest computer effort will result in a solution sequence with R_1 near the maximum limit $2N + 1$ for $N = 4$.

APPENDIX II
GENERAL EVEN FUNCTION SOLUTIONS FOR N = 4

The computation required for obtaining general even function solutions to Eqs. (6) when N = 4 is described here. Relation (C) of Chapter 4 reduces the solution sequence $\{a_n\}_{n=-4}^{4}$ to

$$\{i,\ b_R,\ c_R - i\,0.5\,b_R^2,\ d_R - ib_Rc_R,\ e, \ldots.\}$$

As a shorthand notation, let Eq. (n, k) denote equation

$$\sum_{n=-N}^{N-k} a_n a^*_{n+k} = 0$$

of the 2N - 1 Eqs. (6) of Chapter 4.

$$\text{Eq. } (4,\ 4) \Longrightarrow e_I = -(b_Rd_R + 0.5\,c_R^2 + 0.125\,b_R^4)$$

$$\text{Eq. } (4,\ 3) \Longrightarrow -2b_Rc_R + 2b_Re_R + 2c_R(d_R + 0.5\,b_R^3) = 0$$

and

$$2b_Re_R + 2c_R(d_R + 0.5\,b_R^3 - b_R) = 0$$

Using e_I from Eq. (4, 4)

$$\text{Eq. } (4,\ 2) \Longrightarrow b_R^2(-1 + 1.5\,c_R^2 + b_Rd_R + 0.125\,b_R^4) + 2b_Rd_R + d_R^2 + 2c_Re_R = 0$$

$$\text{Eq. (4, 1)} \Rightarrow 2b_R c_R(1 + b_R d_R + 0.125\, b_R^4 + 0.5\, c_R^2)$$

$$+ 2c_R(d_R + 0.5\, b_R^3) + 2e_R d_R = 0$$

If $d_R = 0$, it can be shown that $R_1 < 6$, hence this case will be ignored in the programming described below. Assuming d_R differs from zero, the equations above reduce to the equation

$$\sum_{n=0}^{4} (Z_{n+1} c_R^{2n}) = 0$$

The coefficients $Z(n + 1)$ are defined in terms of the parameter $BR = b_R$ by the algebraic steps in the subroutine COEFPN(BR, Z) given below.

```
SUBROUTINE COEFPN(BR, Z)
DIMENSION Z(11)
BR2=BR*BR
BR4=BR2*BR2
BA1=BR2*(2.+BR2+0.1875*BR4)
BA2=0.5*BR2
AL=0.25*BR*(4.+BR2)
AL2=AL*AL
AL3=AL*AL2
C2=BR*(2.+BR2)
AC1=BR2*(-1.+.125*BR4)
BC1=.5*BR2-2.
AC0=-2.*BR*(1.+0.5*BR2+0.125*BR4)
E1=3.*AL2+C2*2.*AL+AC1+BA1
E2=BA2+BC1
E12=E2*E1
E22=E2*E2
E11=E1*E1
P0=BA1*E11
P2=BA2*E11+BA1*2.*E12
P4=BA1*E22+2.*BA2*E12
P6=BA2*E22
F31=AL3+3.*AL*BA1
```

```
G31=3.*AL*BA2
H0=F31+C2*(AL2+BA1)+AL*AC1
H2=G31+C2*BA2+AL*BC1+AC0
Q0=H0*H0
Q2=H0*H2*2.
Q4=-BR*H0*2.+H2*H2
Q6=-2.*BR*H2
Q8=BR2
Z(1)=Q0-P0
Z(2)=Q2-P2
Z(3)=Q4-P4
Z(4)=Q6-P6
Z(5)=Q8
RETURN
END
```

If the variable ZREAL denotes a positive real root of the polynomial

$$\sum_{n=0}^{4} Z_{n+1} w^n = 0$$

then subroutine ZORDGN given below calculates the sequence $\{a_n\}_{n=-4}^{4}$ where

$$a_n = ZAR(n + 5) + iZAI(n + 5)$$

Choosing $-\sqrt{ZREAL}$ instead of $\sqrt{ZREAL}$ for c_R in this subroutine would simply change the sign of a few of the sequence terms ZAR(n) and ZAI(n).

```
      SUBROUTINE ZORDGN(BR, ZREAL, ZAR, ZAI, ZMOD)
      DIMENSION ZAR(13), ZAI(13), ZMOD(13)
      CR=SQRT(ZREAL)
      BR2=BR*BR
      BR4=BR2*BR2
      AL=0.25*BR*(4.+BR2)
      BA1=BR2*(2.+BR2+0.1875*BR4)
      BA2=0.5*BR2
      DR=AL+SQRT(BA1+BA2*ZREAL)
      EI=-(BR*DR+0.5*ZREAL+BR4*0.125)
      ER=-BR*(CR/DR)*(1.+BR*DR+0.5*BR2
     1+0.125*BR4+0.5*ZREAL)-CR
      ZAR(1)=0.
      ZAR(2)=BR
      ZAR(3)=CR
      ZAR(4)=DR
      ZAR(5)=ER
      ZAI(1)=1.
      ZAI(2)=0.
      ZAI(3)=-BR2*0.5
      ZAI(4)=-BR*CR
      ZAI(5)=EI
      D0 20 I=1,4
      ZAR(5+I)=ZAR(5-I)
20    ZAI(5+I)=ZAI(5-I)
      D0 30 I=1,9
30    ZMOD(I)=ZAR(I)*ZAR(I) + ZAI(I)*ZAI(I)
      RETURN
      END
```

The main program used these subroutines to plot the redundancy characteristics of solution sequences when BR was varied from -4 to 4 in 0.01 increment steps.

Appropriate program logic, in the form of a subroutine, monitored all the conditions imposed in the algebraic steps above. The solution sequence which maximized R_1 was part of the output data from the program. Finally, to assure that no errors were made, an additional subroutine determined directly that each sequence generated satisfied Eqs. (6) of Chapter 4.

APPENDIX III
GENERAL EVEN FUNCTION SOLUTIONS FOR N = 5

The difficulty in obtaining general even function solutions to Eqs. (6) for N greater than 4 is presented here. It will be shown that iterative methods requiring an initial guess are necessary to solve the system of nonlinear equations when N is 5.

After imposing Relation (C) of Chapter 4, $\{a_n\}_{n=-5}^{5}$ becomes

$$\{i,\ b_R,\ c_R - i\,0.5\,b_R^2,\ d_R - ib_Rc_R,\ e_R - i(b_Rd_R + 0.5\,c_R^2 + 0.125\,b_R^4),\ f_R + if_I, \ldots\ldots\}$$

Eqs. (5,5), (5,4),...(5,1) eventually reduce to a system of two nonlinear equations and two unknowns. The two unknowns are c_R and d_R, and the free parameter is b_R. The variables α, z, e_{R1} and e_{R2} are functions of c_R and d_R, and are defined below in order to reduce the burden of listing the two equations. Let

$$\alpha(b_R,\ c_R,\ d_R) \equiv b_Rd_R + 0.5\,c_R^2 + 0.125\,b_R^4$$

$$z(b_R,\ c_R,\ d_R,\ \alpha) \equiv b_R^2(\alpha^2 - 1 + b_R^2c_R^2) + b_R(2d_R + c_R^2d_R - d_R\alpha) + \alpha^2 - \frac{2d_R}{b_R}(-\alpha + 0.5\,d_R^2)$$

$$e_{R1}\left(b_R,\ c_R,\ d_R\right) \equiv -c_R\left(1 + b_R^2 - \frac{d_R}{b_R}\right)$$

$$e_{R2}(b_R,\ c_R,\ d_R,\ z) \equiv \sqrt{c_R^2\left(1 + b_R^2 - \frac{d_R}{b_R}\right)^2 - z}$$

Then the system of two equations that must be solved provided $b_R \neq 0$ is

$$e_{R2}^2\left(-b_R + \frac{2c_R^2}{b_R} - b_R^3 - 2d_R\right)^2 = \left[e_{R1}\left(2b_R + b_R^3 + 2d_R - \frac{2c_R^2}{b_R}\right) + \alpha c_R\left(-b_R^2 + 2b_R + \frac{2}{b_R}\right) + b_R c_R\left(0.5\, b_R^4 + b_R d_R - 2 - c_R^2\right) - \frac{c_R d_R^2}{b_R}\right]^2$$

and

$$e_{R2}^2\left[2d_R + \alpha b_R - \frac{4e_{R1}c_R}{b_R} - \frac{2}{b_R}\left(-\alpha + 0.5\, d_R^2 + 0.5\, b_R^2 c_R^2\right)\right]^2 = \left[2c_R\left(b_R + 0.5\, b_R^3 + d_R\right) + 2e_{R1}d_R - \frac{2e_{R1}}{b_R}\left(-\alpha + 0.5\, d_R^2 + 0.5\, b_R^2 c_R^2 + c_R e_{R1}\right) - \frac{2}{b_R}c_R e_{R2}^2 + \alpha b_R e_{R1} + 2\alpha\, b_R c_R + c_R d_R + 0.5\, b_R^3 c_R\right)\right]^2$$

Once b_R is chosen and these equations are solved, the remaining orders can be determined from equations:

$$e_R = e_{R1} \pm e_{R2}$$

$$f_R = -\frac{1}{b_R}\left(-\alpha + 0.5\, d_R^2 + 0.5\, b_R^2 c_R^2 + c_R e_{R1} \pm c_R e_{R2} + 0.5\, b_R^2 \alpha\right)$$

$$f_I = -\left(b_R e_{R1} \pm b_R e_{R2} + c_R d_R + 0.5\, b_R^3 c_R\right)$$

Iterative methods such as Gauss-Seidel or Newton-Raphson must be used to solve the remaining equations. Since such techniques require an initial guess, the computer time and programming effort to maximize R_1 are very great.

The work required to maximize R_M can be reduced somewhat if it is decided that the only solutions of interest are those where R_M is near the maximum limit. For example, R_1 equals $2N + 1$ if and only if b_R^2, $|c|$, and $|d|$ equal unity. Imposing this condition narrows the choice for (c_R, d_R) to either $(\pm 0.5\sqrt{3}, \pm 0.5)$ or $(\pm 0.5\sqrt{3}, \mp 0.5)$. If it is found that $|f|$ is near 1, the values for (c_R, d_R) suggested can be used as initial guesses for the iterative techniques required to solve the two equation system. If interesting solutions develop, b_R can be varied slightly in order to maximize R_1.

This approach should help reduce the programming effort, if general even function solutions which maximize R_1 are required for $N > 4$.

APPENDIX IV
PINHOLE ARRAY CHARACTERISTICS

This appendix evaluates work performed by a group at RCA [23]. This group reported that a pinhole array with period X could generate redundancy illumination with period X/J where J is an integer. It will be shown that this redundancy modulation is not optimum for high density storage applications since J cannot exceed certain limits.

Consider a grating $q(x) = \sum_{n=-N}^{N} a_n e^{inwx}$ with complex Fourier coefficients $\{a_n\}_{n=-N}^{N}$. It can be shown that

$$|q(x)|^2 = I_0 + \sum_{n=1}^{2N} 2I_n \cos(2\pi n f_0 x - \phi_n)$$

where $w = 2\pi f_0$

$$I_k = \left| \sum_{n=-N}^{N-k} a_n a^*_{n+k} \right|$$

and

$$\phi_n = \arg\left\{ \sum_{n=-N}^{N-k} a_n a^*_{n+k} \right\}$$

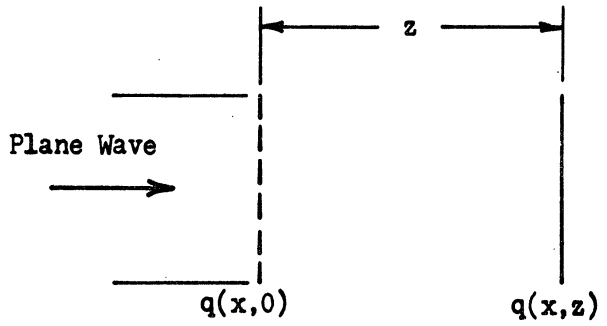

Figure IV-1. Plane Wave Incident on Grating q(x)

The Fresnel diffraction pattern $|q(x, z)|^2$ will now be determined when a plane wave is incident on the grating q(x) as shown in Fig. IV-1.

$$q(x, z) = \sum_{n=-N}^{N} e^{-i\pi\lambda z(nf_0)^2} a_n e^{inwx}$$

Since the new Fourier coefficients are now $\left\{ a_n e^{-i\pi\lambda z(nf_0)^2} \right\}_{n=-N}^{N}$

$$I_k = \left| \sum_{n=-N}^{N-k} a_n a^*_{n+k} e^{i\pi\lambda z f_0^2 [n^2-(n+k)^2]} \right|$$

$$= \left| \sum_{n=-N}^{N-k} a_n a^*_{n+k} e^{i\pi\lambda f_0^2 z(2nk)} \right|$$

The investigators at RCA imposed the condition $\{a_n\}_{n=-N}^{N} = \{1\}_{n=-N}^{N}$. This condition can be easily achieved experimentally using a low duty cycle pinhole array. This means the redundancy parameter

$$R_1 = \frac{\sum |a_n|^2}{\max\{|a_n|^2\}}$$ is equal to 2N + 1 (the number of plane waves).

The coefficient I_k becomes

$$I_k = \left| \sum_{n=-N}^{N-k} e^{i2\pi\lambda f_0^2 znk} \right|$$

Let

$$\pi\lambda z f_0^2 = \pi c$$

Then

$$z = \frac{c}{\lambda f_0^2}$$

If c = 1, z represents the self-imaging distance and

$$I_k = \left| \sum_{n=-N}^{N-k} e^{i2\pi k \frac{n}{(1/c)}} \right|$$

Note that if k << N and N becomes very large

$$I_k \approx \left| \sum_{n=-\infty}^{\infty} e^{i2\pi k \frac{n}{(1/c)}} \right| = \left| \sum_{n=-\infty}^{\infty} \delta\left(k - \frac{n}{c} \right) \right|$$

thus if $c = 1/J$ where J is a positive integer,

$$I_k \approx \left| \sum_{n=-\infty}^{\infty} \delta(k - nJ) \right|$$

and

$$I_k \approx 0 \qquad \text{if} \qquad k \neq nJ$$

Let

$$S = \sum_{n=-N}^{N-k} e^{i2\pi \frac{kn}{J}}$$

If $k \neq 0$,

$$S\left(e^{i\frac{2\pi k}{J}} - 1 \right) = e^{i2\pi k \frac{(N-k+1)}{J}} - e^{-i2\pi k \frac{N}{J}}$$

and

$$I_k = |S| = \left| \frac{\sin\left[\frac{2\pi k}{J} \left\{ N + \frac{1}{2}(1 - k) \right\} \right]}{\sin\left(\pi \frac{k}{J} \right)} \right|$$

If J = 2, it is clear that $I_k = 0$ for k = 1, 3, 5, ... Let N = L(J/2), where L is a positive integer. Then if

$$\left| q\left(x, \frac{1}{J\lambda f_0^2} \right) \right|^2 = I_0 + \sum_{n=1}^{2N} 2I_n \cos (2\pi n f_0 x - \phi_n)$$

$$I_0 = 2N + 1$$

and

$$I_k = \left| \frac{\sin \left[\frac{\pi k}{J} (1 - k) \right]}{\sin \left(\frac{\pi k}{J} \right)} \right| \quad \text{if } k > 0$$

Thus, in general, the condition $I_k \approx 0$ if $k \neq nJ$ does not hold unless $J = 2$. It can easily be shown that $J = 2$ implies $\arg \{a_n a^*_{n+1}\} = \pm\pi/2$. For example, if $N = 3$ and $J = 2$,

$$\{a_n\}_{n=-3}^{3} = \{-i, 1, -i, 1, -i, 1, -i\}$$

Since $a_{-n} = a_n$ and there are an odd number of sequence terms, the condition $I_k = 0$ if $k \neq 2n$ is rather obvious. Consider the case $N = 3$ where

$$\{a_n\}_{n=-3}^{3} = \{1\}_{n=-3}^{3}$$

If $z = 0$,

$$\frac{2}{2N + 1} \{I_k\}_{k=1}^{6} = \{1.71, 1.43, 1.14, 0.86, 0.57, 0.29\}$$

If $J = 2$ or $z = 1/2$, the self-imaging distance

$$\frac{2}{2N+1}\{I_k\}_{k=1}^{6} = \{0.,\ 1.43,\ 0.,\ 0.86,\ 0.,\ 0.29\}$$

If J = 3 or z = $0.3\overline{3}$, the self-imaging distance of the grating

$$\frac{2}{2N+1}\{I_k\}_{k=1}^{6} = \{0.,\ 0.29,\ 1.14,\ 0.,\ 0.29,\ 0.29\}$$

For J = 3, note that $\frac{2}{2N+1} I_2 = 0.29$ is rather large, since $\frac{1}{2N+1} I_0 = 1.$

Instead of demanding that R_1 equal the maximum limit 2N + 1, consider a grating $q(x) = \text{rect}\,(x/A) * \sum_{n=-\infty}^{\infty} \delta(x - n)$ where the constant A < 1. The amplitude transmittance of q(x) is shown below.

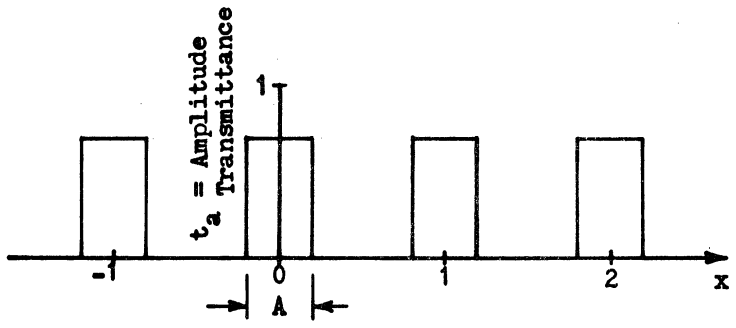

Figure IV-2. Amplitude Transmittance

Let RDC = 1/A be the reciprocal of the duty cycle of the function q(x). If

$$q(x) = \sum_{n=-\infty}^{\infty} a_n e^{inwx} \quad \text{where } w = 2\pi f_o$$

then

$$a_n \propto \text{sinc}\left(\frac{n}{RDC}\right) \quad \text{where sinc } x \equiv \frac{\sin \pi x}{\pi x}$$

This function is shown in Fig. IV-3.

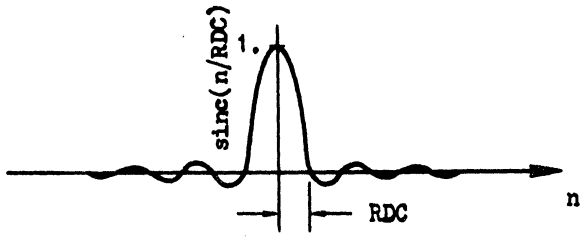

Figure IV-3. Sinc Function

If RDC is a positive integer, the number of nonzero orders within the main lobe of the sinc function is 2 * RDC - 1. Suppose that a low-pass optical filter is used to filter out all but the lowest 2N + 1 orders generated by this grating. Now

$$I_k = \left| \sum_{n=-N}^{N-k} a_n a^*_{n+k} e^{\frac{i2\pi kn}{J}} \right|$$

if

$$\left| q\left(x, \frac{1}{J\lambda f_0^{\,2}} \right) \right|^2 = I_0 + \sum_{n=1}^{2N} 2I_n \cos\left(2\pi n f_0 x - \phi_n\right)$$

If 2N + 1 does not exceed 2 * RDC - 1, then

$$\{\arg(a_n)\}_{n=-N}^{N} = \{0\}_{n=-N}^{N}$$

and $|a_n|$ decreases monitonically as $|n|$ increases. Table IV-1 given below shows the dependence of $\{2I_k\}_{k=1}^{J}$ on RDC, J, and the number of plane waves 2N + 1. It is seen that the condition $I_k \approx 0$ if $k \neq nJ$ is more accurate if the Fourier series coefficients are heavily weighted.

In Table IV-1

$$R_1 \equiv \frac{\sum_{n=-N}^{N} |a_n|^2}{\max_n \{|a_n|^2\}}$$

and q(x, z) has been normalized so that $I_0 = 1$.

In Table IV-1 it is shown that if RDC is adjusted so that R_1 is one-half the maximum limit 2N + 1, the frequency of the diffuser noise is about one-half the maximum limit $2Nf_0$.

Note that if $R_1 = \frac{1}{2}(2N + 1)$, $(2 * RDC - 1) \approx 2N + 1$. This implies that $\frac{|a_n|^2}{|a_0|^2} \to 0$ as $|n| \to N$ and thus the power spectrum of q is not uniform. Since RCA's actual system did not require

a fringe pattern finer than the basic period of the pinhole array, the coefficients $\{a_n\}_{n=-10}^{10}$ used for their system were not heavily weighted.

A computer program which was written to evaluate the self-imaging characteristics of gratings was used to obtain the numerical data presented in this appendix.

Table IV-1. Pinhole Array Data

RDC	(2 * RDC - 1)	(2N + 1)	R_1	J	$\{2I_k\}_{k=1}^{J}$ for $I_0 = 1$
5	9	9	4.51	2	{0., 1.63}
5	9	9	4.51	3	{0.0086, 0., 1.27}
5	9	9	4.51	4	{0.02, 0.02, 0.0096, 0.879}
5	9	9	4.51	5	{0.106, 0.023, 0.026, 0.216, 0.532}
5	9	9	4.51	6	{0.33, 0., 0., 0.059, 0.2933, 0.269}
5	9	9	4.51	8	{0.78, 0.03, 0.006, 0.04, 0.05, 0.11, 0.097, 0.024}
50	99	9	8.92	4	{0.001, 0.22, 0.31, 1.11}
11	21	21	9.93	9	{0.013, 0.004, 0.0029, 0.0043, 0.001, 0.0053, 0.013, 0.042, 0.86}
20	39	21	15.87	9	{0.06, 0.05, 0.004, 0.06, 0.020, 0.0034, 0.030, 0.21, 1.15}
40	79	21	19.50	9	{0.15, 0.082, 0.001, 0.087, 0.030, 0.001, 0.05, 0.261, 1.15}